CLOSED-LOOP CONTROL OF A SOFT ROBOTIC XY-TABLE TO MANIPULATE DELICATE OBJECTS

A THESIS SUBMITTED TO AUCKLAND UNIVERSITY OF TECHNOLOGY
IN PARTIAL FULFILMENT OF THE REQUIREMENTS FOR THE DEGREE OF
MASTER OF ENGINEERING

Supervisor

Dr. Martin Stommel

By

Hong-Quan Nguyen

Student ID: 17998890

School of Engineering, Computer and Mathematical Sciences

2020

Abstract

At present, soft robotic engineering is rapidly emerging as a significant part of the robotics. Recent research concerns a range of potential applications in terms of manipulating and transporting delicate work-pieces in the industrial production line. With the characteristics of soft materials, soft robots can bring a higher level of safety for human and operating objects during the interaction. Additionally, the flexible and soft structure of these robots allows them to adapt naturally to various environments without complicated control systems. Inspired by the caterpillar's crawling gait, a particular kind of soft robot called a "soft table" has been proposed to solve applications in the bio-mimetic, medical and industrial field. This table is capable of translating and rotating objects on the top surface deriving from the deformation of its top surface. For constructing this deformation, an open-loop controller has been adopted to the soft table to produce surface movements in the current studies. Several studies have replicated this locomotion in their prototypes such as a novel soft machine table (Deng, Stommel & Xu, 2016) and other one developed at Auckland University of Technology (AUT) (Maratas, 2018). If Deng's prototype has been consisted of a soft upper surface and rigid, non-moving sidewalls. Whereas, Maratas's prototype achieves a more excellent working range by flexible sidewalls. The drawback of this fashion, however, is that the actuators bend unpredictably along their length. Additionally, operated by an open-loop control, the system does not sense the deformation of the actuators. In this study, these shortcomings are solved by integrating a sensor to measure the system state,

and by enhancing either the stability or the flexibility of the soft sidewalls by origami techniques.

The new soft XY-table proposed in this research study consists of an array of actuators, each of which is made by origami paper covered with a soft material. Origami folding paper technology from Japan has proved its ability related to high stiffness and broad elongation. Consequently, the soft origami actuator is capable of extending or contracting more widely along the vertical direction. This actuator hence not only expands its working range flexibly, but also creates a transformation on the top surface. Without rigid sidewalls, the proposed table is able to reduce the limitation of the movement amplitude on the top surface. Furthermore, an infrared sensor is embedded inside the actuator to control and monitor the robot's operation.

To validate the proposed methodology, several techniques have been applied with regards to constructing a system fashion, a pneumatic system, manufacturing of soft origami actuator, integrating the sensor, and calibrating the sensor as well. Working principle of the control system is based on inflating or deflating the air inside the actuator. It leads to an up and down movement of the actuator. A combination of these movements is to construct an object manipulation on top. A feedback signal from the sensor is necessary to monitor the operating state of the system. Our findings show that the working range of the new model is better than the previous one, and the sensors work correctly.

In conclusion, this study manages to develop an entirely soft XY-table created from soft origami actuators, the pneumatic system and the feedback controller. This table offers potential applications in industrial and medical fields to handle fragile objects. Because of the modularity of the system, the soft actuators can be easily assembled

in other designs apart from the table to meet the demands of further applications in healthcare, industrial automation, and food processing.

Contents

List of Tables

List of Figures

Attestation of Authorship

I hereby declare that this submission is my own work and that, to the best of my knowledge and belief, it contains no material previously published or written by another person nor material which to a substantial extent has been accepted for the qualification of any other degree or diploma of a university or other institution of higher learning.

Signature of student

Acknowledgements

First of all, I would like to acknowledge my primary supervisor Dr. Stommel, who has had to suffer most during the course of writing this thesis. Dr. Stommel has been the best possible supervisor I could have had, exhibiting extreme patience in allowing me to find my own way and express my own perspective. I could not have asked for better guidance and support. Dr. Stommel went way beyond the call of duty in the amount of time and effort he spent in giving me his reflections on both my research and my writing. I would particularly like to acknowledge Mr. Maratas who inspired me to investigate in this prototype of soft origami robotic table. I would like to thank AUT for the various ways in which it has supported me through this thesis.

Chapter 1

Introduction

1.1 Overview

In recent years, the term “Soft robotics” has gained numerous interest with different industrial and medical applications. The soft robot is generally defined as a robot which is either partly or entirely made from soft materials, especially the softness of the actuating components. There are many prototypes of soft robots which have been researched for applications in various fields. Some of these potential applications are proved to be applicable in industrial production lines for transporting fruits and gripping fragile goods. Medical applications, which support patients and the elder in their movement, are also considered as another potential field of soft robots. The shapes of soft robots are also very diverse, they can be like a starfish, a worm, a round shape, or a square shape. The transformation in shapes of soft robots is made by the driven force and characteristics of their materials to get adapted to the different surrounding environments. As a consequence, soft robots are entailed with far more flexible and adaptive abilities than the rigid robots which are generally manufactured by rigid linkages and discrete joints. The soft robots can, therefore, replicate the morphology and mechanical functions of animals in nature; for example, the elephant

(a) Partly soft gripper robot

(b) Entirely soft gripper robot

Figure 1.1: Examples of soft robot

trunk (J. Wilson, Li, Chen & George, 1993), starfish shape (Mao et al., 2014), caterpillar movements (Stommel, Xu, Lim & Kadmiry, 2014), and octopus arms (Kier & Stella, 2007). Nevertheless, soft robots cannot displace hard robots completely; they instead provide such new capabilities which cannot be found in rigid robots as movements with a high degree of freedom and safe contact in human-robot interaction.

1.2 Rationale

At present, the soft robot has been investigated to determine more and more feasible applications for human life. These robots can flexibly operate with their partially or completely soft body, as shown in Figure 1.1. Different studies have been implemented successfully and show that the advantages of soft materials for soft robots to adapt to diverse environments. However, it is still found to be challenging to handle the delicate work-pieces, to maintain the working safety when human and robots are in close contact, to expand the elongation range, and to monitor the state of the system.

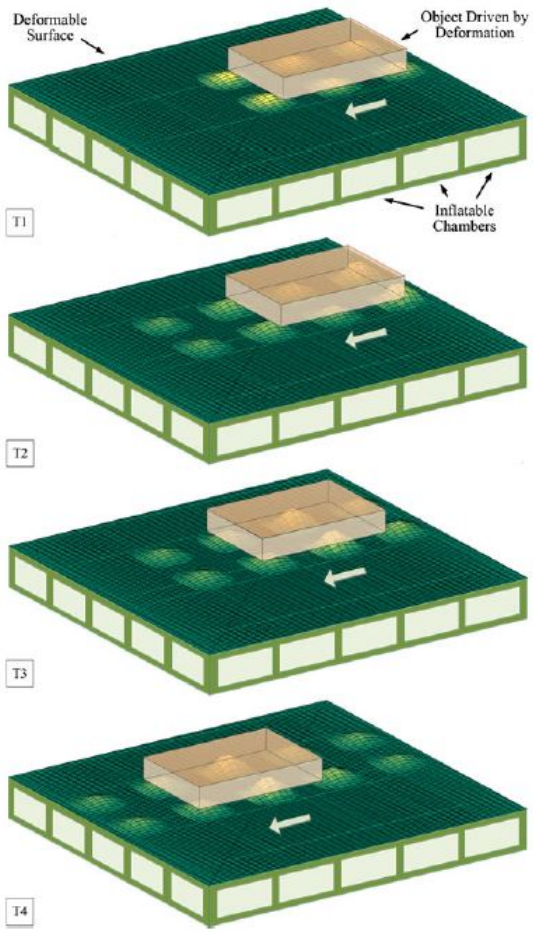

Figure 1.2: A novel soft machine table robot (Deng et al., 2016)

First of all, the rigid part that is used to construct the robots poses hazards when being in close contact with human or delicate work-pieces (Whitesides, 2018). Furthermore, it is challenging for robots to work simultaneously with multiple objects. A novel shape of soft robots called XY-soft table robot has been then developed by Deng et al. (2016), as shown in Figure 1.2, to improve the capability of manipulating objects. Inspired by the caterpillar's crawling gait, this table robot is able to create either translational movements or rotational movements on the top surface (Deng et al., 2016).

Secondly, this prototype of the table robot manipulates work-pieces by the deformation

of the top layer. The softness or deformation of the surface material influences significantly its extension and contraction range along the vertical direction. Thus, it is necessary to develop a prototype which is capable of operating in a broad range. Maratas's design (2018) proposed a wider working range of the table's deformation with origami actuators, but this deformation is derived from an open-loop control algorithm with fixed time steps. The system, therefore, cannot sense the manipulation of actuators to send out suitable control signal which corresponds to changes during the operating process.

Several studies have been conducted to apply the closed-loop controller. Computer vision and the sensor are adopted to measure the deformation on top (Hashem et al., 2016). Nevertheless, the drawback lies in the object's dimension. The external camera cannot detect the deformation beneath the object because the object blinds this deformation. Another solution has been proposed with an ultrasound sensor being located at the end of the extensor actuator (Al-Ibadi, Nefti-Meziani & Davis, 2018) to measure its elongation. This sensor, however, only performs properly with a rigid reflecting plane. When being applied in a completely soft design, most of the reflecting energy is absorbed; thus, this measurement result is no longer accurate. To handle this issue, several studies have managed to develop theory and experimental prototype of the closed-loop controller for the soft robot.

To work out solutions to the above-mentioned challenges, this study proposes a practical model which manages to solve these drawbacks with more proper technical solutions. In particular, this research proposes an entirely soft XY-table that consists of soft origami actuators, a pneumatic system, and a feedback controller. The origami actuator can bring about a better working range, which means that the magnitude of deformation on the top layer is wider. A sinusoidal wave which is created and

represents the deformation is also shown to be smoother and more powerful. In addition, a proximity sensor is embedded into the soft origami actuator to measure the elongation of each actuator without any obstacles. Consequently, working states of the system are monitored properly, and there are better adaptive responses to the changes.

1.3 Objectives and Scope

The overarching goals of the thesis are to present (1) the fundamental structures of soft robotic XY-table which is able to manipulate the objects by translating and rotating within a broad elongation range along the vertical direction, and (2) the closed-loop controller based on a feedback signal from the sensor to monitor the operation states of the system. The proposed prototype consists of three major components including a soft origami actuator, a pneumatic system, and a feedback controller. These components not only provide more flexible applications but also higher possibilities to improve the system's performance. In depth, the study proposes a novel prototype with very high practicality and manages to present significant contributions to the field as follows:

- A soft origami with a broad range of extension and contraction.
- A solution to integrate sensor to monitor operating states of the system.
- A design of soft origami actuators with the high level of stability and tightness, and easy maintenance of its components.
- A feedback signal controller to enhance the performance of the system.

This leads to the following research questions (RQs):

RQ 1: How can a sensor embedded inside the soft origami actuator operate properly?

RQ 2: How can a soft origami actuator operate to create the translational and rotational

locomotion?

RQ 3: How can the prototype be controlled by a closed-loop controller?

1.4 Thesis structure

A brief overview of the remaining chapters is provided here:
A wide ranging background review of soft robotics is provided to help set the context for the research and depict the relevant information about the soft table robot in **Chapter 2**.

Chapter 3 then presents several conceptual models of the current research and its parts.

Chapter 4 describes several designs of the prototype and how to fabricate them.

Chapter 5 introduces actual experiments to test the operation of the system and validate the results.

Chapter 6 begins with a review of the main findings of all experiments conducted in the research before comparing these findings with those from other studies reported in the literature.

Chapter 7 gives an overview of what the thesis has achieved and a brief summary of the method. It then summarizes the implications and limitations with reference to the research questions posed in chapter one. Finally, areas of further research are sketched out.

Chapter 2

Literature Review

Recently, soft robotics is emerging as an exciting field. Its applications are able to apply to many aspects of life. It is considered the solution to major drawbacks of conventional robots with regard to the safety in close contact, the diversity in shape, and movement methods. Meanwhile, the classical robot is made from rigid materials and in fixed shapes, the soft robot is constructed from soft materials with high capability of changing its shapes to suit different operating environments. Therefore, the soft robot has such benefits as handling delicate objects properly, quickly adapting to changes in the working environment without any refurbishments. As a result, a large number of research studies have been conducted to propose and investigate the reliability of soft robots, one of which is a soft table robot. The soft table robot is investigated to deliver delicate objects in the industrial production lines. This table transports the objects based on the deformation of its top surface. However, these prototypes are still under the developmental stage due to the absence of a closed-loop control algorithm and a feasible design. Thanks to the development of materials and sensor technology, these issues are now possibly solved. This chapter begins with a brief look at table robot with its definition and then provides detailed information about its classification and principal components.

2.1 Definition of soft robot

To provide a precise interpretation of the “soft robotic” term, some definitions have been presented. Chen et al. (2017) define soft robotics as a field investigating how to make use of the soft materials to build up a robot which can provide a required level of softness to both its own environment and its receiver. Based on this definition, the researchers who investigate in the specific branch of soft robotics also present their definitions of the soft table robot. It is defined as a soft XY machine table which is capable of manipulating objects not only in translational direction but also rotational direction on the surface (Deng et al., 2016). However, this definition has not presented insights into how movements are made.

A complete and detailed definition of the soft table robot is necessary to understand about this research and support to future work as well. In this study, the soft table is defined as a robot which has the top surface made from a soft material and is capable of manipulating an object in both translational and rotational movement through deformation of its surface. This soft table robot is called "The Tabbot" in this current research.

2.2 Types of soft robots

Thanks to the properties of soft materials, the soft robots are designed in diverse shapes to adapt to various functional features. From these identical shapes or functions, soft robots can be subdivided into three categories including walking robots, grippers, and soft tables.

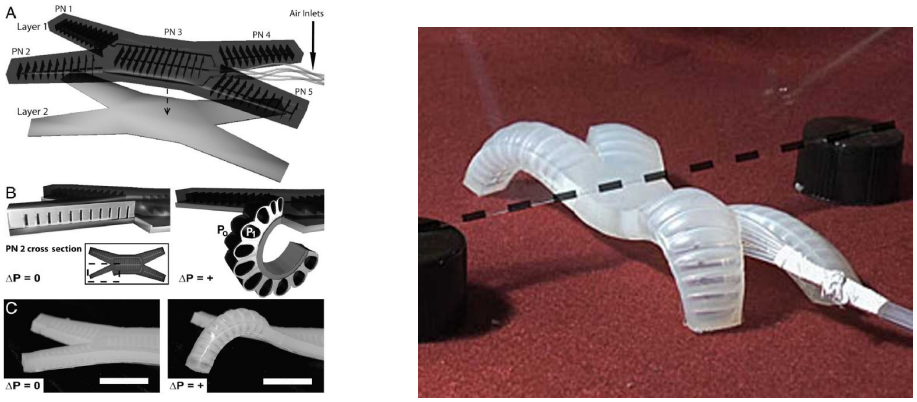

(a) Schematic representation (b) Operating to pass through an obstacle

Figure 2.1: Tettrapod (Shepherd et al., 2011)

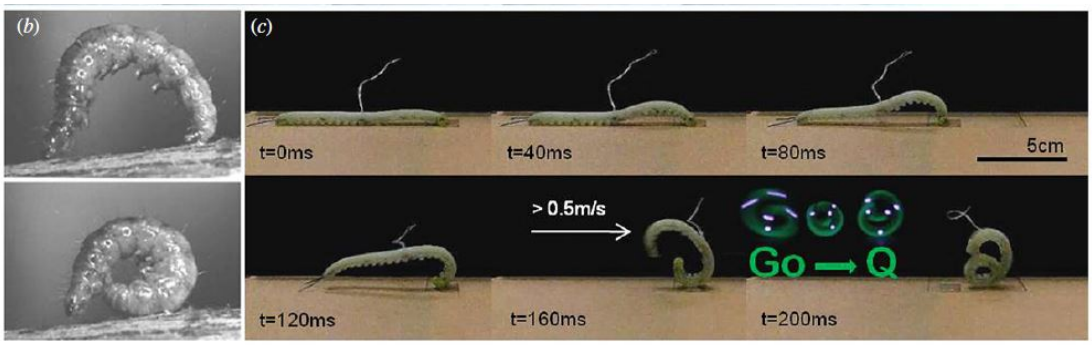

Figure 2.2: GoQBot (Lin et al., 2011)

2.2.1 Walking robots

Shepherd et al. (2011) presented a walking robot, named Quadrupedal, as shown in Figure 2.1. This robot is able to generate locomotion relied on five pneumatic actuators which are the representative for two front legs, two rear legs, and one body. A unique combination of these actuators makes them flexible to lomocate and easy to pass through an obstacle, as shown in Figure 2.1b.

Another prototype of walking robots, called the “GoQBot" was proposed (Lin et al., 2011). It is inspired by the caterpillar rolling to produce its movement, as shown in Figure 2.2. Beside the normal crawling gait, this robot is capable of curling up to speed

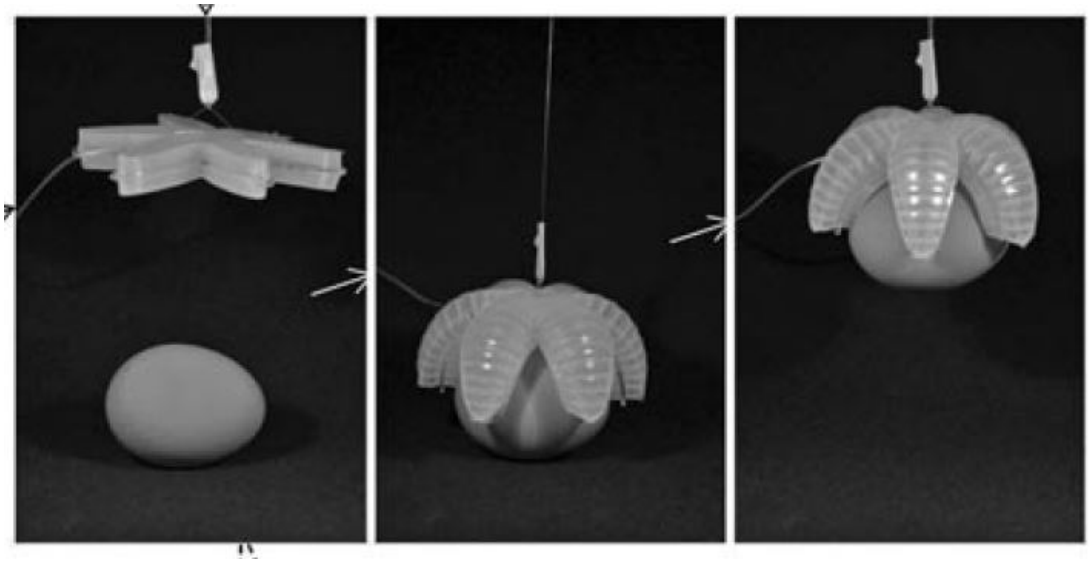

Figure 2.3: Soft gripper robot (Laschi et al., 2012)

up.

However, the sensor has not been adopted in both of these robots. Their movement is controlled by human or fixed time steps. The deformation ability of the robot mostly depends on the deformation of soft material behaviour.

2.2.2 Gripper robots

The gripper robot or hand robot is inspired by starfish or octopus robots (Laschi et al., 2012). It uses its "fingers" to grab and lift up the object, as shown in Figure 2.3. When these fingers are inflated with air, they curl to fit the object and lift it up (Ilievski, Mazzeo, Shepherd, Chen & Whitesides, 2011). Inversely, when the pressure in these fingers is decompressed, they get back to the rest position and release the object.

In this type of gripper robots, no sensor is adopted in the operating process. They are mostly controlled manually like the walking robots.

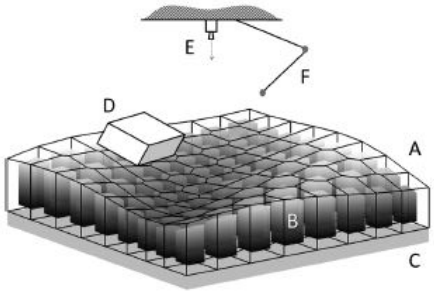

(a) Peristaltic table (Stommel & Xu, 2015)

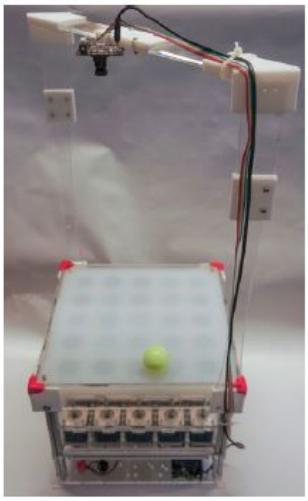

(b) Hybrid soft table (Hashem et al., 2016)

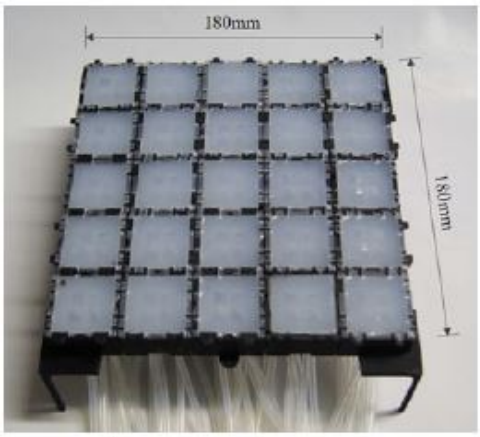

(c) Soft machine table (Deng et al., 2016)

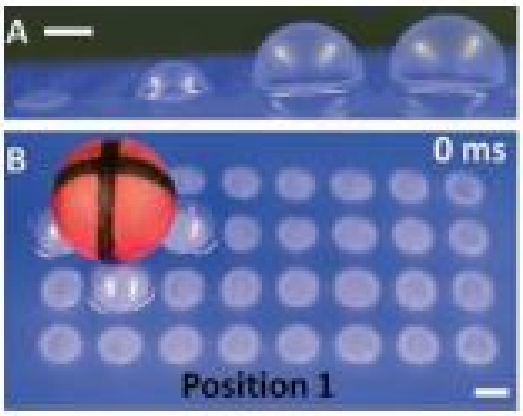

(d) Braille design (Mosadegh et al., 2014)

Figure 2.4: Examples of soft machine table

2.2.3 Soft table robots

The soft table robots can be categorized into rigid actuators, hybrid actuators, and soft actuators. These actuators exert a deformation on top to move the object. To guarantee the continuous manipulation and safe interaction when working with the delicate work-pieces, several prototypes of the XY-soft table robot have been proposed; for instance, a peristaltic sorting table, a hybrid soft bodied XY peristaltic table, and a soft machine table in Figure 2.4. The Braille design adopts the deformation of the air chamber to move the objects. These air chambers around the object are controlled

to guide the movement (Mosadegh et al., 2014). However, this prototype just works properly with the round objects. Deng et al. (2016) and Hashem et al. (2016) replicate the caterpillar's crawling gait to manipulate the objects. The efficiency and quality of the table robots have been improved when this table is capable of manipulating flat objects in both translational and rotational movements. On the other hand, Hashem et al. (2016) design generates movements by rigid rods underneath the top surface. It causes damages to the delicate objects. Additionally, most of the tables have fixed side-wall in between the actuators. The deformation only occurs on the top surface. Thus, an overarching challenge of these tables is the limitation of the deformations on top. It depends on the expandable feature of the soft materials. These deformations are quite small, thus resulting in the restrictions of moving objects. Finally, these soft tables are controlled by an open-loop controller. Several previous studies has adopted an external camera to get feedback signal (Stommel & Xu, 2015). They, nevertheless, faces a challenge from the object itself when these cameras cannot detect any deformation beneath this object.

To deal with the limitation of elongation of the sidewall, Maratas (2018) proposed his design which is constructed by an origami actuator, as shown in Figure 2.5. This prototype has improved the elongation of the table thanks to the characteristics of the origami structure. It can extend and contract in a wider range (L. Wilson et al., 2013). However, origami actuators in Maratas's (2018) design are not homogeneous. They bend unpredictably in any direction. It is challenging in the control process when these actuators' height is not detected properly. Moreover, his prototype is still controlled by the open-loop controller. A sensor has not been adopted in this prototype yet.

From these drawbacks mentioned above, inspired by underlying theories and experimental prototypes, this study proposes a new prototype of the soft table robot

Figure 2.5: First prototype of the origami table robot (Maratas, 2018)

which is able to expand the deformation range of the top surface and create the feedback signal through a sensor. It is also useful to improve the quality and efficiency of the soft table and able to bring this table closely to practical applications in the industry and life.

2.3 Soft actuators

In general, an actuator is a significant part of a robot. The actuator converses energy from a power generator to a desired mechanical power (Chen et al., 2017). With regards to the material behaviours and functions of the actuators, actuators are categorized into different groups. Within the scope of this study, the soft actuator is the main focus to construct the soft table robot.

2.3.1 Types of soft actuators

The soft actuator can be defined as a device that is made of soft materials and capable of transforming energy from the generator to manipulate other devices (Whitesides, 2018). The soft actuator is one of the main components to make the soft robot. To adapt to various movements, several existing prototypes of the actuators have been developed such as:

- Dielectric elastomeric actuator (DEA): it adopts high voltages to exert an electrostatic force and actuation (O'Halloran, O'malley & McHugh, 2008). Furthermore, it requires a rigid stage to support the elastomer. Therefore, it does not suit the soft robot, and it is not safe, either.

- Shape memory alloys (SMA) actuators (Kim et al., 2009): it bases on an alloy behavior to create a shape of the actuator. However, this actuator is influenced dramatically by heat (Zhakypov, Huang & Paik, 2016).

- Piezoelectric actuators (Adriaens, De Koning & Banning, 2000): it uses the electric field to change the geometry (Chee, Tong & Steven, 1998). It, therefore, leads to their dependence on the polarization of the dielectric materials which are used to make the actuators.

- Electro-active polymer actuators (Benslimane, Kiil & Tryson, 2010).

- Pneumatic/hydraulic actuators (Bihlmaier, 1982): it uses air or fluid to make movements. This actuator is clean and safe, and it is suitable to be applied to the soft robots.

- Soft origami actuators inspired by Kresling model (L. Wilson et al., 2013): it bases on the pneumatic actuator. An origami structure, however, has been applied with its support structure to increase its stiffness and moving flexibility. It is the

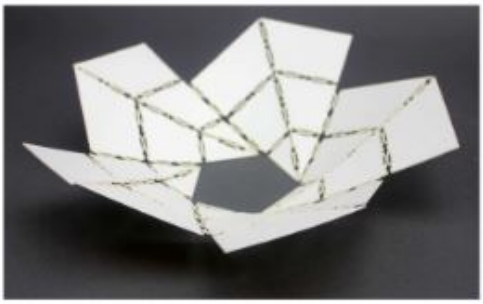

(a) Aerospace application - Parabolic antenna (Morgan et al., 2016)

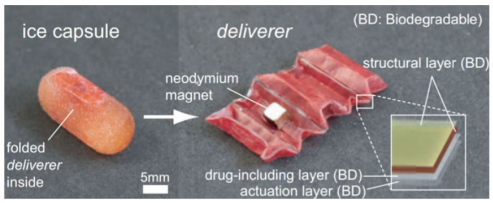

(b) Medical application - Capsuled gastrointestinal microsurgery (Johnson et al., 2017)

(c) Packaging application - Container (Dai & Caldwell, 2010)

(d) Architecture application - Building structure (Tachi, 2010)

Figure 2.6: Examples of origami applications

first time when the origami structure is applied successfully in Maratas's soft table (2018). Nevertheless, there are still drawbacks in the manufacturing process to acquire the homogeneity among the samples, stiffness, and air tightness of the actuator.

To fill the gaps in the literature, this research adopts Kresling's folding pattern and ecoflex00-30 silicone to construct the soft origami actuator and the soft origami table robot.

2.3.2 Soft origami actuator

The origami soft actuator is constructed by the origami paper and ecoflex00-30 silicone. The origami paper acts as the support structure of the actuator. This structure is to shape the actuator. Ecoflex00-30 is coated on both internal and external sides of this origami

structure so that the actuator can be softer and stronger. Maratas (2018) presented the first prototype of the origami actuator, which is used to construct a soft table robot, relying on these advantages of this origami structure.

The origami term is to describe the Japanese art of folding paper. From a flat sheet, it is able to build up various 3-D shapes with high strain and stability (Tachi, 2010). It is increasingly being applied in the engineering designs in various fields. Thanks to its advantages such as lightweight and high strain performance up to 900% (Whitesides, 2018), this technique has been applied in such a variety of mechanical engineering fields as the aerospace applications (Morgan et al., 2016), biomedical applications (Johnson et al., 2017), packaging applications (Dai & Caldwell, 2010), and architectural applications (Tachi, 2010), as shown in Figure 2.6.

Inspired by the origami sunshield for space telescopes (L. Wilson et al., 2013) and Maratas's (2018) design, this study proposes a prototype of the soft origami actuator with high softness, moving flexibility, and easy manufacturing to solve the existing drawbacks raised in the previous research.

2.4 Pneumatic system

In general, several soft robots including the soft gripper, walking soft robots often use a pneumatic network (Pneunets) (Whitesides, 2018). These robots are normally small in size, and the deformation of their actuators is different along their length. These actuators are constructed by a number of small air-chambers, as shown in Figure 2.1 & 2.2. The structure and deformation of each actuator determine the shape of the robot and its movement. It is difficult to apply the Pneunets to the soft table robot because the actuators of table robot operate independently and only deform along the vertical

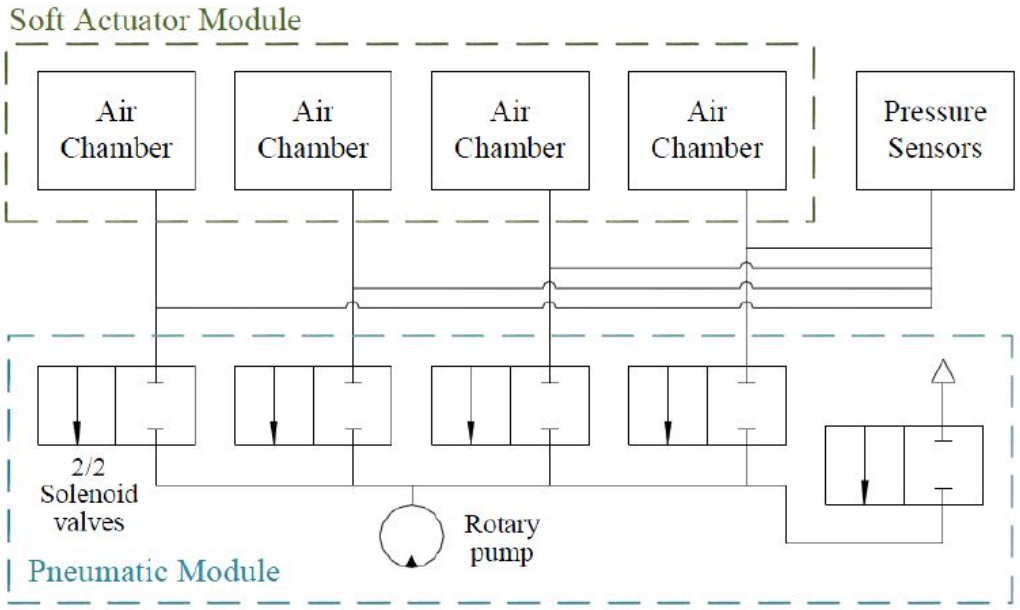

Figure 2.7: Schematic of pneumatic system proposed by Deng (2016)

direction.

The pneumatic system is beneficial in exerting a high force and is not affected by temperature. It also uses clean energy and is easy to be maintained (Kim, Laschi & Trimmer, 2013). Thus, the pneumatic system is suitable to be applied to the table's actuators to manipulate work-pieces (Deng et al., 2016), as shown in Figure 2.7. This design uses one air pump to inflate air into each air-chamber through corresponding 2/2 solenoid valve. In the deflating process, an exhausting valve is set on, and the air inside the air-chamber is evacuated outside by the atmosphere difference between inside air-chamber and the environment. This actuator returns its rest position when the air goes out completely. This system is restricted in the downward movement because there is no vacuum force to make the actuator go downward, thus leading to limitations in the elongation range of the actuator.

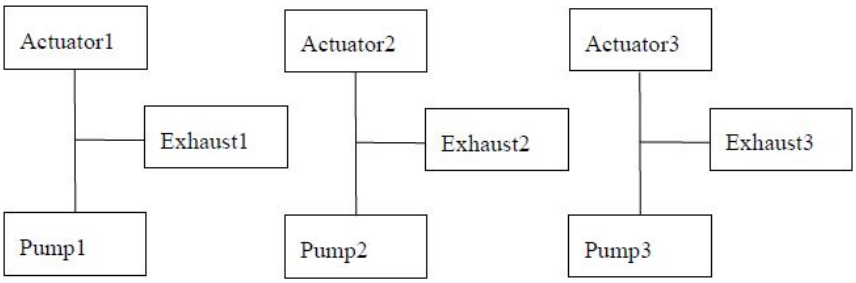

Figure 2.8: Schematic of pneumatic system of Maratas (2018)

In another research, Maratas (2018) has presented a schematic of the implemented pneumatic system, as shown in Figure 2.8. This system just adopted one air pump for pressurizing the air and one 2/2-way solenoid valve for deflating the air. This principle faces a challenge when deflating the air outside. It is impossible to control this deflating process because the air that is deflated outside naturally depends on the difference between the inside and outside pressure of the actuator. Especially, when there is an object on top of the table, the object's weight produces a force that makes the actuator move downward unpredictably and uncontrollably.

Inspired by a double-acting cylinder's operation (Thomas, Maul & Jayawiyanto, 2005), as shown in Figure 2.9, the cylinder is replaced by the soft origami actuator, and the exhaust valve (2/2-way solenoid valve) is removed. The pneumatic system in this study is maximized with one air pump and two 3/2-way solenoid valves to create upward movements and downward movements through the pressure and vacuum process respectively.

2.5 Proximity sensor

Technically, many different methods are proposed to measure deformation on the top surface of the robot by using an internal or external sensor. With the external sensor,

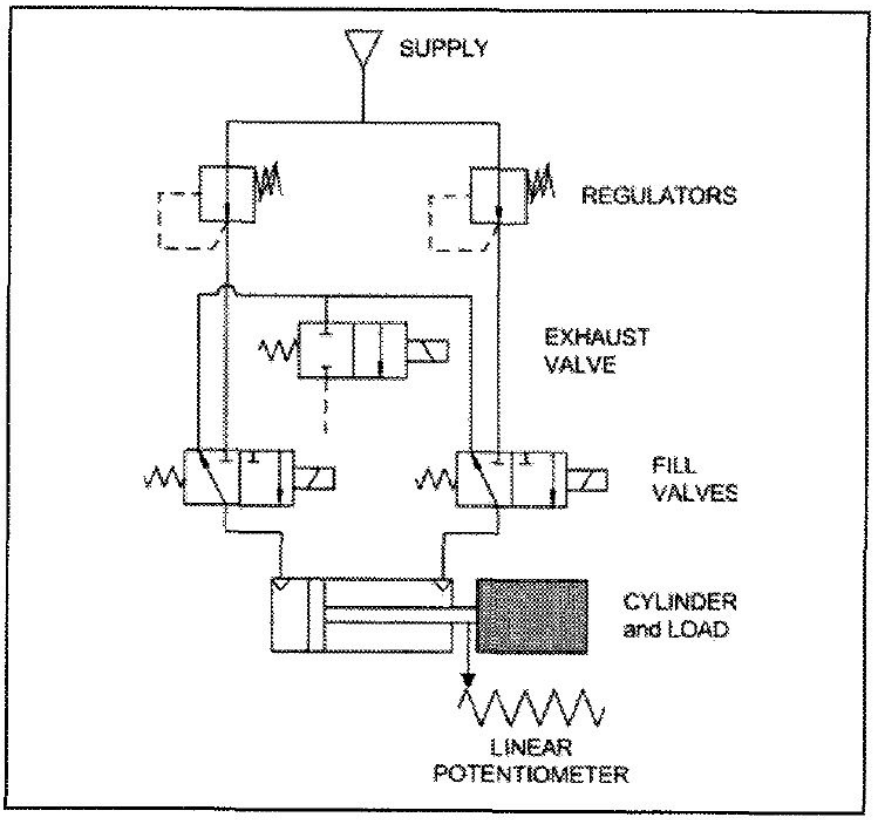

Figure 2.9: Schematic of pneumatic system of Thomas (2005)

a major challenge of detecting the deformation is that it is blinded by the working object itself. It is therefore not capable of detecting the deformation beneath this object. Meanwhile it is easier to detect the deformation with the use internal sensor that is planted directly into the object. It is able to avoid disturbances caused by any obstacle.

2.5.1 Types of proximity sensors

A proximity sensor is a sensor which is capable of detecting the present or appropriate location of an object without any contact (Johnston, 1977). Based on the principle of the sensors, they are subdivided into classes including (Benniu, Junqian, Kaihong & Zhixiang, 2007):

- Inductive sensor: uses the magnetic field to detect an object. It only applies to

detect metallic objects.

- Capacitive sensor: based on changing capacitance between two electrodes. It is not suitable for small objects.
- Optical sensor: uses a special kind of light, such as laser and infrared light to detect the objects. However, the laser sensor has a narrow detecting area.
- Ultrasound sensor: based on the reflection of an ultrasound. It is easy to be disturbed by the resonance of reflected sounds.

2.5.2 Infrared sensors

The purpose of this study is to integrate the sensor inside the soft actuator. An infrared (IR) sensor is considered as the most suitable because it has small dimensions, wider sensing range, fewer disturbances and more proper working with the soft materials. Thien et al. (2016) proposed an infrared sensor, named APDS-9960, to detect the elongation of an actuator. A major function of this sensor is gesture detection. Hence, a sensor which is specialized on detecting the distance is in need. Furthermore, this research just presented an experimental model. It, however, revealed that the infrared sensor was capable of working properly under the soft actuator with a white reflecting plate.

An IR proximity sensor specialized for distance measurement that is adopted is called VCNL4010. This sensor is able to measure the height within 200mm (DiCola, n.d.). However, the height of this sensor is measured in the raw unit, and there is not any general equation to directly converse from the raw unit to the height unit. The dependency of this conversion is non-linear, so it is necessary to investigate this sensor and determine the sensor's regression function.

2.5.3 Colour effect on IR sensor performance

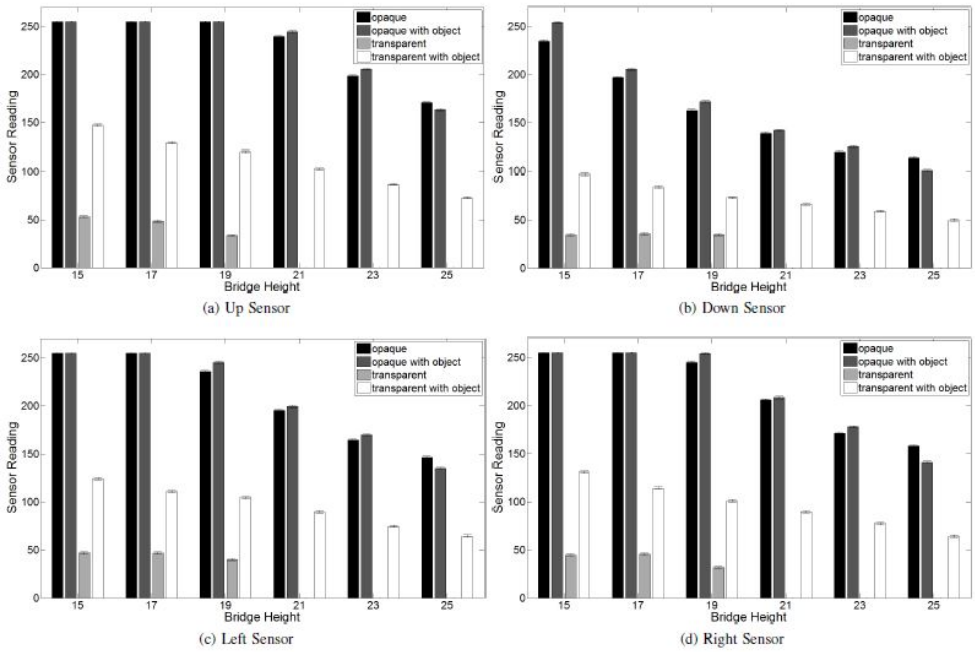

Figure 2.10: Colour effect on reflection of IR sensor (Thien et al., 2016)

One of the important factors that affect the sensor performance is the colour of the reflected plane. The previous studies reveal that the sensor performs the best with the reflected plane being coloured in white (Mollah, n.d.; Thien et al., 2016), as shown in Figure 2.10. However, the colour of the sidewall has not been considered in these studies yet. The method to embed the sensor inside the actuator has not been described thoroughly since their research just presents the principle and experimental model without any actual prototype.

This study, hence, proposes a complete prototype of a soft actuator which is integrated with the infrared sensor. In addition, the sidewall's colour is investigated to present the best working condition of the sensor. Consequently, the elongation of the

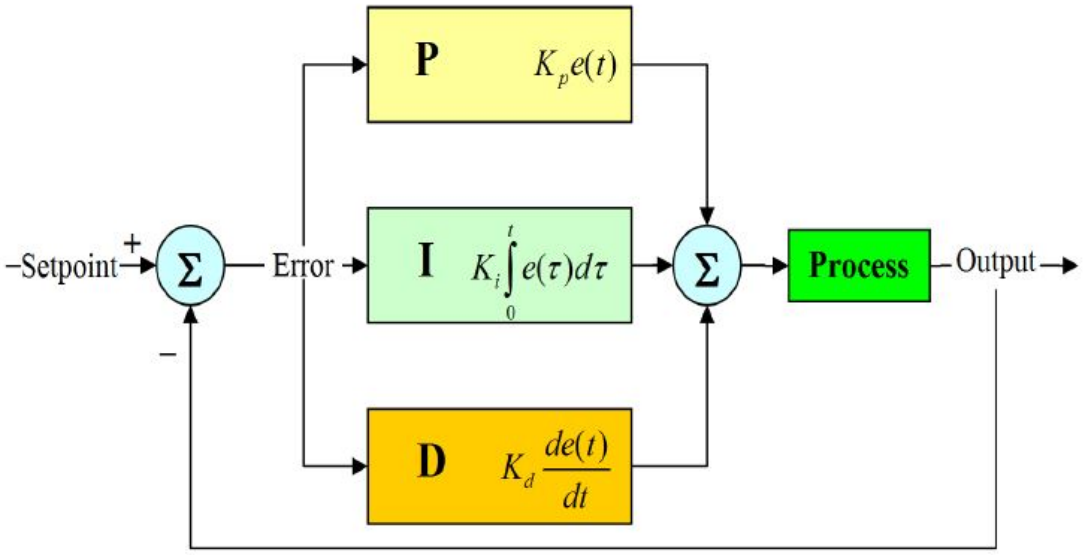

Figure 2.11: General concept of PID controller

actuator is able to be measured properly prior to getting back to the micro-controller. It is useful to construct a closed-loop controller which has not been employed in the working process of the current soft robotic table.

2.6 PID controller

A PID controller is a control loop feedback mechanism. The PID controller uses three components including proportional, integral, and derivative terms to control the performance of an object, as shown in Figure 2.11. This PID controller calculates an error which is defined by the difference between the set point value and the process value (Araki, 2009; Oguntoyinbo et al., 2009). Depending on the magnitude of the error, this controller sends out the appropriate control signal so that the object can reach the set point value in the shortest time period.

2.6.1 Types of PID controller

Based on the principle of signal processing, the PID controller is classified into two types: continuous-time PID controller and discrete-time PID controller (Mohamed, Abdalaziz, Ahmed & Ahmed, 2017).

- Continuous-time PID controller works based on analog signal in time domain (MathWorks, n.d.).
- Discrete-time PID controller works based on digital signal in Z domain (MathWorks, n.d.).

2.6.2 Finding PID gains

It is challenging to find out the best suitable gains of the PID controller. Ogata and Yang (2010) proposed several methods to find the PID gains related to fuzzy logic and neural networks. Adopting a micro-controller to find PID gains is also investigated by Fadali and Visioli (2013). This process requires a large amount of time to determine the gains of PID controller. Hence, this research chooses to implement a built-in tool in Matlab software to simplify the finding process.

2.7 Movement control

To manipulate the objects on the soft table robot's surface, many researchers have investigated various methods of the movement control by replicating the caterpillar's crawling gait to create the sinusoidal wave of the surface deformation.

2.7.1 Replication of caterpillar's crawling gait

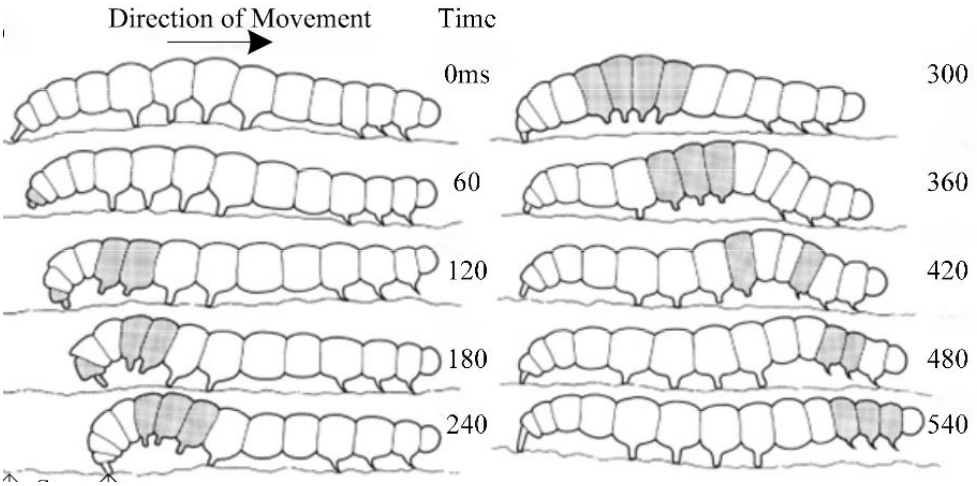

Figure 2.12: Operating of proleg

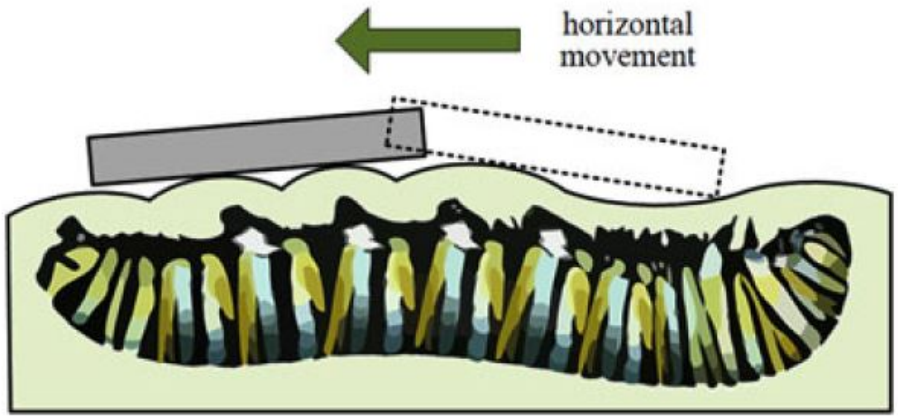

Figure 2.13: Inverted locomotion concept (Deng et al., 2016)

The locomotion of caterpillar has been investigated with more focus on the benefits of its easy manufacturing and simple operation. Deng et al. (2016) proposed a soft table robot which mimics the caterpillar's crawling gait to produce manipulation. Deng's research investigated the principle of rear legs (prolegs) to make the caterpillar movement, and then applied this principle to create this soft table robot. Theoretically, the proleg is

lifted up and swung ahead to create movement. Depending on the moving velocity, the adjacent proleg is also lifted up and swung forward but in a delayed period of time, as shown in Figure 2.12. This process is repeated and propagated among different prolegs to create the caterpillar movement. This principle is proved to be suitable to create the movement on the top surface of the table by swapping the role of the ground and the caterpiller (Deng et al., 2016). To be specific, the prolegs still make a move; however, the moving object is the ground, and the static object is the caterpillar, as shown in Figure 2.13. In each typical operating cycle of the proleg, these legs are lifted up and down simultaneously. Thus the ground, but not the caterpillar, is translated by a specific distance.

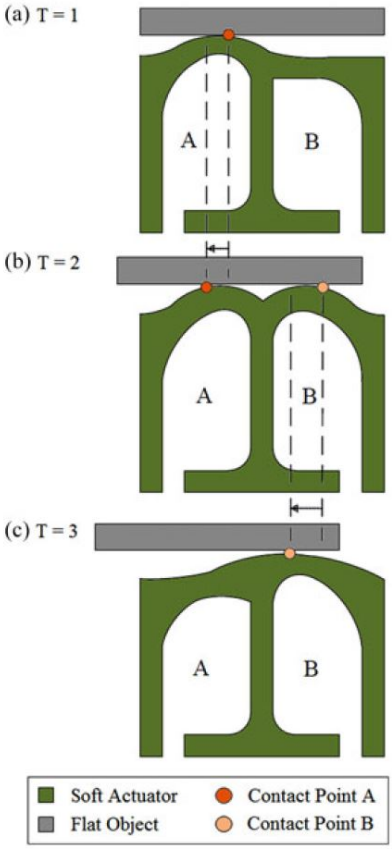

Figure 2.14: Movement concept (Deng et al., 2016)

To create the translational movement on top, two air chambers in one actuator are tested, as shown in Figure 2.14. Initially, two air chambers are inflated with air to create the numerous contact points between the object and the actuator, and the object is lifted up by the movement of these contact points. When chamber A is deflated, and the air in chamber B is kept stable, a new contact point between the object and chamber B is created. This process is similar to operation of the prolegs. As a result, the object moves from chamber B to chamber A.

To generate rotational movement on top, it requires four air chambers of one actuator to work together. With regards to the clockwise rotation, two upper air chambers create a translational movement from left to right, while two lower air chambers create an opposite movement from right to left. Two opposite moving patterns play the role of a pair of torques that is applied to the object to create its rotational movement. Meanwhile, counter-clockwise rotation is produced with the same method but in the opposite direction.

However, Deng et al.'s prototype (2016) has the rigid sidewalls in between actuators. Each actuator consists of four air chambers with the soft sidewall in between the air chambers. With the rigid sidewalls, there is no interaction among actuators, and the horizontal movement of the object merely depends on the deformation of the air chambers' surface in each actuator. Consequently, the movement of the object is small, and this prototype only lifts the object up to 4mm height. The average horizontal speed is approximately 30mm/min, and the average rotational speed is 1 degree/second.

2.7.2 Sinusoidal wave of surface deformation

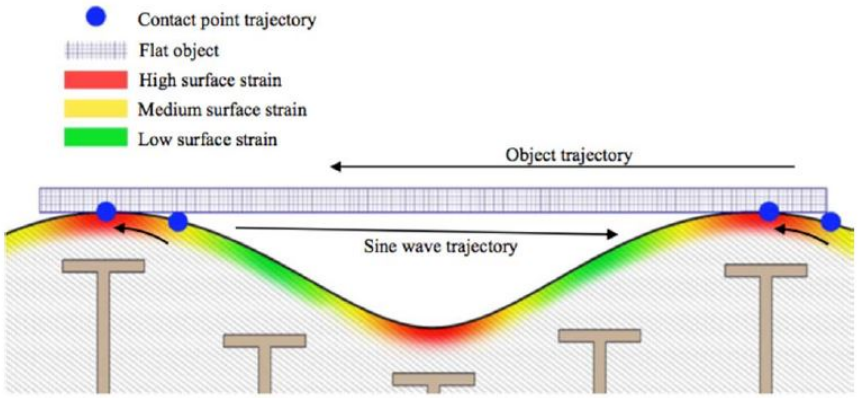

Figure 2.15: Deformation on top with a typical sinusoidal wave (Hashem et al., 2016)

To create a sinusoidal wave of the table's surface deformation, Hashem et al. (2016) controls the upward and downward movement of each actuator by a discrete sinusoidal wave, as shown in Figure 2.15. The sampling period in the research of Hashem et al. (2016) is equal to the number of the actuators. When the actuator contacts the object, a contact point is created. This contact point is moved by the translation of the sine wave. However, the rotational movement is not mentioned in his research. Besides, there are still rigid sidewalls in between the actuators, so there is no interaction between actuators. Fixed points on the rigid sidewall prevent the movement of the table's surface.

Inspired by the sinusoidal wave and the caterpillar's crawling gait, this research proposes a movement method of the top surface. The caterpillar's crawling gait is to rotate the object, while the sinusoidal wave is to make the object slide on this wave's gradient. By adopting soft actuators without rigid sidewalls, fixed points are completely removed, thus creating smooth movement of the table's surface. The proposed movement method that is named Tabbot wave by the researcher is capable of propagating movements on top to produce either the translational movement or the rotational movement.

Chapter 3

Theoretical modelling

The significant advantage of the soft robots is that they are capable of replicating completely the locomotion of some animals in nature and removing the limitation of the degree of freedoms (DOFs). Therefore, the soft robot is able to operate more flexibly and easily in diverse environments. Inspired by the caterpillar's crawling gait, Deng et al. (2016) presented a first prototype of the soft table robot which is able to manipulate objects on top. To further develop improvements of the first prototype, this research approach is to construct a fundamental soft table robot which is capable of manipulating the objects in both translating and rotating movement. In addition, the elongation ability of the table also needs to be improved to create a more powerful deformation. The deformation is, hence, helpful to handle either round objects or flat objects. Finally, this table is provided with a closed-loop controller through the sensor to monitor the operation states of the system properly. This chapter aims to present the underlying theories to model the Tabbot.

3.1 Soft origami table robot

Inspired by Deng et al.'s prototype (2016) and Maratas's prototype (2018), this study proposes a new prototype of the soft table being constructed to manipulate objects on top. This table consists of four main components including origami actuators, pneumatic system, feedback controller, and electrical system, as shown in Figure 3.1. These soft origami actuators are able to extend and contract in the vertical direction. The pneumatic system exerts a pressure and vacuum force to produce the extension and contraction movements respectively. The feedback controller is to measure and monitor the system state during the operating process. The electrical system is to supply power to electrical components including the air pump, solenoid valve, sensor, micro-controller, and others.

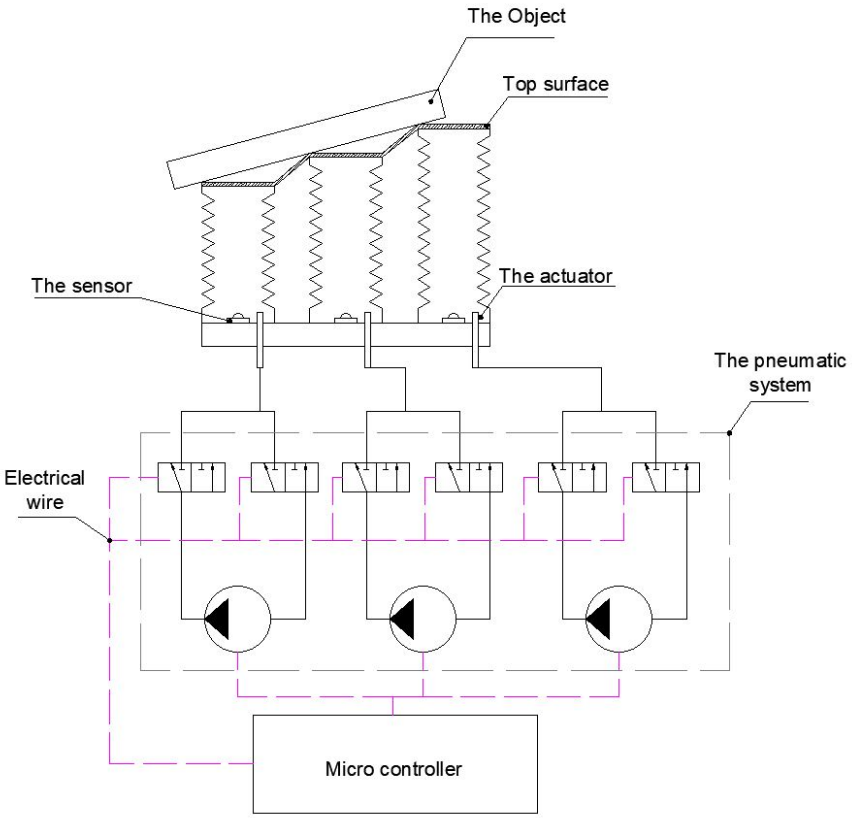

Figure 3.1: Schematic of table robot structure

The research approach is to propose a complete prototype of the soft table robot

with seven actuators that are arranged in the honey comb shape. This honey comb shape is simple to be scaled up to larger dimensions. The hexagonal shapes are arranged together like honey comb or square shape. In the honey comb shape, the gaps in between actuators that are the smallest and the most homogeneous, as shown in Figure 3.2. The proposed soft origami table robot, called Tabbot, is capable of elongating in both up and down directions. Each actuator is controlled by an air pump with two 3/2-way solenoid valves. The elongation process is sensed by an embedded sensor. These basic elements are combined together to construct the Tabbot. A micro-controller is adopted to monitor and control the operation states of the system.

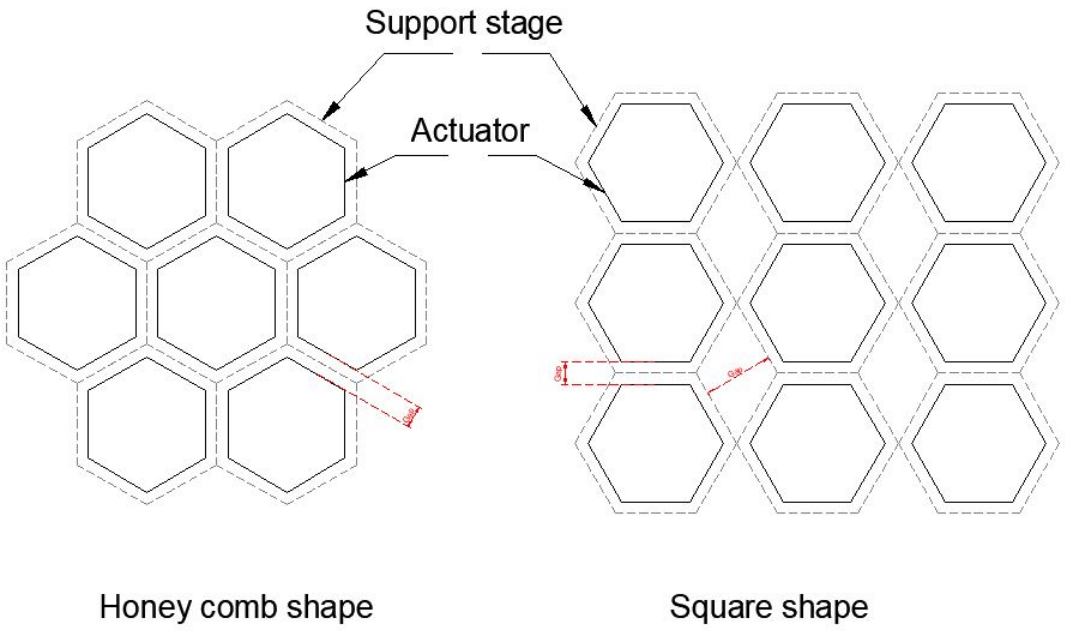

Figure 3.2: Actuator arrangement

3.2 Soft origami actuator

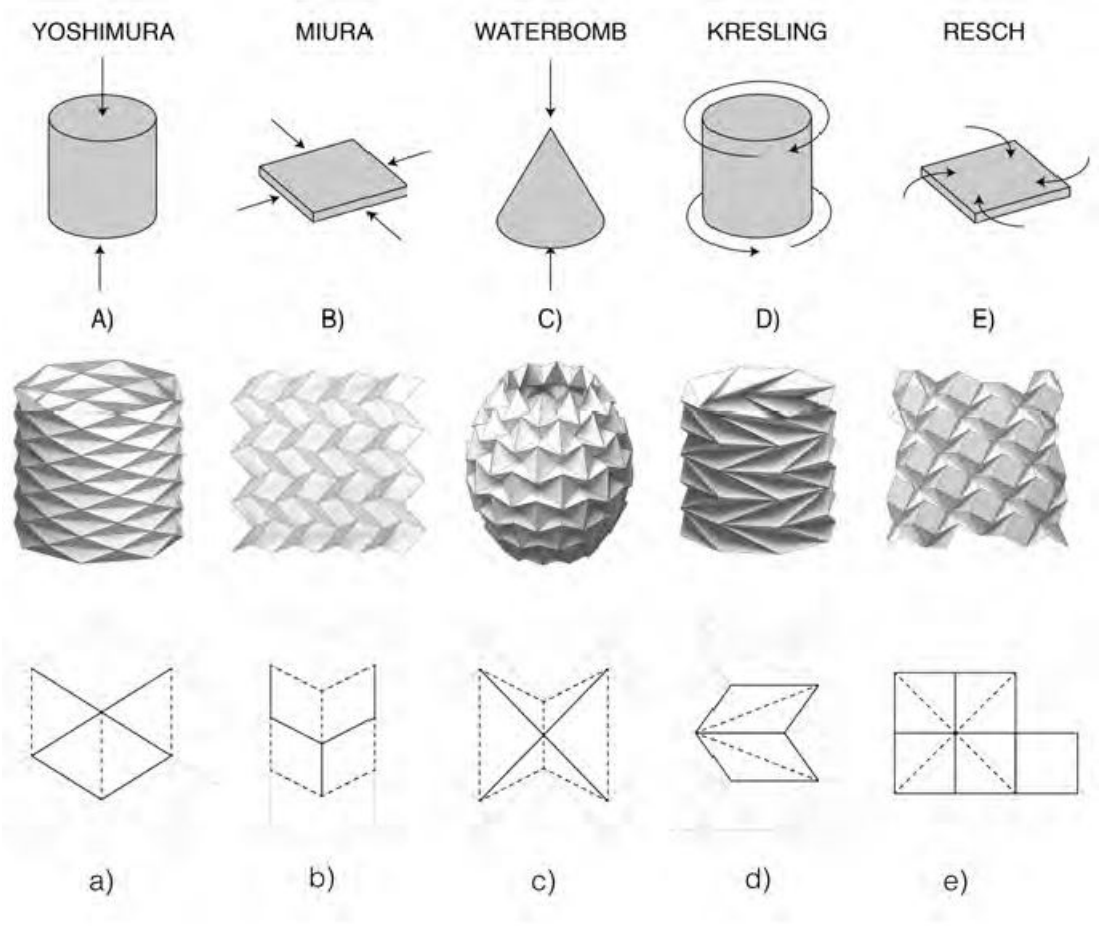

Figure 3.3: Natural Folding: Top: Illustration of Force + Matter. Middle: Expression of Folded Form. Bottom: crease patterns. a/A- Yoshimura, b/B- Miura, c/C- Waterbomb d/D- Kresling, e/E- Resch (Gardiner et al., 2018)

The actuator is considered an essential part of the robot. It affects how the robot operates and how the robot is controlled. Furthermore, it also affects the performance of the whole system. Several origami patterns, which are applied to the support structure of the actuator, have been investigated to determine the best performance; for instance, the waterbomb, Kresling, or Miura pattern, as shown in Figure 3.3.

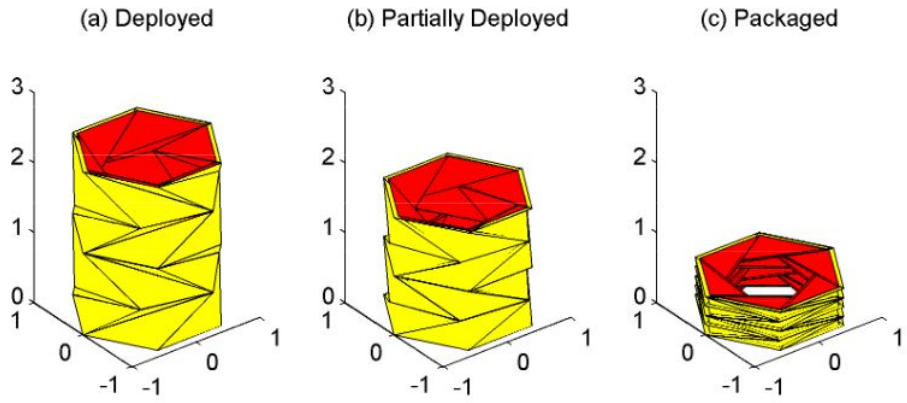

Figure 3.4: Kresling model in operating process (L. Wilson et al., 2013)

Origami engineering is derived from the Japanese paper-folding art. This engineering has proved its potential applications in numerous areas. From a flat sheet, a 3-D object is folded by specific origami patterns such as Yoshimura, Miura, Waterbomb, Kresling, or Resch. There are, however, some drawbacks displayed in these prototypes. For instance, Miura and Resch patterns create the rotational movement when elongating. Waterbomb pattern creates the deformation along the horizontal direction. Therefore, it is difficult to fabricate an origami actuator with these patterns to control the motions properly. Yoshimura and Kresling patterns are considered suitable with elongation, but Kresling pattern is finally chosen after it is improved with the hexagon pattern, as shown in Figure 3.4. The Kresling patterns has been presented with numerous advantages. First, it is easier to be fabricated, assembled together and arranged in a broader array. Adjacent levels are arranged oppositely to remove the rotational movement of the actuator when elongating. The movement of the actuator is merely linear along the vertical direction.

Finally, the Kresling pattern is seen as a suitable design for the cylinder actuator which is adopted in this study. The origami actuator is capable of contracting or

extending along the vertical axis of the actuator without any singular deformation in other directions before it reaches the minimum or maximum elongation. This pattern is applied to the soft origami actuator which is able to meet operating requirements of the system in terms of the stiffness, air tightness, and easy maintenance. The soft origami actuator is constructed with a broad elongation, ease of attaching a sensor, and possibility of building up a larger scale table.

3.3 Pneumatic system

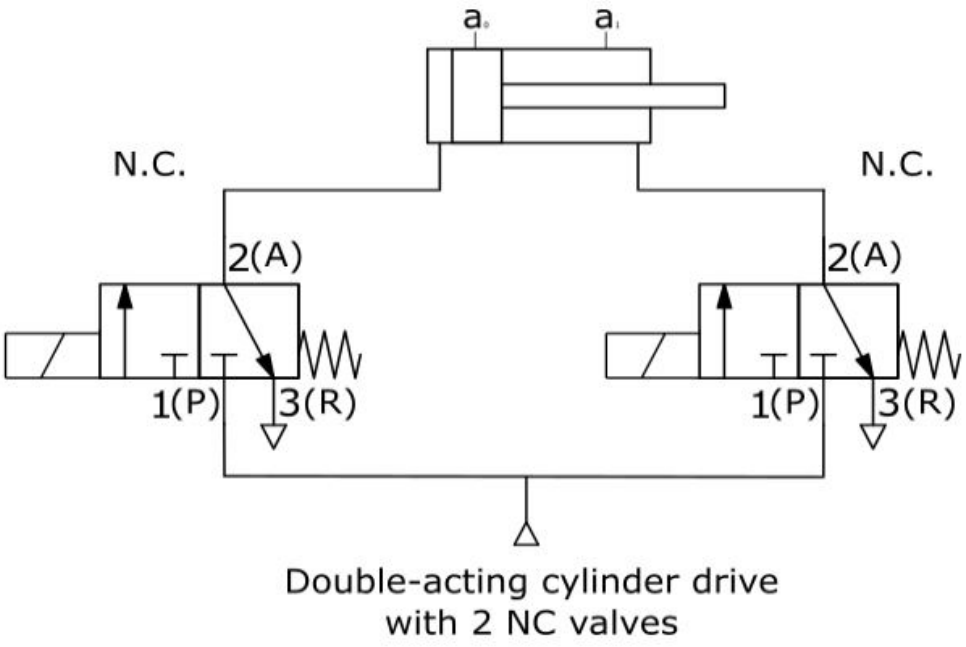

Figure 3.5: Schematic of pneumatic system applied to the cylinder (Van Varseveld & Bone, 1997)

With the features of easy maintenance and cleanliness, the pneumatic system is more suitable for the applications that are required to be lightweight and cost-effective. It is applied widely in both manipulating robots and gripper robots. This study is inspired by Van Varseveld and Bone's principle (1997). Their proposed principle is implemented

to control a double-acting cylinder driven by On/Off solenoid valves, as shown in Figure 3.5. Firstly, a left hand side valve is on, and a right hand side valve is off. At the time, the right air chamber is connected to the environment outside via the right valve. An air pump is used to inflate air to the left chamber through the left-hand side valve. The pressure in the left chamber rises and forces the stroke to move. Consequently, the air in the right chamber is compressed out through the right valve, and a stroke moves to the right side. Inversely, when the right valve is set on, and the left one is set off, the air is pumped into the right chamber. At the time, the left chamber is connected to the environment via the left valve. Following the same way, the air in the left chamber is compressed out via the left valve. It leads the stroke to return to the initial position.

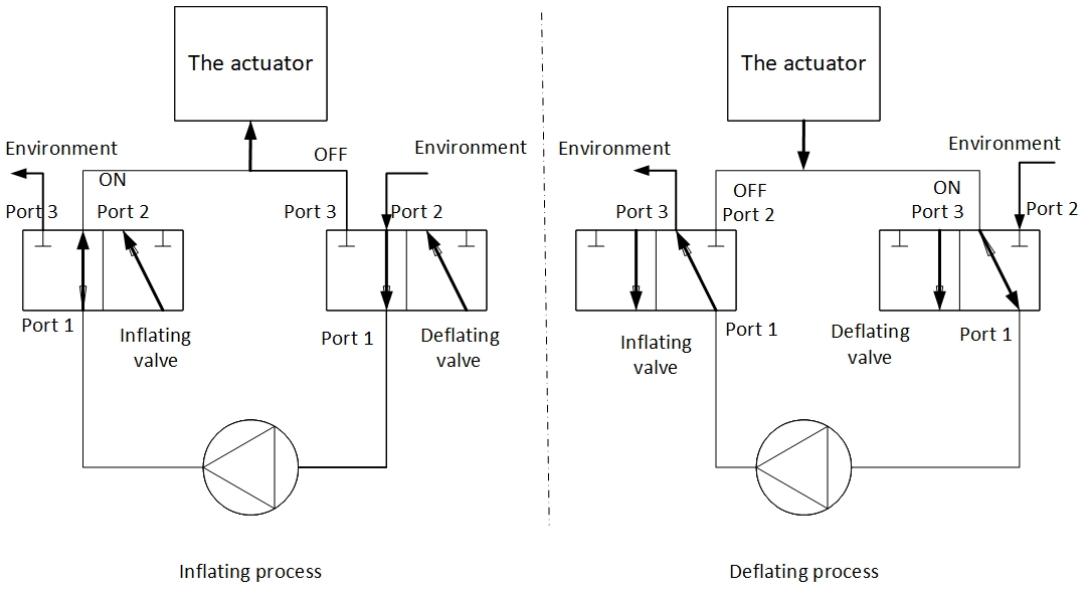

Figure 3.6: Operating pneumatic system schematic

Based on this principle, the cylinder is replaced by the soft origami actuator, and a different method of connecting the solenoid valves is adopted to create the actuator movement, as shown in Figure 3.6 because the proposed actuator consists of only one air chamber. An air pump has its input and output port connected to the inflating and

deflating valve respectively. The air is inflated into the actuator from outside through the inflating valve in the pressuring phase. Meanwhile, the air inside the actuator is compressed out the environment through the deflating valve in the compressing phase. The air pump takes over the pressuring process and vacuum process to create the upward or downward movements of the actuator respectively.

3.4 Movement method

Based on the research approach, the pneumatic system is employed for seven actuators. However, the inflating or deflating process for each actuator is synchronised and controlled by the micro-controller to produce translational and rotational movements. These actuators take the similar role to the caterpillar's prolegs. The elongations of different actuators are combined together to generate the deformation like the propagated wave on top.

To generalise the movement of each actuators, a sine equation is used to represent the actuator's movement, described as below:

$$y = Asin(2\pi f.t + n\phi) \tag{3.1}$$

where:

A: is the amplitude of the actuator movement.

f: is the frequency of the actuator movement.

t: is the time.

ϕ: is the initial phase of the actuator.

n: is the constant which depends on the number of segments into which a period of the sine wave is divided.

y: the height of the actuator.

In this research, a series of three actuators is investigated. The constants in the equation including A, f, ϕ are the same for different actuators. The graph that shows the movement of these actuator is presented in Figure 3.7. Depending on the desirable characteristics of the movement of the object, these constants are changed to suit the specific scenarios.

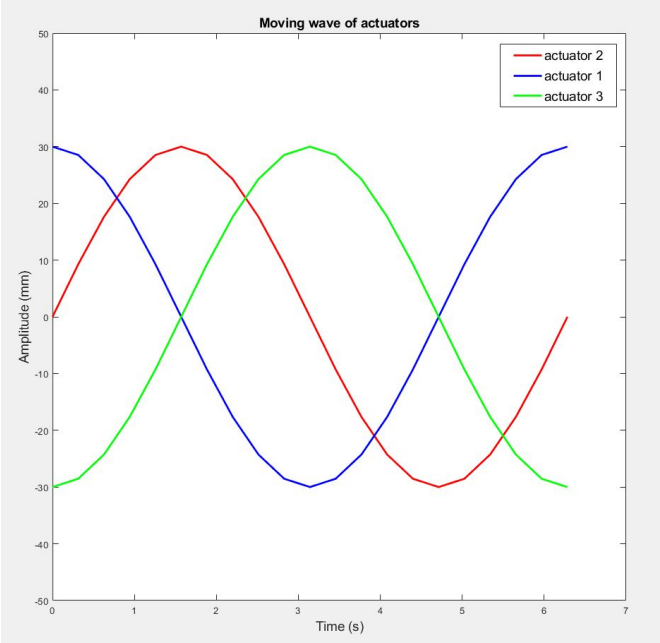

Figure 3.7: Example of moving wave of actuators

The translational movement is created by a series of actuators. In Figure 3.8a, the right actuator goes to the highest amplitude, the middle actuator is at the rest position, and the left actuator is at the lowest amplitude. A combination of the heights of three actuators creates a gradient like the sinusoidal wave's gradient (Hashem et al., 2016; Mosadegh et al., 2014). Thanks to the gravity force, the object tends to slide on this surface. The sliding movement is not made in the models of Deng et al. (2016), Hashem et al. (2016), and Mosadegh et al. (2014) because there are the fixed sidewalls in between

the actuators. Hence, the deformation of the actuator in their research just follows the upward direction. Meanwhile, the movement in this current research is created by the extension and contraction of the actuator following the equation 3.1. Indeed, the Tabbot wave is capable of propagating among these actuators to translate the object, as shown in Figure 3.8b. Furthermore, with the same movement principle, two series of these actuators, which travel in the opposite moving directions, create pairs of opposite Tabbot waves. These pairs are considered the pairs of torques to produce a rotational movement, as shown in Figure 3.9. A new movement method is finally proposed to manipulate the objects in either translational movement or rotational movement.

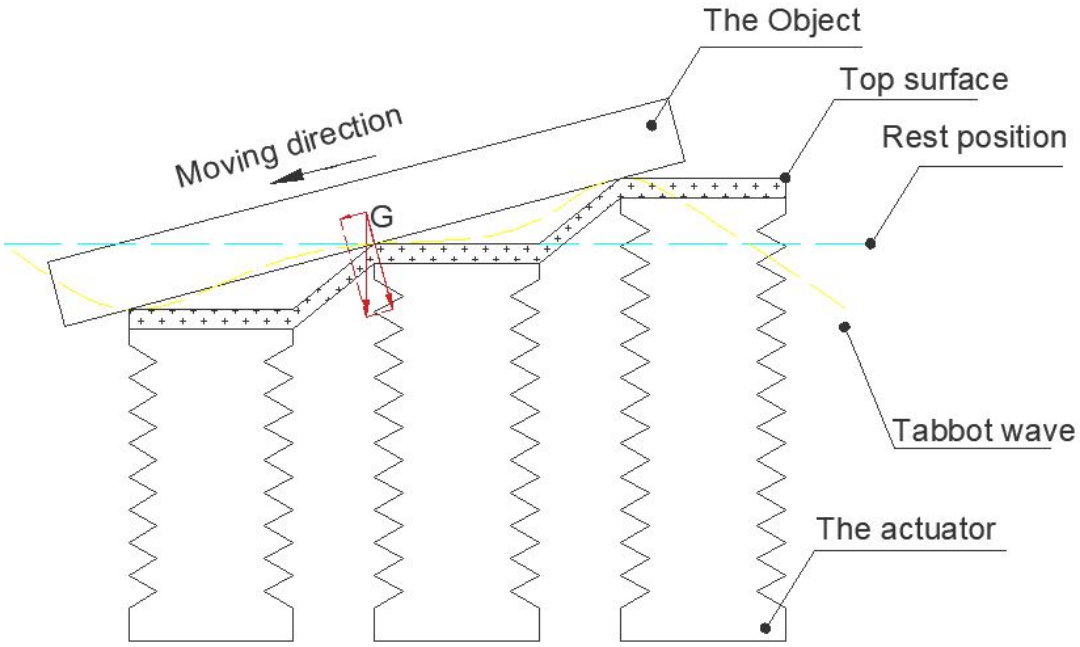

(a) Front view of translating movement

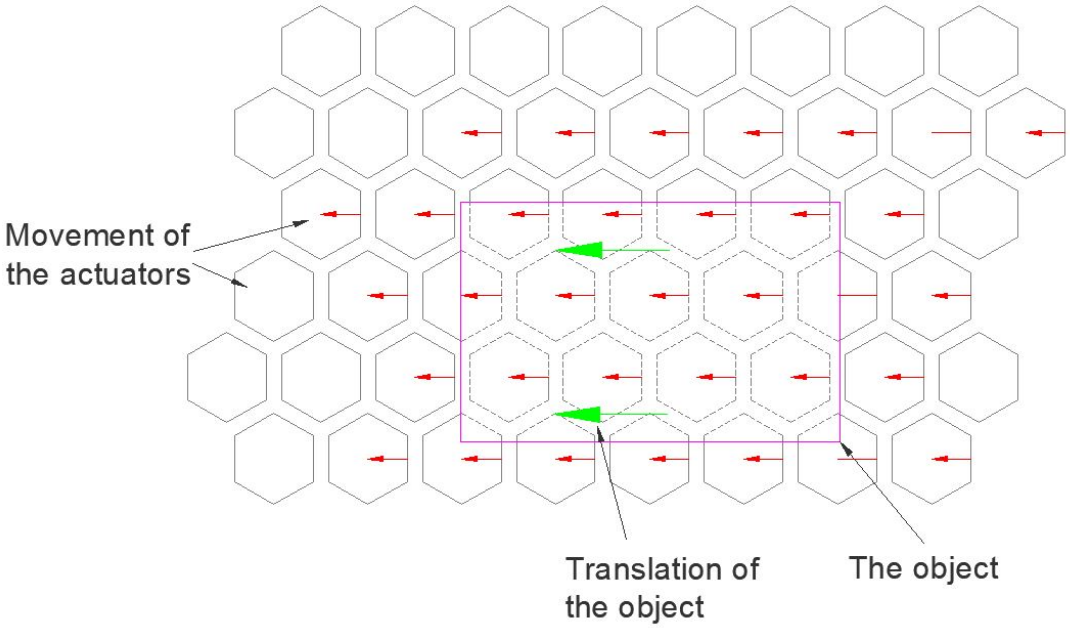

(b) Top view of translating movement

Figure 3.8: Principle of translational movement

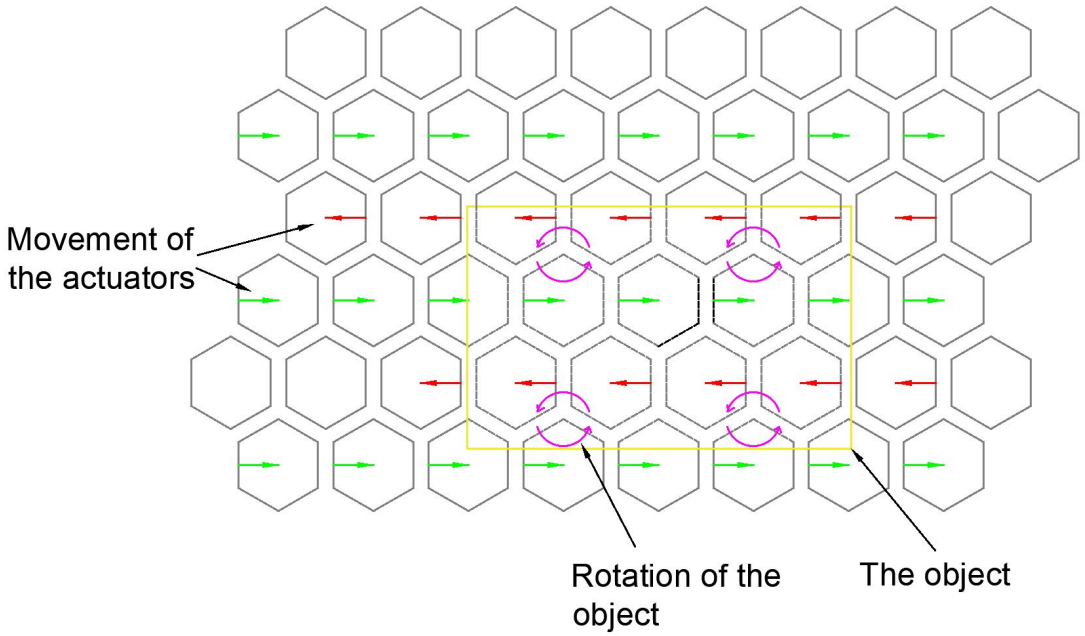

Figure 3.9: Principle of rotational movement

Chapter 4

Design and Fabrication

Based on the above-mentioned theoretical principle in Chapter 3, several designs and fabrications of prototypes of a soft origami actuator with an embedded sensor, pneumatic system, electrical system, and PID model have been presented to answer three research questions in Chapter 1. This chapter first describes the designing and fabricating process before making final decisions on the design of these prototypes.

4.1 Soft origami actuator with an embedded sensor

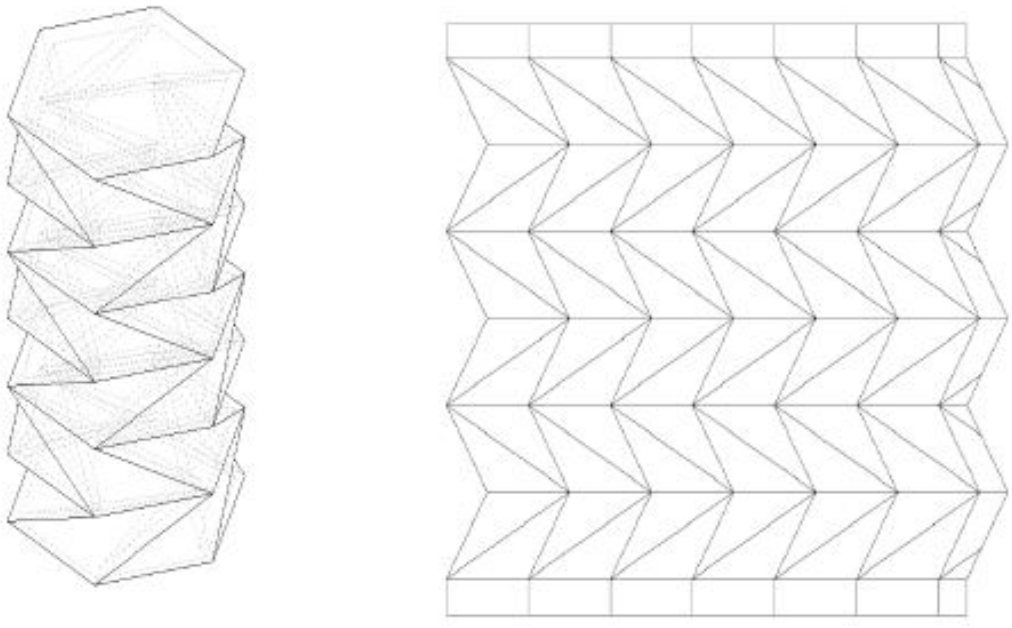

Figure 4.1: A hexagon origami pattern

Based on the literature review and theoretical modelling, the Kresling's pattern has been chosen as the support structure of the actuator, as shown in Figure 4.1. This actuator is divided into three parts including, as shown in Figure 4.2:

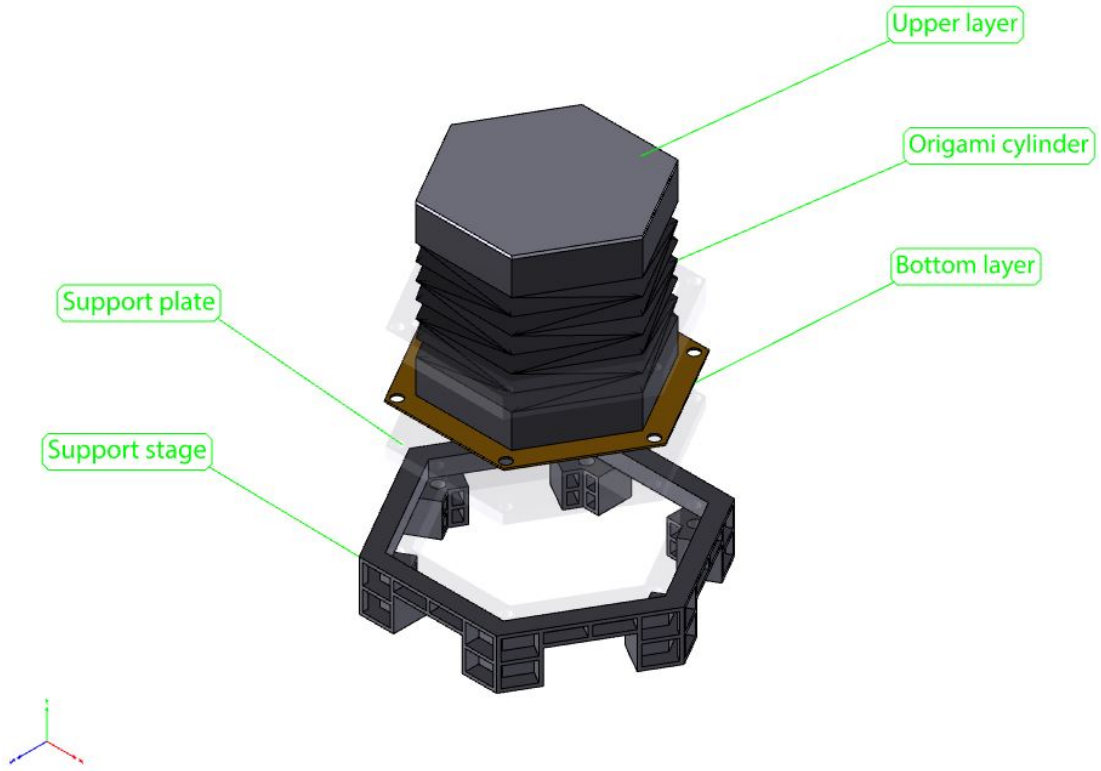

Figure 4.2: Structure of actuator

- Upper layer is cast by silicone with 6mm thickness. It covers one end of the origami cylinder and sticks to the top surface of the Tabbot.
- Origami cylinder is made from origami paper covered by silicone on both sides. The origami cylinder is able to extend and contract along the vertical direction.
- Bottom layer is a fringe that is made of silicone to connect the origami cylinder and the support stage.

With different combinations of these three parts, three designs of the actuators are manufactured to evaluate the ability of attaching a sensor to the actuator, as well as the air tightness of the actuator. Three designs, as shown in Figure 4.3, are described as below:

(a) Design 1

(b) Design 2

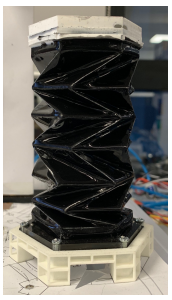

(c) Design 3

Figure 4.3: Origami cylinder

- Design 1, the origami cylinder is coated with silicone on both internal and external sides of the sidewall by painting. The upper layer is then stuck down the origami cylinder by silicone glue. This design does not have the bottom layer, and the origami cylinder is connected directly to the support plate by glue.

- Design 2, the origami cylinder is manufactured in the same way as in design 1. However, the upper layer is dipped in the cylinder and sealed by glue. Moreover, the origami cylinder has a bottom layer to increase the contact area with the support stage.

- Design 3, the origami cylinder has several cantilevers on top, it is dipped in the silicone liquid. With support of the cantilevers, the upper layer and the cylinder is cast as one integral unit, and the bottom layer is the same as that of design 2.

4.1.1 Upper layer

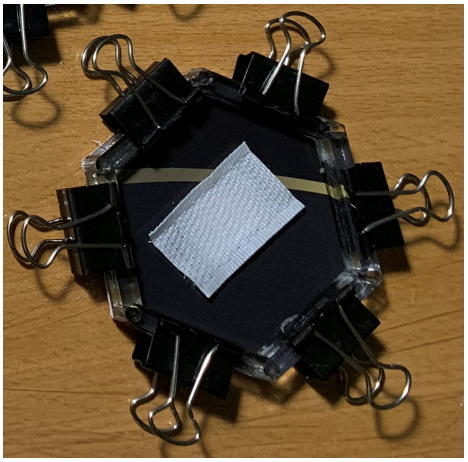

(a) Establishing a mould

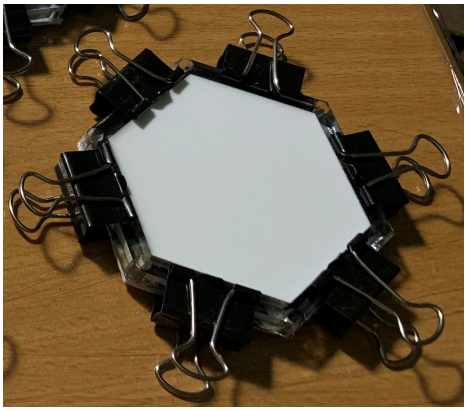

(b) Silicone filled in mould

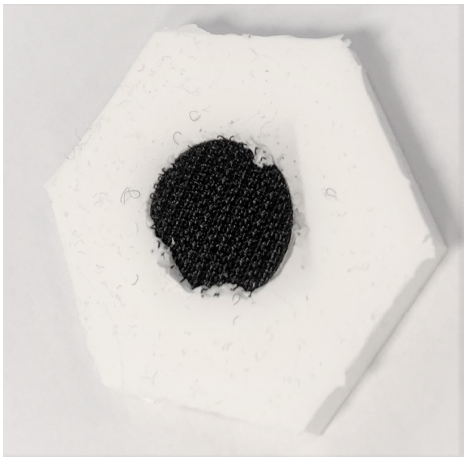

(c) Final product

Figure 4.4: Process to mould upper layer

The upper layer is cast entirely from white Ecoflex00-30. Initially, a mould is made to support the casting process, as shown in Figure 4.4a. A velcro is attached to the bottom plate in the middle. This velcro consists of two parts. the hook is attached to the upper layer of the actuator, and the loop is attached to the cover sheet of the Tabbot. This velcro functions as the soft re-configurable connection between the actuator and the cover sheet. The clips are used to prevent silicone from leaking out during the casting process. The silicone is then filled in these moulds, as shown in Figure 4.4b. It takes about three or four hours to cure the silicone. Finally, the upper layer is shaped, as shown in Figure 4.4c.

4.1.2 Origami cylinder

(a) Paper with Kresling pattern (b) Coating black silicone inside (c) Coating black silicone outside

Figure 4.5: Fabricating origami cylinder by coating silicone

The origami paper plays a role as the support structure of the actuator on which a thin silicone film (Ecoflex 00-30) is coated on both interior side and exterior side. An A4 white paper 80 GSM is selected to create this structure. The origami pattern is printed out on this paper, as shown in Figure 4.5a, before being coated with silicone. In design 1 and 2, the paper sheet is folded to shape the origami cylinder. This part is then spread out on the plate before the silicone rubber (Ecoflex) is painted on the interior side, as shown in Figure 4.5b. It takes about three hours to cure the silicone. At this time,

the guidelines and vertices of this part emerge and are gradually formed. The origami cylinder then needs to be folded and sealed before the exterior side is painted, as shown in Figure 4.5.

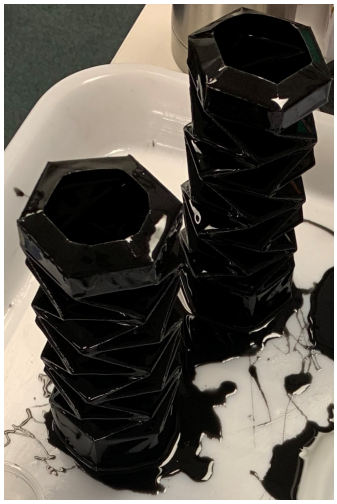

Figure 4.6: Fabricating origami cylinder by sinking in silicone

In design 3 of the actuator, the origami cylinder is dipped in the silicone liquid. After the origami pattern is folded and shaped like a cylinder, this cylinder is sunk into a mixed ecoflex 00-30 volume, as shown in Figure 4.6. This model is kept along the vertical direction, and it also takes about three hours for the silicone to cure.

4.1.3 Bottom layer

To keep the air chamber tight, the bottom layer is mounted to the origami cylinder. Some paper cantilevers are made, and then silicone is coated on these cantilevers. As a result, the contacting area between the bottom layer and support plate is dramatically increasing, as shown in Figure 4.7. Thanks to the cantilevers, the clamping force and air pressure inside the chamber keep the actuator tighter.

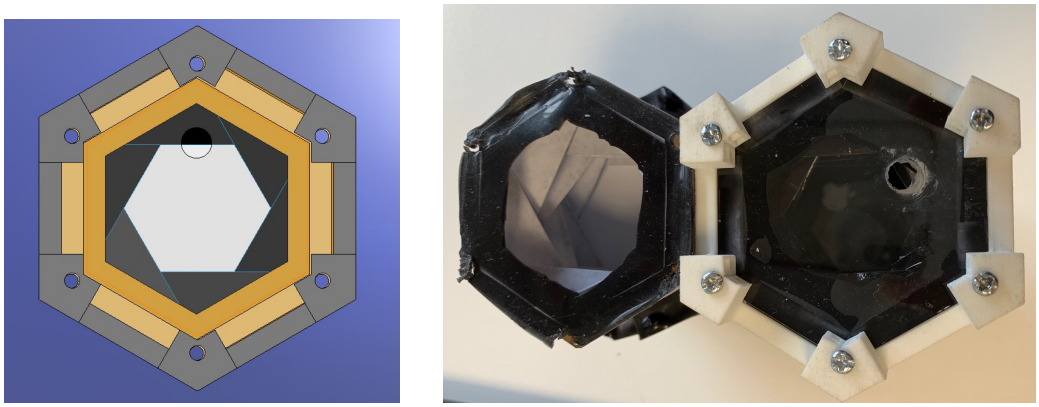

(a) Bottom layer in simulation (b) Bottom layer in a practical model

Figure 4.7: Bottom layer

In reference with the literature and design decision, three designs of the soft origami have been produced. However, to answer the first research question related to embedding the sensor inside the actuator, several experiments are conducted to evaluate the ability of detecting actuator's elongation, the air tightness of the air chamber, and ease of maintaining the actuator.

4.2 Pneumatic system

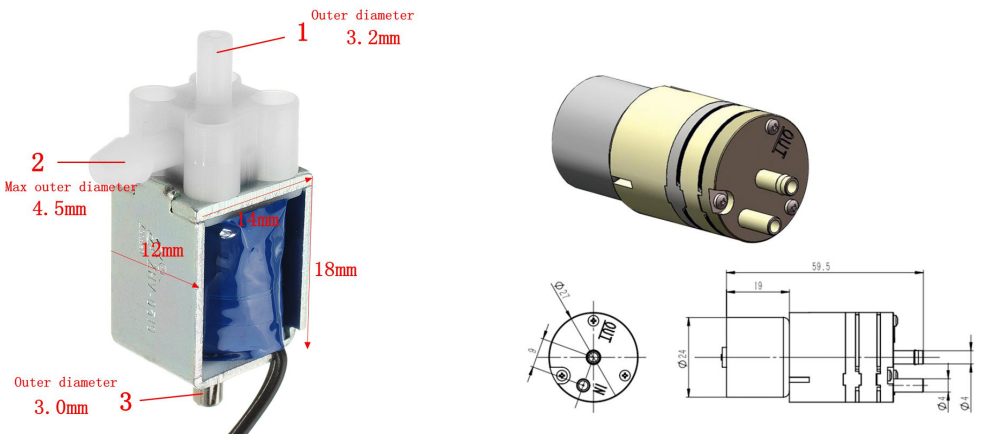

(a) 3/2-way solenoid valve (b) Air pump

Figure 4.8: Pneumatic components

Based on the air supply theory that is mentioned above, a pneumatic system is designed to supply air to the Tabbot with seven actuators. The research approach is to construct the system to maximize its functions. Each air pump is used to supply air to the actuator through two 3/2-way solenoid valves. This valve is normally closed, and port 1 is linked to port 3, as shown in Figure 4.8a. When this valve is on, port 1 is linked to port 2. In this research, the inflating valve and deflating valve are connected to the output and input of the air pump respectively. As shown in Figure 3.6, the inflating valve is set on in the whole inflating process; meanwhile, the deflating valve is set off. At this point, the air is supplied from the environment outside to the input of the air pump through the deflating valve. The air is then inflated from the air pump to the actuator through the inflating valve. Since the deflating valve is closed, the link between the actuator and the deflating valve is blocked. Consequently, the actuator is forced to go upward. In the reverse process, when the inflating valve is off, and the deflating valve is on, the link from the actuator to the inflating valve is blocked. The air inside the actuator is deflated by the air pump via the deflating valve. The air is then released out to the environment via the inflating valve. Consequently, the actuator goes downward. It is one typical operating cycle of the actuator.

When different actuators are combined together, the air supply principle is the same for separated actuators. However, this process should be combined and repeated under the control of an algorithm to make specific deformation trajectory of the top surface.

(a) Fundamental cell: top-view

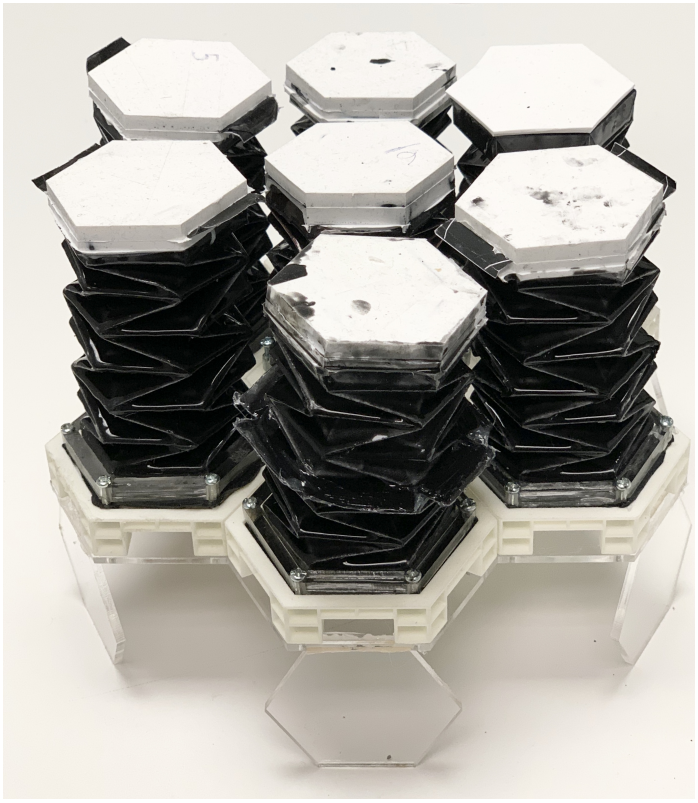

(b) Fundamental cell: front-view

Figure 4.9: Fundamental cell arranged in hexagon symmetry

The research approach is to build a fundamental cell which is able to be expanded to a larger table. A fundamental cell involving seven actuators is arranged as in Figure 4.9. This prototype uses only one air pump and two 3/2-way solenoid valves for both inflation and deflation, as shown in Figure 3.6. Hence, this design has reduced significantly the number of the air pumps and solenoid valves. It leads to the reduction in the physical dimensions of the practical prototype. Also, it is feasible to be scaled up to a larger prototype. By optimising the number of the components in the system, it is also possible to simplify the control algorithm and help the control process to be more stable with the use of the closed-loop controller.

4.3 Electrical system

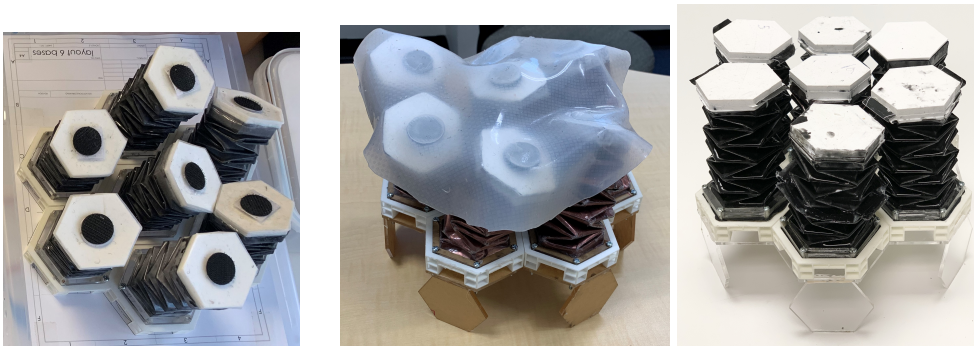

(a) Prototype 1 (b) Prototype 2 (c) Prototype 3

Figure 4.10: Different prototypes of Tabbot

(The cover sheet is temporarily removed for inside look)

The research approach is to build up a fundamental actuator which is able to be scaled up to a bigger table with various dimensions. A fundamental cell involving seven actuators is proposed, as shown in Figure 4.10. The electrical system, therefore, consists of numerous components as listed in Table 4.1.

Table 4.1: Basic components of electrical system

Electrical component list			
No	Name	Code	Quantity
1	Micro-controller	Arduino Uno	01
2	I2C multiplexer	TCA9548A	01
3	PWM expander	PCA9685	01
4	Motor driver	L6203	07
5	Air pump	KVP-04	07
6	3/2 way solenoid valve	N/A	14
7	IR proximity sensor	VCNL4010	07
8	NPN Darlington transistor arrays	ULN2803A	02
9	5V power supply	N/A	01
10	12V power supply	N/A	01

Apart from the physical architecture of seven actuators, an electrical system is designed to drive seven air pumps (KVP-04) via seven motor drivers (based on H-bridge which uses L6203 chip), and fourteen 3/2-way solenoid valves. The electrical system also reads data from seven IR proximity sensors (VCNL4010) with fixed I2C address. These components are all controlled by a micro-controller (Arduino Uno); however, it raises a big problem. Since the Arduino Uno has only one I2C port and 14 digital

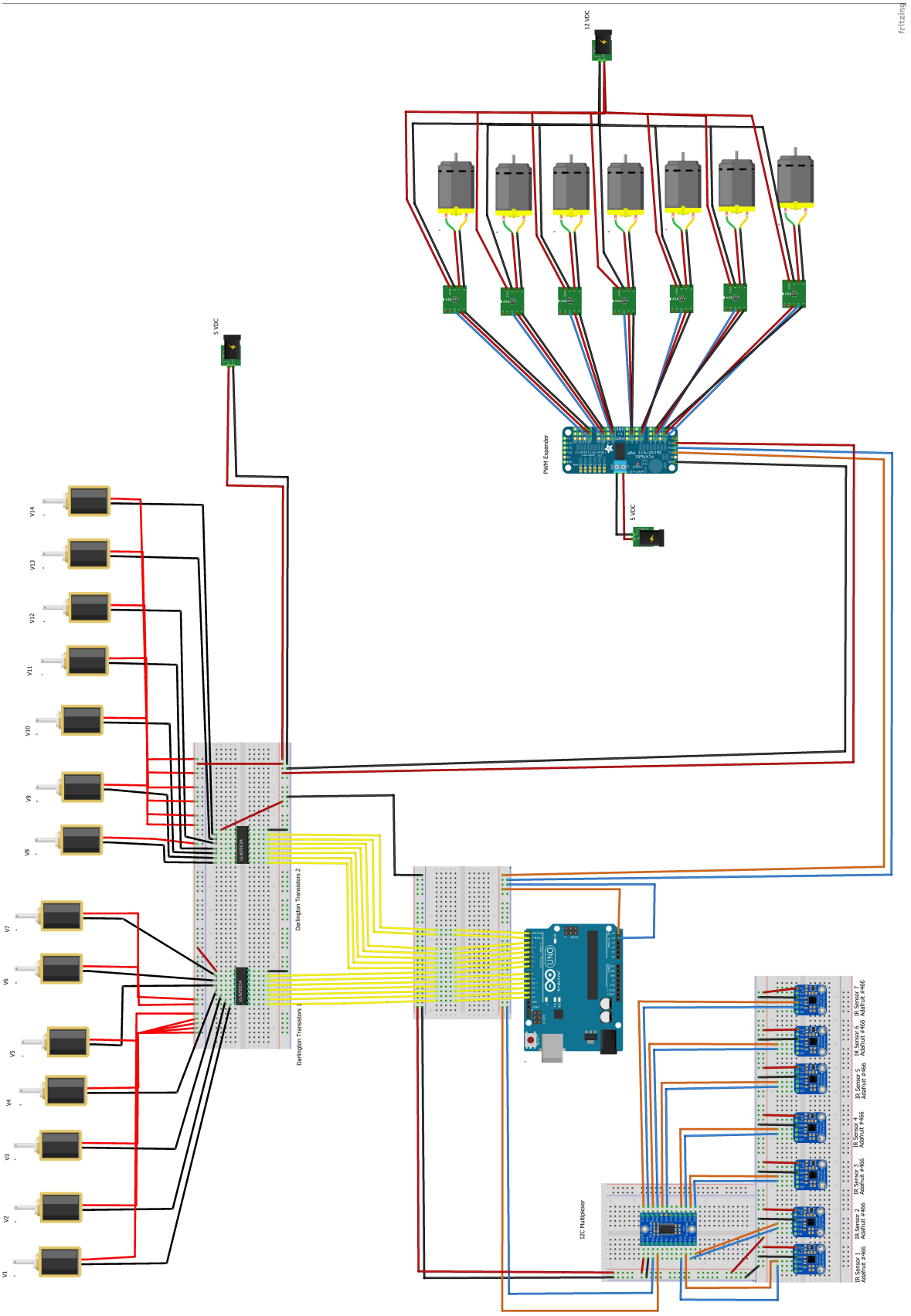

Figure 4.11: General electric schematic

ports including six PWM ports, it cannot assign the temporary I2C addresses to the devices with the same I2C address. In addition, with only six PWM ports, Arduino Uno is unable to provide PWM signals to control seven air pumps used in this research. The other eight digital ports in Arduino Uno are technically incapable of controlling 14 solenoid valves simultaneously. The researcher, therefore, comes up with an idea of employing expandable devices such as I2C multiplexer and PWM expander. Firstly, the I2C multiplexer (TCA9548A) is able to drive eight I2C devices with the same fixed I2C address, and the maximum driving capacity is up to 64 devices. Secondly, the PWM expander (PCA9685) is able to drive 16 PWM devices at the same time. The final electrical schematic is shown in Figure 4.11 including the IR proximity sensor, air pump, and solenoid system.

4.3.1 Circuit driving IR proximity sensor

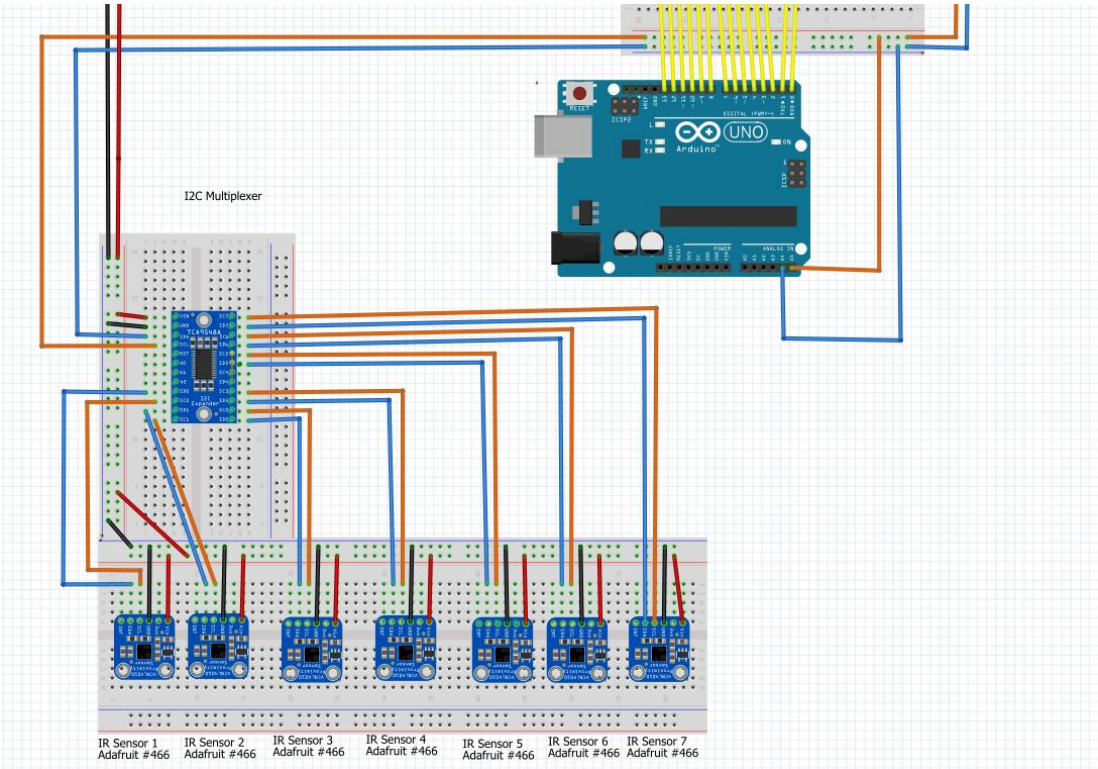

Figure 4.12: Circuit driving IR proximity sensor

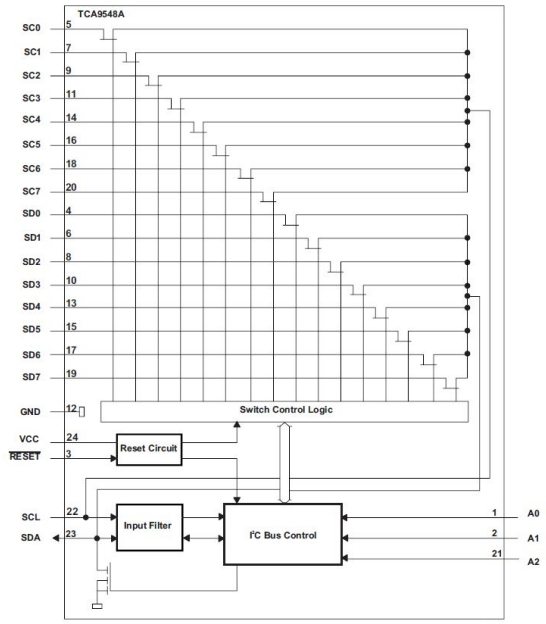

Figure 4.13: TCA9548A functional block diagram (TexasInstruments, n.d.-a)

As seen from the data sheet documented for the sensors (DiCola, n.d.), the IR proximity sensor is capable of detecting the object within its working range. The working range of IR proximity sensor depends on the energy level of the emitted and received light that the sensor transmits and receives respectively. This energy is driven by the current flowing through the sensor. Seven sensors are wired up to the I2C multiplexer because these sensors have the fixed I2C address, while the micro controller (Arduino Uno R3) has only one I2C port, as shown in Figure 4.12. Thus, the I2C multiplexer (TCA9548A) is adopted to assign a temporary I2C address to each sensor. This I2C multiplexer sweeps eight ports around 100ms. Therefore, only one sensor is turned on at the time, and the concern related to the same I2C address is able to be solved with an acceptable shifting time among the sensors. A proposed functional block diagram of the multiplexer is shown in Figure 4.13 (TexasInstruments, n.d.-a).

4.3.2 Circuit driving air pump

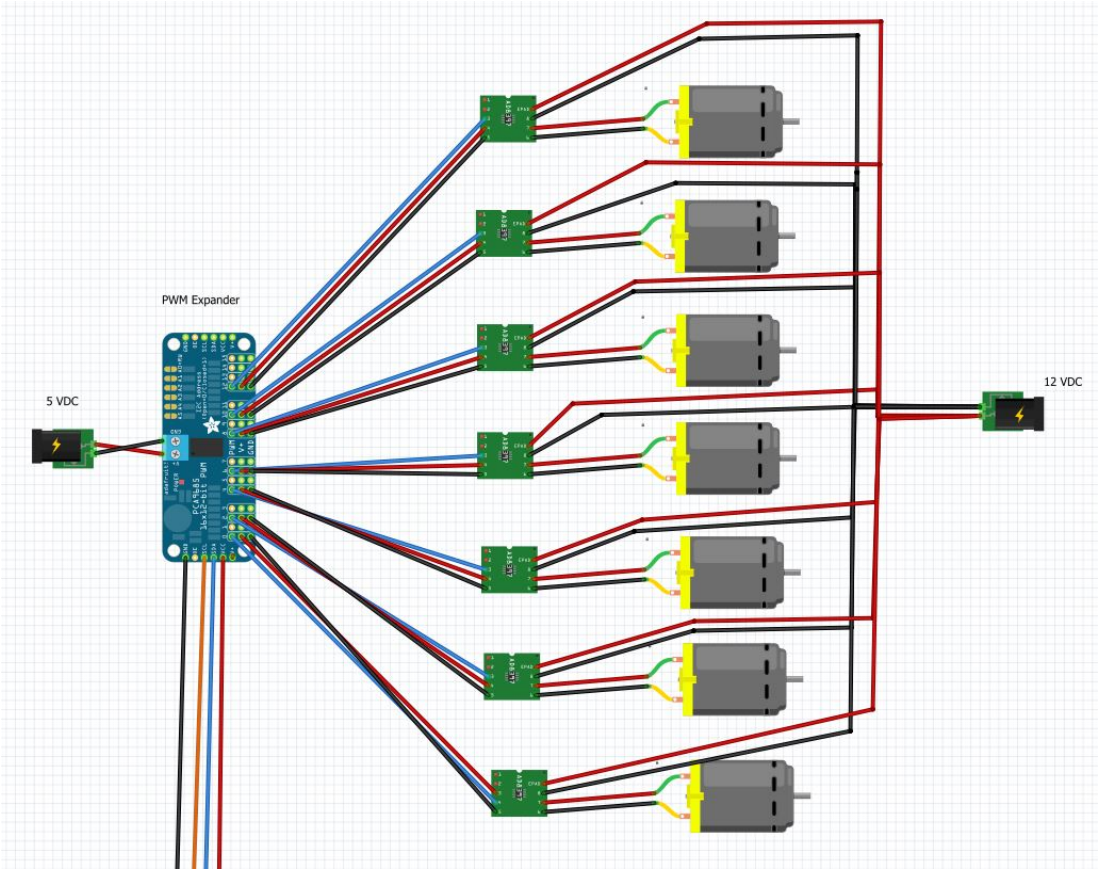

Figure 4.14: Circuit driving air pump

The air pump that is adopted in this research has model code KVP04-1.1-12. Its power supply is 12 voltage, and the current is 320 milli-Ampere (Kamoer, n.d.). The micro-controller does not suffice to drive the air pump directly. Several H-bridge circuits are employed to drive this pump such as L298, L298N. However, these breakouts with L298 are delicate and uncertain. Therefore, another H-Bridge breakout based on chip L6203 is finally selected for its high stability and reliability. Each H-Bridge breakout is capable of driving the air pump. Totally, the fundamental cell with seven actuators needs seven H-Bridge breakouts to drive seven air pumps. However, Arduino Uno R3 micro-controller just has six PWM ports. The researcher thus chooses a PWM expander with 16 PWM channels (PCA9685). This PWM expander is controlled by I2C bus

(Adafruit, n.d.). The I2C multiplexer has 8 pins, seven of which are wired up to the sensors, and the last pin is connected to the PWM expander. This configuration of the system is designed to maximize the efficiency of all components.

The air pump does not change its direction during the operating process. The solenoid valves are in charge of reversing the airflow. Hence, the motor driver which controls the air pump does not need to change the driving current. The air pump is connected to the motor driver, and these motor drivers are then wired up to the PWM expander prior to being connected to the micro-controller, as shown in Figure 4.14.

4.3.3 Circuit driving solenoid valve

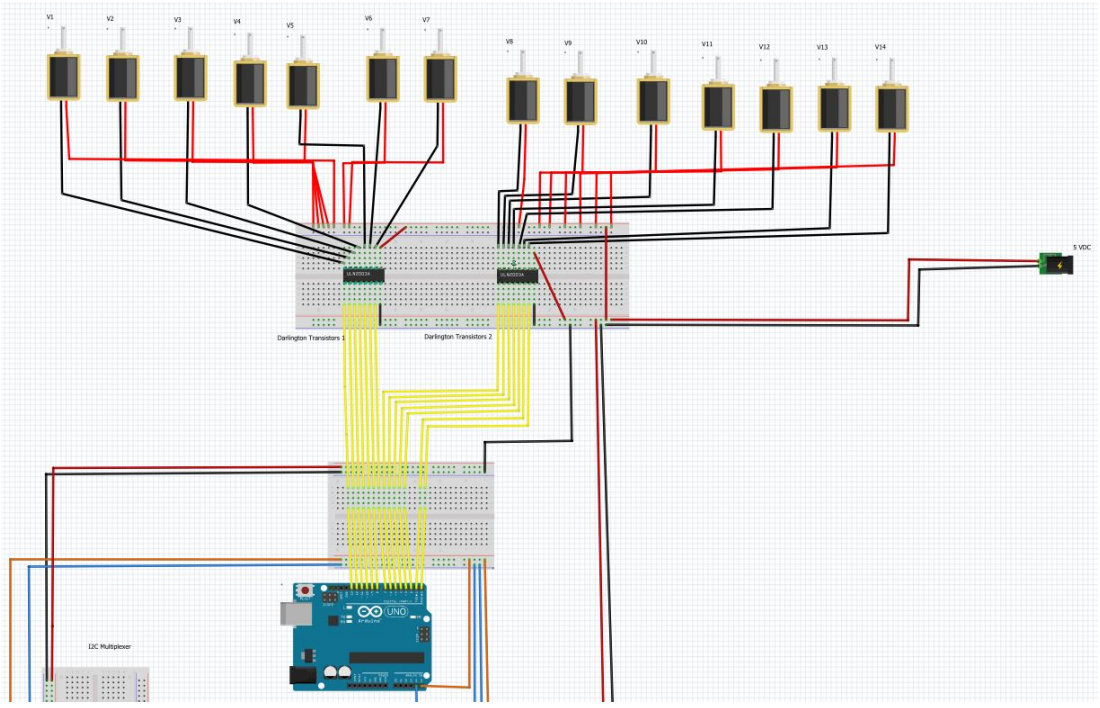

Figure 4.15: Circuit driving solenoid valve

Each solenoid valve is operated at the 220mA current, and the behaviour of this load is inductive. Therefore, these valves can not be wired up directly to the micro-controller.

An NPN Darlington transistor array is considered as the appropriate solution. It is capable of driving a load with a maximum value of 50V and 500mA (TexasInstruments, n.d.-b). In addition, the internal free wheeling diodes are built in to suppress the kick-back voltage of the inductive loads. Each actuator needs two solenoid valves. Totally, 14 solenoid valves are necessary for one fundamental cell. These 14 pins control valves are then hooked up to 14 digital pins of the micro-controller, as shown in Figure 4.15.

4.4 PID model

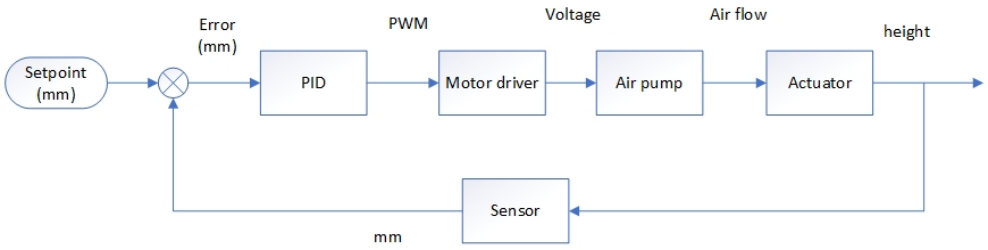

Figure 4.16: PID model schematic

In accordance with the theory of PID algorithm, a PID controller is constructed to control the velocity of the air pump and drive the actuator so that it can reach the desired height in the shortest time period. There are various types of PID controllers such as continuous-time and discrete PID controller. A discrete PID controller however has proved its advantages in terms of implementation errors, speed, and accuracy (Mohamed et al., 2017). The proposed model is shown in Figure 4.16. The desired height here is a reference variable to specify whether the actuator is going to reach this value. An IR proximity sensor named VCNL4010 is used to measure the height of the actuator. An error between desired height and the actual height is calculated by a micro-controller (Arduino Uno) to present suitable control signals for the motor driver.

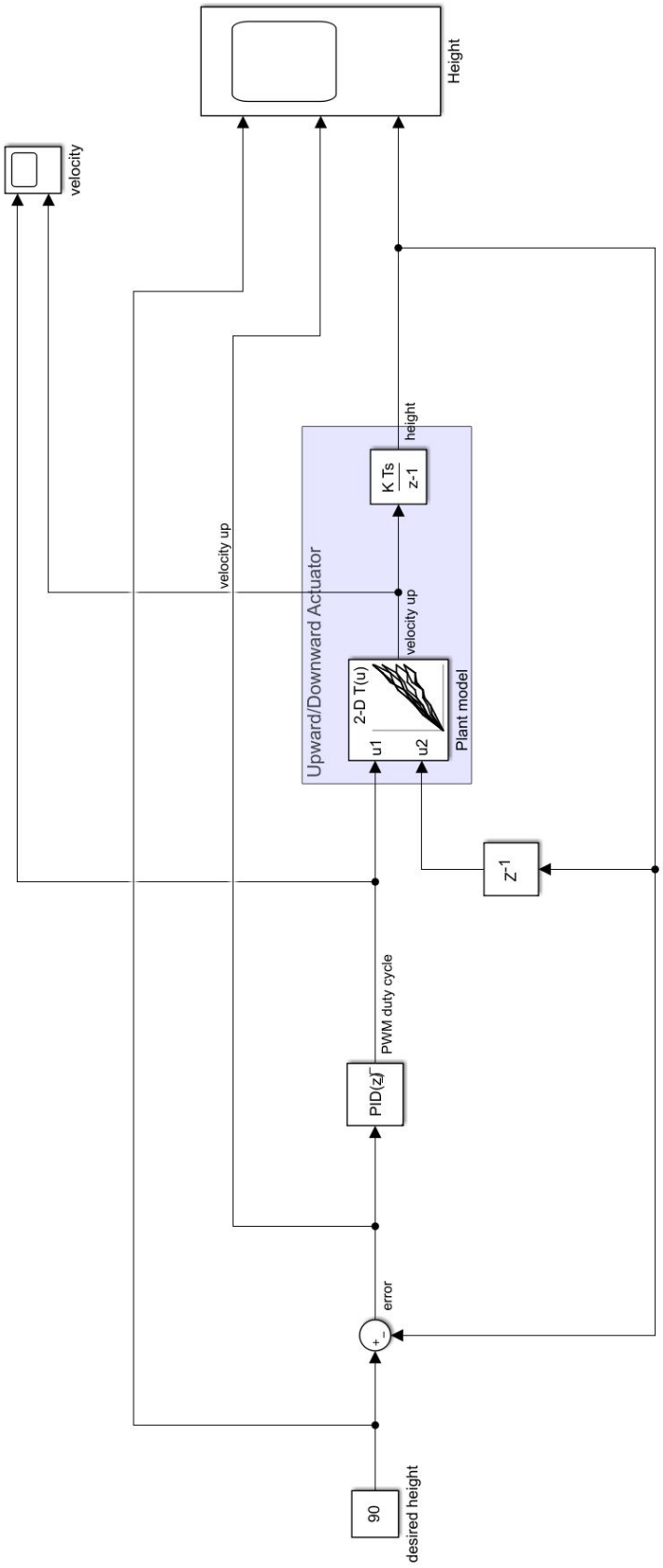

Figure 4.17: Prototype of PID control schematic

This research uses MATLAB and SIMULINK software to develop the PID controller to control the air pump. This air pump runs the plant model of the soft origami actuator, as shown in Figure 4.17. This plant model is constructed from data that is collected during the actuator's operation, and it is presented in a lookup table. To find out the P, I, D gain, the PID tuner tool in MATLAB/SIMULINK is applied. This research adopts two types of PID controller: the continuous-time and discrete PID controller. The software is helpful to reduce the calculating time and support the design and control process. As a result, the P, I, D gains presented in the research can be easily deployed in the actual hardware and offer a high possibility of modification and adaptation to different hardware.

4.5 Movement design

To manipulate the objects on the Tabbot's top surface, the translational movement and rotational movement are investigated. This section is to investigate how these movements are created based on the principle described in Chapter 3.

4.5.1 Translational movement

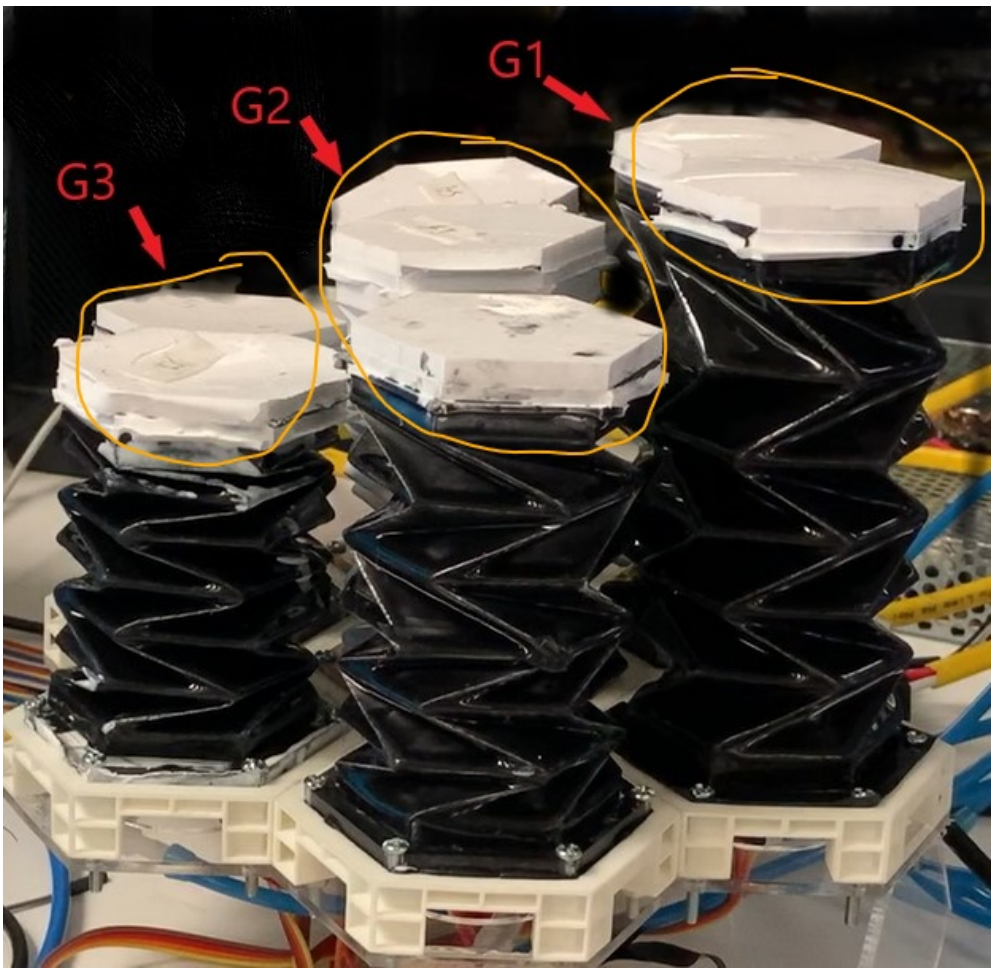

Figure 4.18: Actuator groups

The Tabbot with seven actuators are divided into three different groups, namely G1, G2 and G3, as shown in Figure 4.18. To translate an object from the right to the left, the amplitude of G3 is the smallest, followed by G2 with the second smallest amplitude, and G1 has the largest amplitude. All of them have the same neutral/rest position. These groups of actuators fluctuate around these rest position following a specific frequency. When G1 is at the highest position, G2 is in the middle position, and G3 is at the lowest position, they all create a gradient. The gravity force of the object pushes the object to slide on the created gradient of the table's surface to create its movements.

In specifically, a typical cycle of the movement is divided into four steps. Initially, all groups including G1, G2, and G3 are at the rest position. Afterwards, G1 is inflated to go upward to the highest position, G2 is at the rest position, and G3 is deflated to go downward to the lowest position. A gradient on the top surface is created, the object is thus pushed to slide on this surface, from right to left.

Secondly, G1 goes down to the rest position, G2 goes up to the maximum height, and G3 goes up the rest position.

Thirdly, G1 keeps going down to the minimum height, G2 goes down to the rest position, and G3 keeps going up to the maximum height.

Finally, G1 goes up the the rest position, G2 keeps going down to the minimum height, and G3 goes down to the rest position.

These steps are illustrated in Figure 4.19. This process is repeated continuously to create the propagated wave, called Tabbot wave, on the Tabbot's surface. The Tabbot wave can manipulate the object to any horizontal direction on the top surface, following the above-mentioned principle.

4.5.2 Rotational movement

With the same grouping method as described in Section 4.5.1, each group of actuators creates its own Tabbot wave. In particular, G1 and G3 have two actuators each, and these actuators go up and down together. G2 has three actuators which are operated in the same principle, but in the opposite direction to the actuators in G1 and G3. The odd

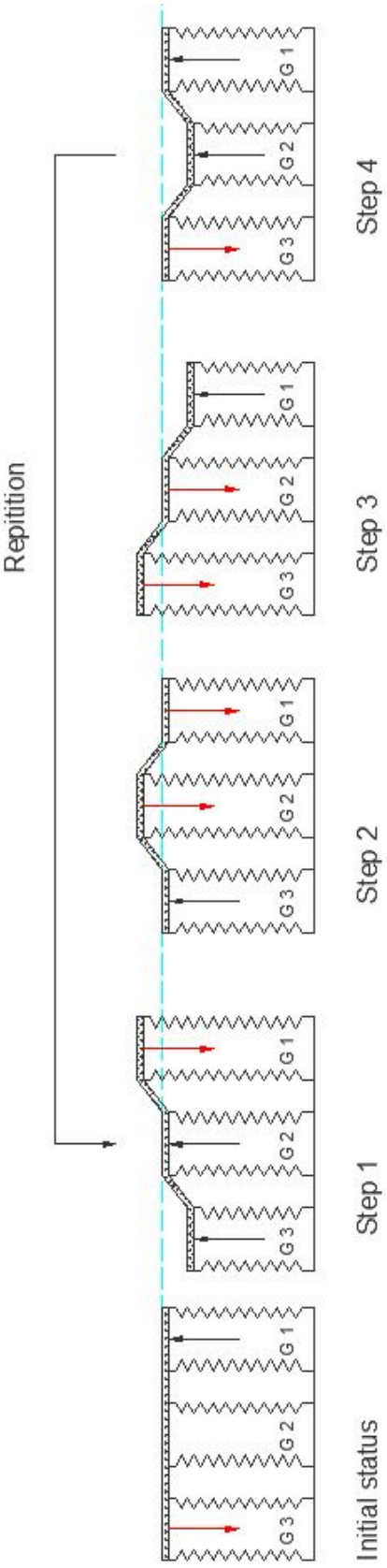

Figure 4.19: Typical period Tabbot wave

group, G1 and G3, is to propagate the Tabbot wave in one direction. Meanwhile, the even group, G2, is to propagate the Tabbot wave in the opposite direction. A pair of an odd and an even group of actuators is considered a pair of torques applied on the object. Consequently, the object is rotated on the table's surface.

Chapter 5

Experiments

This chapter reports on the experiments that are conducted to test the actual operation of the proposed designs. Each experiment is configured with the specific scenario that presents answers to the research questions. Some variables are therefore changed in different conditions to determine the best parameters and structures of the soft table robot to maximize its performance for high accuracy in the operating, monitoring process, easy manufacturing, and easy maintenance.

5.1 Experiment 1: Testing of air leakage

The primary purpose of this experiment is to provide experimental evidence of air leakage so as to finalize which design suffices meet of requirements raised in this research with regards to the air tightness, stiffness, flexibility, and easy maintenance. This experiment is also helpful to answer the research question regarding how to embed a sensor in the actuator. Three designs fabricated by different methods are studied. In design 1 of the actuator, the origami cylinder is shaped like a cylinder. The upper layer is sealed to one end of the origami cylinder, and the other end is directly sealed to the stage without a bottom layer. The design 2 and design 3 both have the bottom layer.

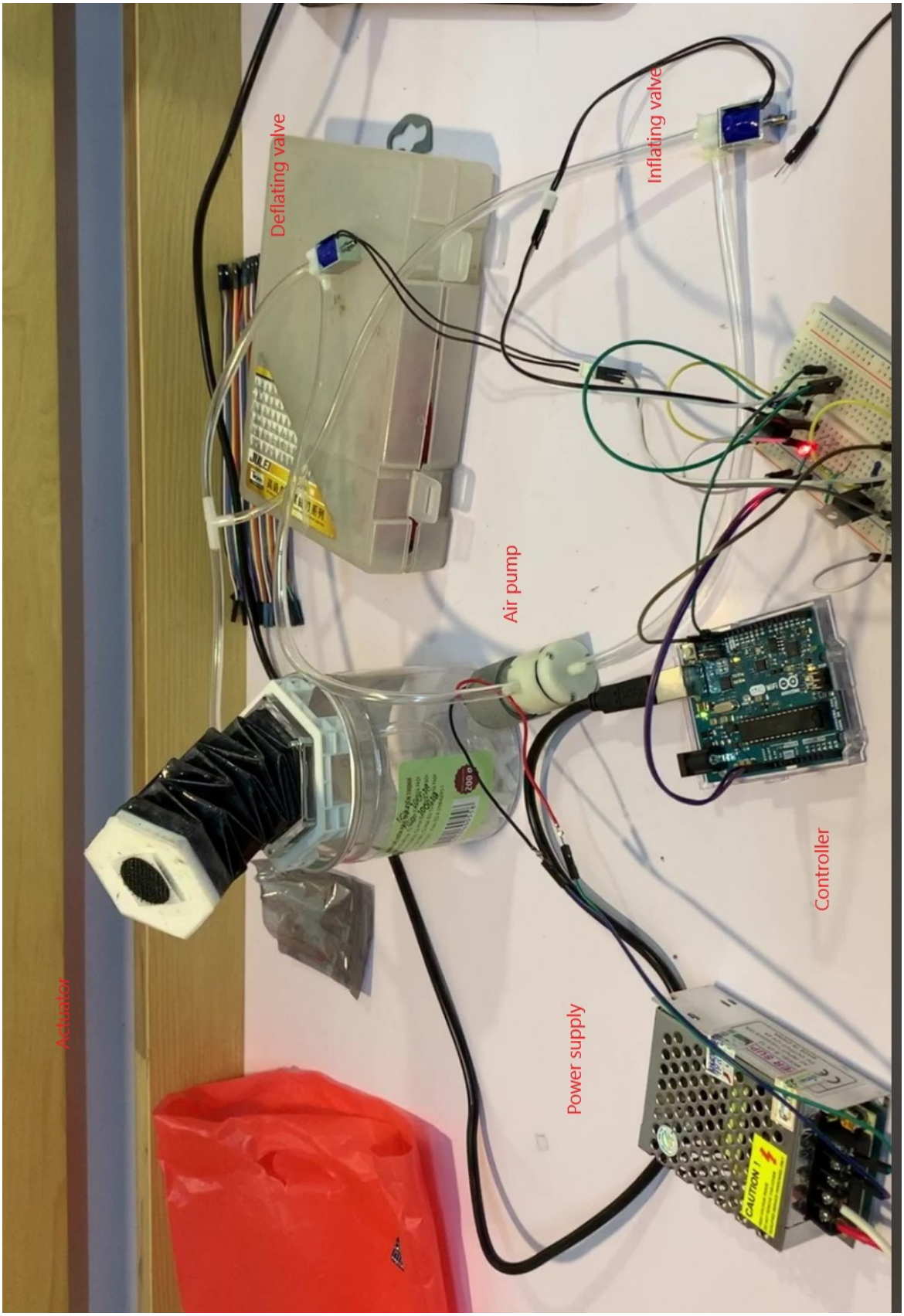

Figure 5.1: Schematic of experimental testing of air leakage

The design 2, however, does not have cantilevers on top. The upper layer is instead sunk into the origami cylinder and then sealed by silicone glue. The upper layer of the design 3 is directly moulded with the top end of the origami cylinder. The experiment is set up, as shown in Figure 5.1. These three different designs are tested sequentially. In each test, the amount of air pressure is supplied from the minimum to maximum level multiple times. After 100 times, the evidence of air leakage in these designs is recorded to determine the best design of soft origami actuator by manually detecting distortions and abnormalities of the actuator.

5.2 Experiment 2: Testing of sensor placement

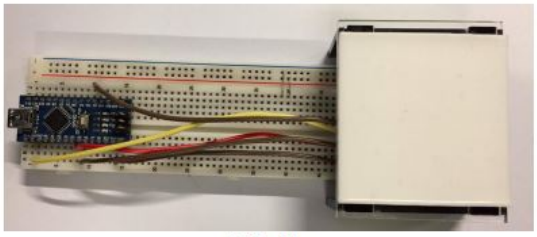

(a) Top View

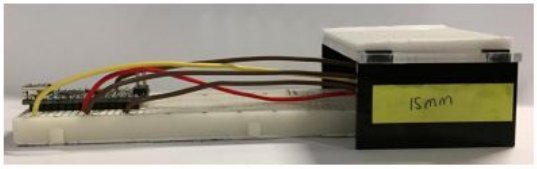

(b) Side View

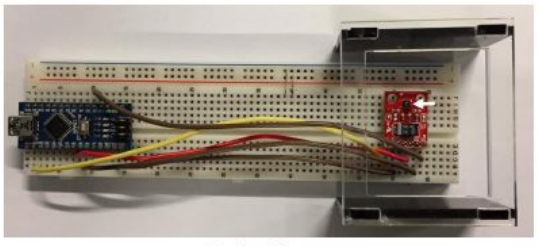

(c) Open Support

Figure 5.2: Experiment setting (Thien et al., 2016)

This experiment is set up to find out which sensor placement shows the highest accuracy in measuring the elongation of actuators while still providing high air tightness and

easy maintenance. Thien et al. (2016) suggested an experiment to measure changes in the height of actuators by using a proximity sensor (called APDS 9960), as shown in Figure 5.2. Thien et al.'s (2016) experiment just presents an experimental model of the actuator with only a top surface. Additionally, the main function of a sensor adopted in their experiment is gesture detection, but it is not actually specialized in distance detection. Consequently, the researcher decides to use an infrared proximity sensor provided by Adafruit company because it has compact dimensions and adaptable working range within 200mm. The operation of this sensor relies on receiving the reflected infrared light from the measured object. The sensor is also small enough to be embedded into the actuator because its bounding dimensions of the printed circuit board (PCB) are 18mm x 16.5mm, and the maximum thickness of PCB with the tallest surface-mount technology (SMT) component included is only 3.15mm. However, the sensor value and detected distance are in an inverse proportion. It means that when the object gets close to the sensor, the sensor value is large. When the object is far from the sensor, this value is small. Moreover, this dependency is non-linear, and there are no general equations to transfer from the sensor value to the distance unit and vice versa. It is therefore important to work out a conversion equation or a regression function between the raw sensor value and the detected distance.

The rigid bridge which has a configurable height is set up to measure various values. The experiment is conducted in three steps as follows:

- Step 1:Preliminary measurement of the height. The sensor is set up to measure the height of the bridge at different values.
- Step 2: Measurement of the height of the actuator with the sensor placed outside. The bottom plate of the actuator is transparent so that IR light can pass through.
- Step 3: Measurement of the height of the actuator with the sensor embedded

inside. The sensor is attached on the bottom plate of the actuator.

5.2.1 Preliminary measurement of the height

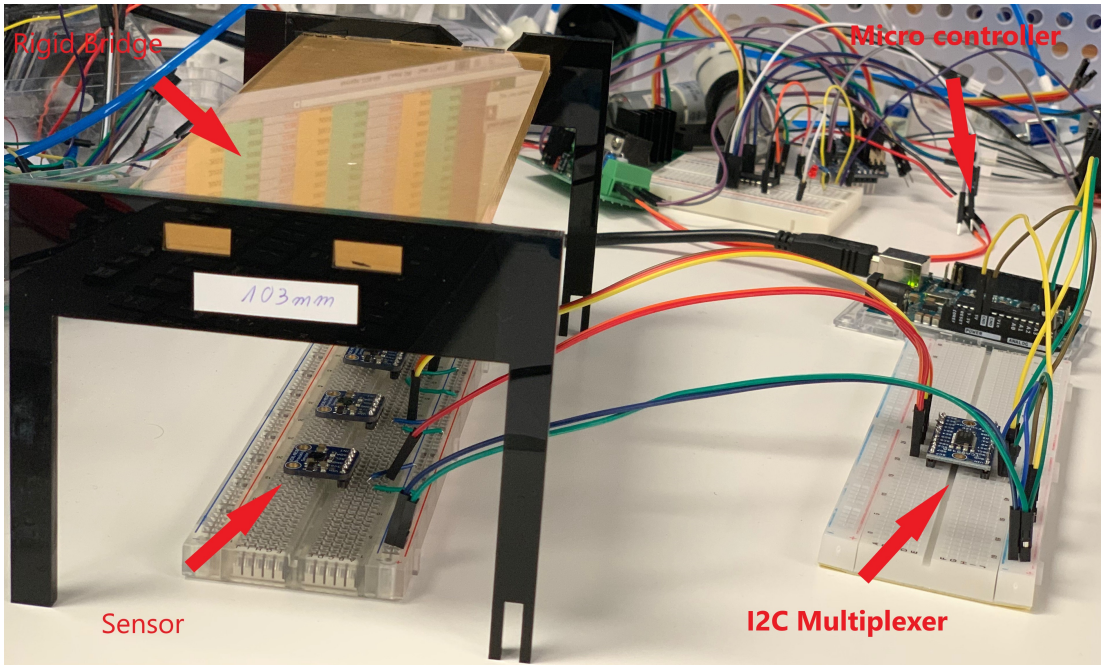

Figure 5.3: Preliminary measurement with bridge

First of all, this experiment is conducted to specify a general equation which can be applied for all sensors. A rigid bridge, which has a configurable height within the sensor's working range, is set up at a specific height. The bridge's height is changed by replacing different legs with a 10mm increment each time. A MATLAB program is written to collect data, the data is stored in a computer. The data is then analysed to investigate the general behaviour of the sensor. Three sensors are adopted at the same time in order to find out a general equation for all sensors, as shown in Figure 5.3. This general equation is to convert raw values of sensors into height unit and helps to develop the closed-loop controller.

5.2.2 Sensor placed outside

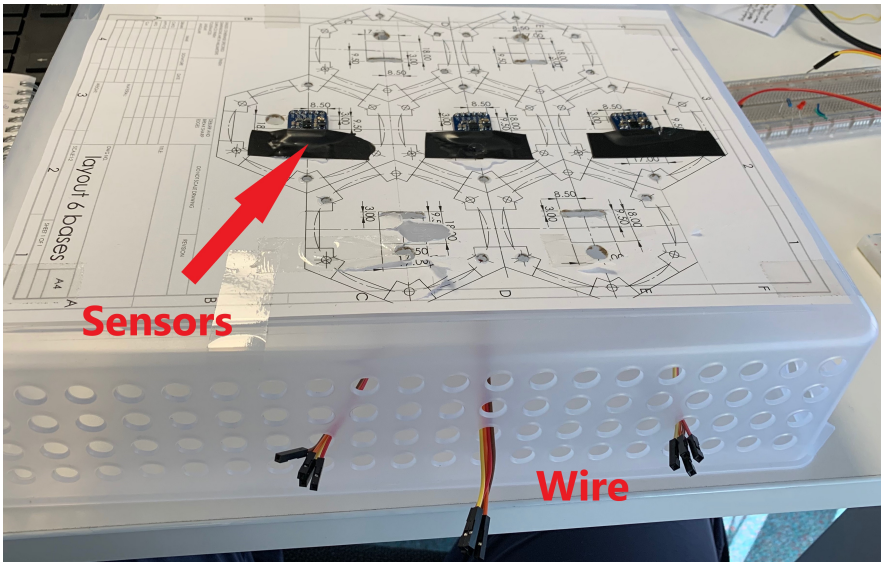

(a) Installing sensors

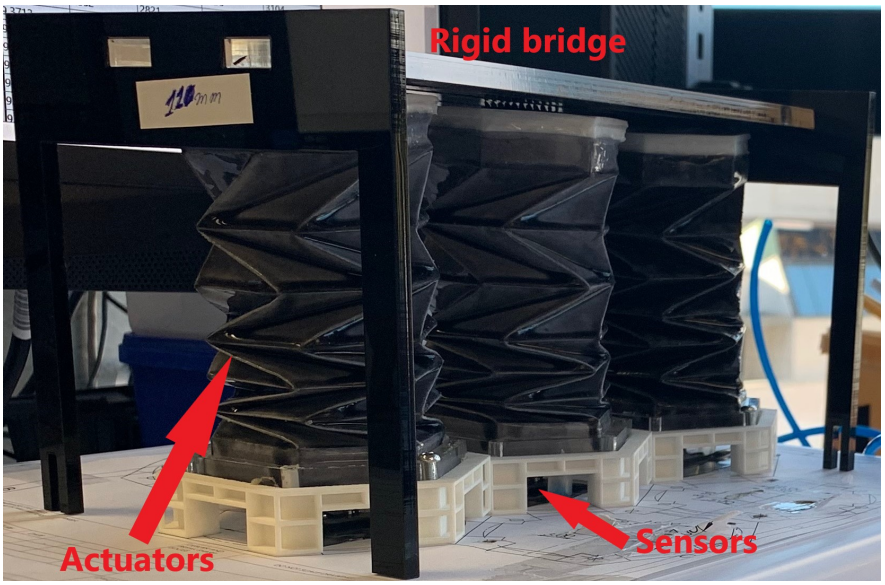

(b) Installing actuators

Figure 5.4: Measurement of height with the sensor placed outside, below actuator and looking upward

The bridge is set up similarly to the above experiment. The increment of the height is also changed by 10mm each time. Three actuators are however placed above the sensor to be tested in each actual condition, as shown in Figure 5.4. A pneumatic

system is attached to push these actuators to reach the height given by the rigid bridge. The support plate that maintains the air pressure within the actuator is made from a transparent Plexiglas with the thickness of 3mm. The IR light emitted from the sensor can pass through this Plexiglas to detect the elongation of the actuator. The sensor data is collected for further analysis.

5.2.3 Sensor embedded inside

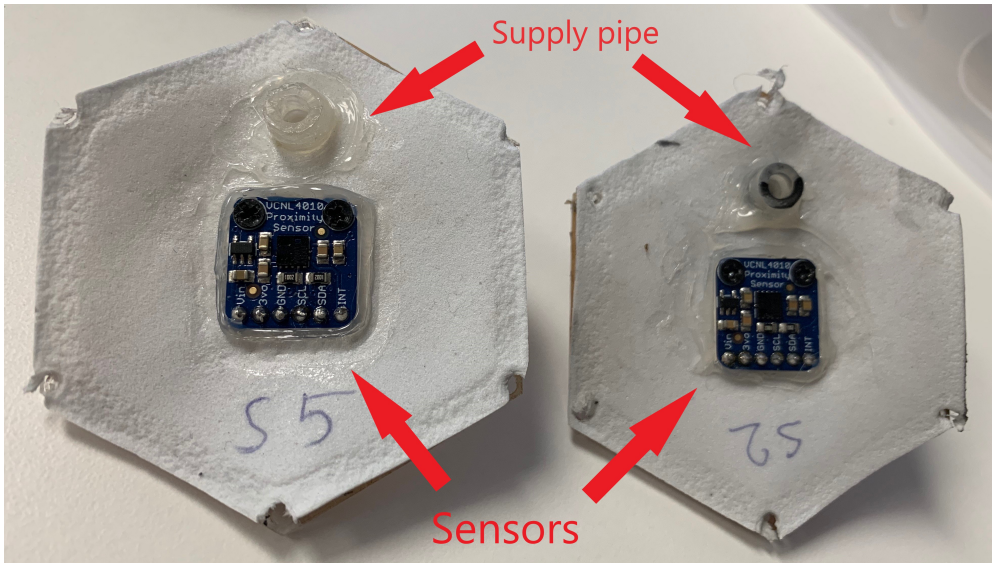

(a) Upside of the support plate

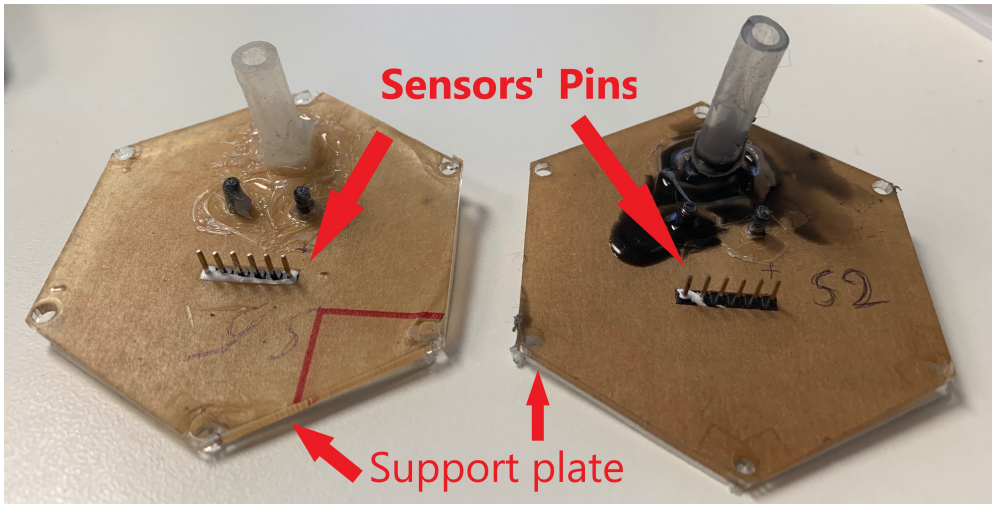

(b) Downside of the support plate

Figure 5.5: Sensor mounted on support plate before placing inside actuator

Thirdly, apart from the structure of the bottom support plate, there are no other changes made in the parameters in the experiments. A sensor is mounted above the bottom support plate by screw. Sensor's connecting pins and air supply pipe are drilled through this support plate to connect to the outside. A gasket is located in between the sensor and support plate to restrict the air leaking outside, as shown in Figure 5.5. Silicone glue is added to contact areas between the sensor and the support plate, and between the supply pipe and the support plate to improve the air tightness of the actuator.

5.3 Experiment 3: Testing of colors of inside sidewall

Colour painted on the sidewall is another significant factor which affects the overall performance of the sensor. White colour is proposed as the best colour for the reflecting surface, as shown in Figure 2.10 (Thien et al., 2016), only effect of the upper layer's colour is investigated in his research. In this current study, three colours of the sidewall are investigated. Three different colours are whole black, black-white, and whole white, all of which are shown respectively in Figure 5.6. The whole black sidewall and white sidewall are fabricated in the same method; however, they are pigmented in different colours. Meanwhile, the hybrid sidewall is split into two separated parts. The higher part of the origami cylinder which is connected to the upper layer is pigmented in white. It means that the white area above the sensor is significantly increased compared to that of the wholly white upper layer. The lower part of the origami cylinder which is connected to the bottom layer is pigmented in black colour. When two parts are created successfully, they are stuck down together. Finally, the sensor is embedded inside this actuator to sense the elongation of the actuator.

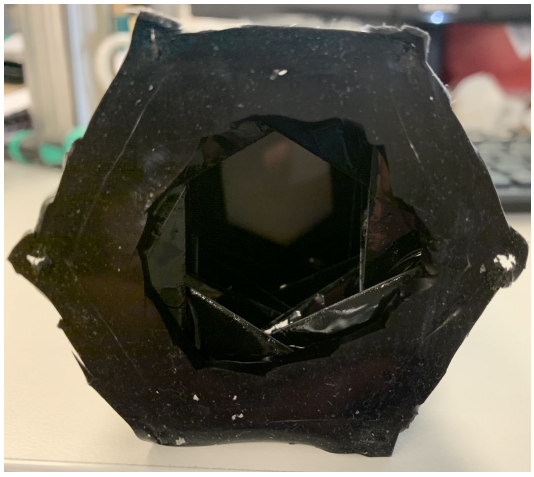

(a) Whole black

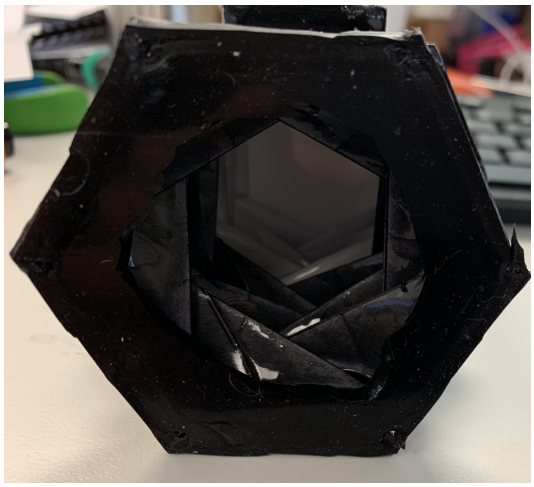

(b) Hybrid black-white

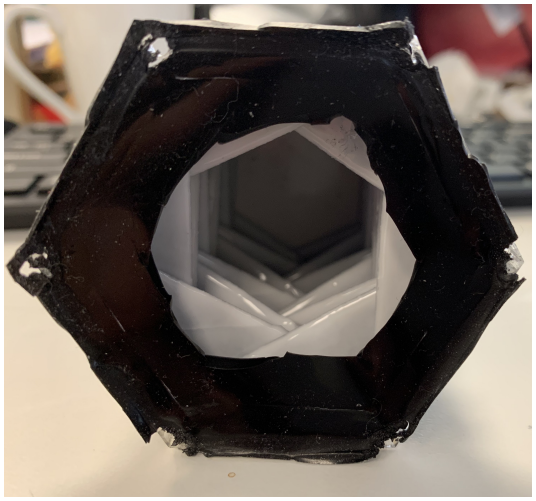

(c) Whole white

Figure 5.6: Colouring sidewall

In this case, the same sensor is used with three different sidewall colour so that sensed data may be consistently compared with the main focus on the effects of the sidewall colour on the sensor performance.

5.4 Experiment 4: Testing of control parameters

In this research, linearizing the soft actuator and constructing a PID controller need to be considered since they affect system performance.

5.4.1 Plant model

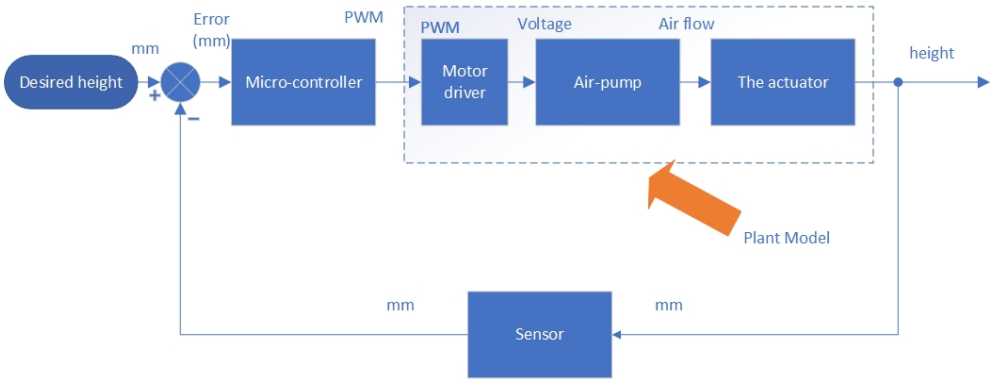

Figure 5.7: Plant model

A plant model that represents the motor driver, air pump, and actuator is shown in Figure 5.7. When the actuator is commanded to travel to a specific height, the micro-controller calculates the distance between the current position and the desired height by the proximity sensor. The output of the controller is a pulse width modulation (PWM) duty cycle which is then fed into a motor driver. This value is directly proportional to the voltage applied to the air pump. An equivalent airflow is either inflated or deflated to make the actuator go upward or go downward respectively. However, the soft actuator is the non-linear object in the control process because of the characteristics of the soft materials. It is hence challenging to present a transfer

function or a state-space equation of the soft actuator. Within the scope of this research, a lookup table representing the characteristics of the soft actuator is therefore proposed.

From the principle mentioned above, this experiment is set up to reveal the relationship between a PWM duty cycle applied to the motor driver and the velocity of the actuator at the specific height. With these manufacturing specifications, the actuator is able to work within a range from 50mm to 140mm. A control program is written in Arduino IDE to monitor the distance by which the actuator can travel in every three seconds at the specific PWM duty cycle value. This experiment is shown in Figure 5.8.

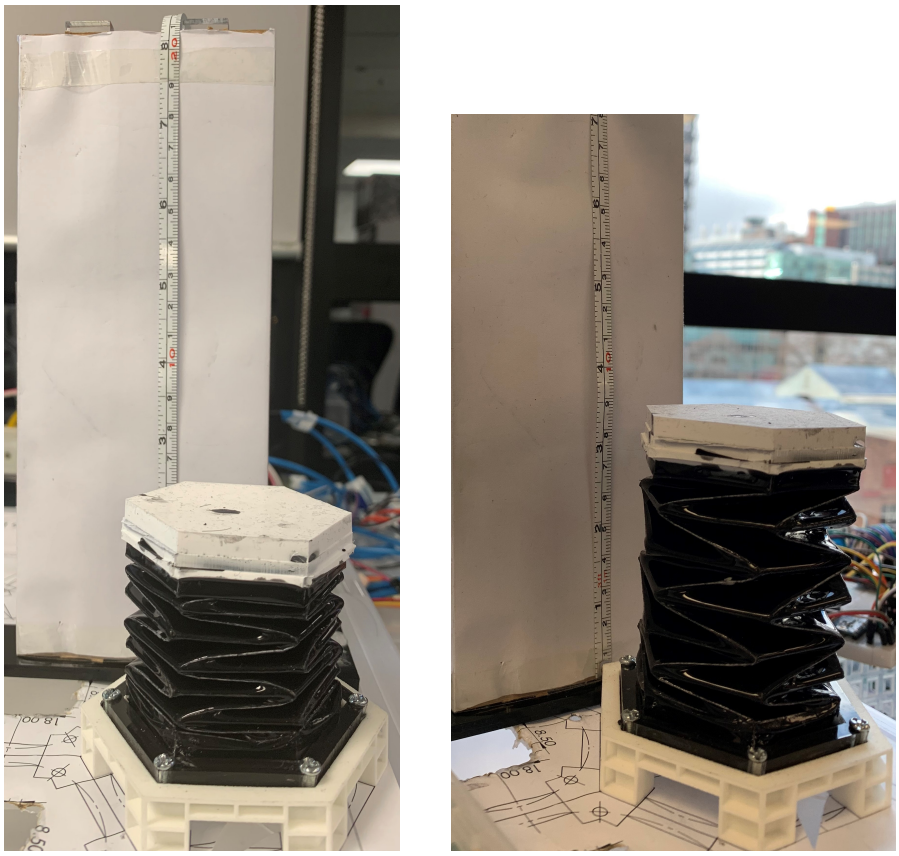

Figure 5.8: Measuring configuration

A ruler is set up in the vertical direction. The first position of the actuator is at the

minimum height of around 50mm. A specific PWM value is programmed and supplied to the motor driver. The air pump injects an amount of air into the actuator. Every three seconds, the actuator's height is recorded manually until it reaches the maximum height. The increasing velocity of the actuator is recorded along with the specific PWM value. When the actuator reaches the maximum height, the air pump function is reversed from inflating to deflating. The actuator then goes down with the same PWM value. The decrease in the velocity is recorded every three seconds in a similar method. This process is repeated with 12.5% increment in the PWM value. All velocity values are saved in a data file for further analysis so as to determine the best parameters of the plant model.

Within the above-mentioned experiment, the measurement process is conducted several times with the same air pump and actuator. However, to propose a plant model of the soft actuator, a typical value of the PWM signal of 50% is chosen. Because this value accounts for 50% of the air pump's power, it clearly shows the changes in the height of the actuator in the whole operating state. Consequently, it is considered the representative value for the actuator's operation.

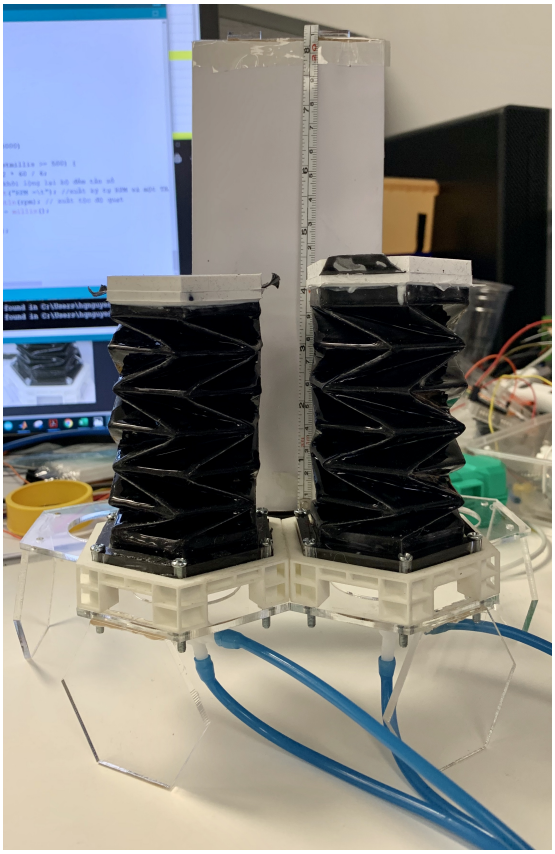

Figure 5.9: Measuring configuration with two actuators

Additionally, two other pairs of the air pump and actuator are tested in the same method, as shown in Figure 5.9. They are named actuator 3, air pump 3, actuator 6, air pump 6. After that, air pump 3 and air pump 6 swap their positions to create two new pairs including actuator 3 and air pump 6; actuator 6 and air pump 3. After that, these two new pairs are measured in the similar method.

5.4.2 PID model

The approach adopted in this experiment is to determine the most suitable set of three gains of proportional, integral, and derivative component in the PID controller. When the desired height is set up, the controller measures the current height of the actuator and compare it with the desired height. An error value is calculated by the subtraction

between the desired height and the current height. This error is then fed into the PID controller to get the equivalent velocity value. The P, I and D gains are calculated so that the actuator can reach the desired height as fast as possible. The current height frequently changes until reaching the desired height, and the controller has to respond properly to these changes and sends out adaptive control signal during the operating process.

A simulated model is constructed in MATLAB/SIMULINK software to investigate gains of the PID controller, as shown in Figure 4.17. There are two PID controllers adopted to measure responses from the system including continuous time PID controller and discrete time PID controller. A tool, called PID tuner, in the software supports to determine these gains of the PID controller. The criteria for the PID controller in terms of rising time, settling time, overshoot, and closed-loop stability are taken into consideration. After analysing trade-offs among these criteria, the most appropriate P, I, D gains are finally selected.

5.5 Experiment 5: Testing of movement design

The purpose of the experiments is to verify how the Tabbot manipulates the objects in translational movement and rotational movement. Thanks to the improvements in the design of the origami actuator, this table is capable of manipulating not only round objects but also square objects. Manipulating the round objects is quite simple because the friction between the objects and the table's surface is small. However, the square objects have a large contact area with the table's surface. The friction in this case is larger. Hence, this experiment is implemented on the square object, as shown in Figure 5.10.

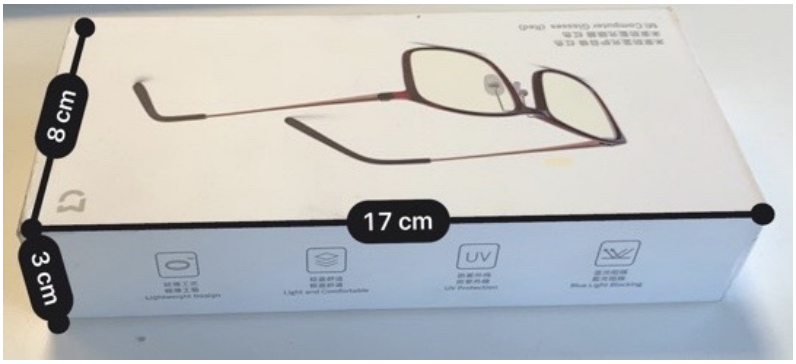

Figure 5.10: Square moving object

A camera recorder is set up to capture the movements of the object. Evidence of the whole moving process is saved for further analysis of the object's movements.

Figure 5.11: Configuration of translational movement

A square object is put on the Tabbot's surface, and ruler is set up to monitor the translational movement of the object, as shown in Figure 5.11. A control program is applied to the micro-controller to monitor the system. The translational movement and rotational movement are tested sequentially. The operation states of the system and the object's movement is recorded for further analysis.

In this part, based on the feedback signal from the IR sensor, the height of the actuator is sensed to control the actuator to reach the desired positions. The operation states of the Tabbot are monitored automatically. It means that the drawbacks found in the previous studies have been handled by adopting the closed-loop controller and having the IR sensor embedded inside the actuator. Furthermore, the PID algorithm is also developed to support the actuators to travel faster and more precisely.

These experiments are significant to determine the behaviours of every single component. This research manages to determine a movement algorithm to manipulate the object in both of translational and rotational movement. The results are going to be discussed in the next chapter.

Chapter 6

Analysis and Discussion

This chapter begins with an overview of the findings of the experiments undertaken for this thesis. These results are compared with those from other studies reported in the literature. Then the implications for the operation of the actuators are considered, addressing the questions of how to create translational and rotational movements in the top surface of the Tabbot. This is followed by a discussion of the sensor placement to provide accurate measurement of the actuator's elongation to give answer to the second research question. Finally, it shows how the deformation of actuators can be controlled in the closed-loop controller to demonstrate the correct functioning of the system.

6.1 Soft origami actuator

The objectives of this research is to manufacture a soft origami actuator with a sensor embedded inside, so several experiments have been conducted with regards to the air leakage of the actuator, sensor placement, and effects of sidewall colour.

6.1.1 Discussion on air leakage of actuator's designs

Based on the results of experimental testing on the air leakage and how to attach an IR sensor to the actuator, three designs are investigated. Design 1 and design 2 are fabricated by coating silicone rubber on both sides of the origami cylinder. The upper layer is stuck down the origami cylinder in design 1. The upper layer of the design 2 is dipped in the origami cylinder and sealed by silicone glue. Since they are not able to stand straight up, their bending pattern is unpredictable and changeable in different models, as shown in Figure 4.9. Especially, the air leakage errors occur at the contact seam on the top side in both of design 1 and design 2, as shown in Figure 6.1. Design 1 does not have the bottom layer, so the origami cylinder is instead directly stuck down the support stage. The air also leaks out at either the top contact area or the bottom contact area. In design 2, the bottom layer is added into the origami cylinder, so the contact area between the bottom layer and the support stage is substantially increased. The clamping force from the screw and pressure inside the air chamber are the primary forces to improve the air tightness at the bottom position. However, the weak point of design 2 is that the upper layer is sealed by glue, thus causing the air leakage at this point, as shown in Figure 6.1b.

(a) Air leakage in design 1

(b) Air leakage in design 2

Figure 6.1: Air leakage errors

In addition, the actuator needs to stand upward so that the emitted light of the sensor can go straight to the upper layer without being bent. However, inhomogeneity in the actuator's shape is found in design 1 and design 2. In particular, they bend in different directions. It is therefore very difficult to detect the height of the top surface. These

different bending patterns also cause errors in the measuring process of the sensor. When the emitted light from the IR proximity sensor partly reaches the top surface, it is then reflected back to the sensor receiver. When the top surface is inclined, the reflected light is reflected back to the sidewall rather than to the sensor receiver. In short, design 1 and design 2 do not function correctly because of the air leakage and unexpected bending.

The origami cylinder of design 3 is sunk into a silicone liquid, and half of the upper layer is dipped in the origami cylinder. Moreover, the entire origami cylinder is also dipped in the silicone liquid. The silicone excess splits out of these surfaces and drops off on the ground. Thanks to the gravity force, the density of the silicone rubber coated on the actuator is homogeneously distributed. As a result, the actuator is able to stand straight up. It, therefore, helps to create a proper reflecting surface, and IR light can reach the top surface with fewer disturbances. The emitted light is reflected directly back to the sensor when it reaches the upper layer without any losses of energy at the sidewall. Hence, the measurement shows higher accuracy, and the system operation is more stable and reliable. To sum up, design 3 presents the highest air tightness and ability to stand straight up along the vertical direction.

6.1.2 Effects of sensor placement

The experiments is to determine what is the best position to mount the sensor. Two major positions including inside and outside the actuator are considered. However, a sensor calibration is necessary to calibrate the sensor in advance. Sensor calibration is helpful to support follow-up experiments to determine the regression function of the sensors.

Sensor calibration

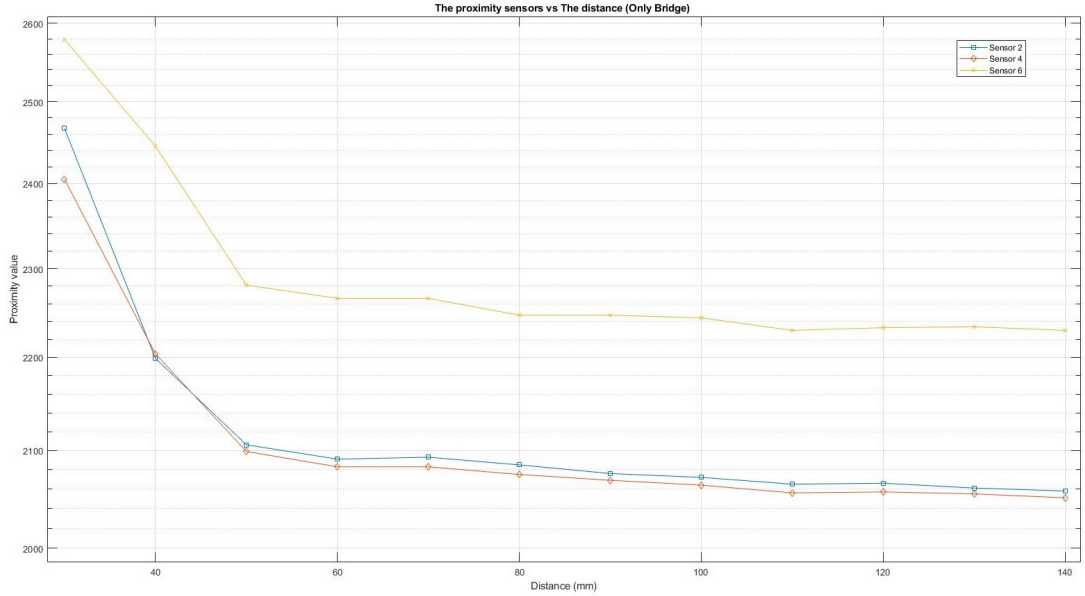

Figure 6.2: Results of sensor calibration

In these experiments, the sensor placement is investigated to determine the best position. The first step is to set up the general configuration to measure the height. The preliminary results of the measurement without actuators show the height detection of sensors, as shown in Figure 6.2. Three sensors are used at the same time; they are called sensor 2, sensor 4 and sensor 6. Generally, the behaviour lines of sensors follow the same pattern. However, an offset value is seen among different sensors. This offset value is small between sensor 2 and sensor 4. Meanwhile, a marked difference is recorded between sensor 6 and the other sensors. The closer the bridge approaches the sensor, the higher sensor value is. The sensor value for sensor 2 decreases dramatically to nearly 350 raw units in the first 20 millimeter, from 30mm to 50mm. In the next range, the value of sensor 2 reduces gradually by about 40 raw units from 2100 raw units at 50 millimeter to 2060 raw units at 140 millimeter. It means that with a wide working range of about 90mm, the sensor value reduces slightly by just only 40 raw units. These changes are similar to those recorded for sensor 4 and sensor 6. It is therefore difficult to distinguish

the changes in the actuator's height within the working range from 50mm to 140mm.

To sum up, the behaviour line of each sensor is in a similar pattern. Because of the offset value, a calibrating process of the sensors is necessary. It is required to bring the different values of sensors back to the same coordinate system. With the similar pattern of the behaviour line, it is possible to build up a general regression function to convert the raw sensor value to the length unit.

Sensor placed outside the actuator

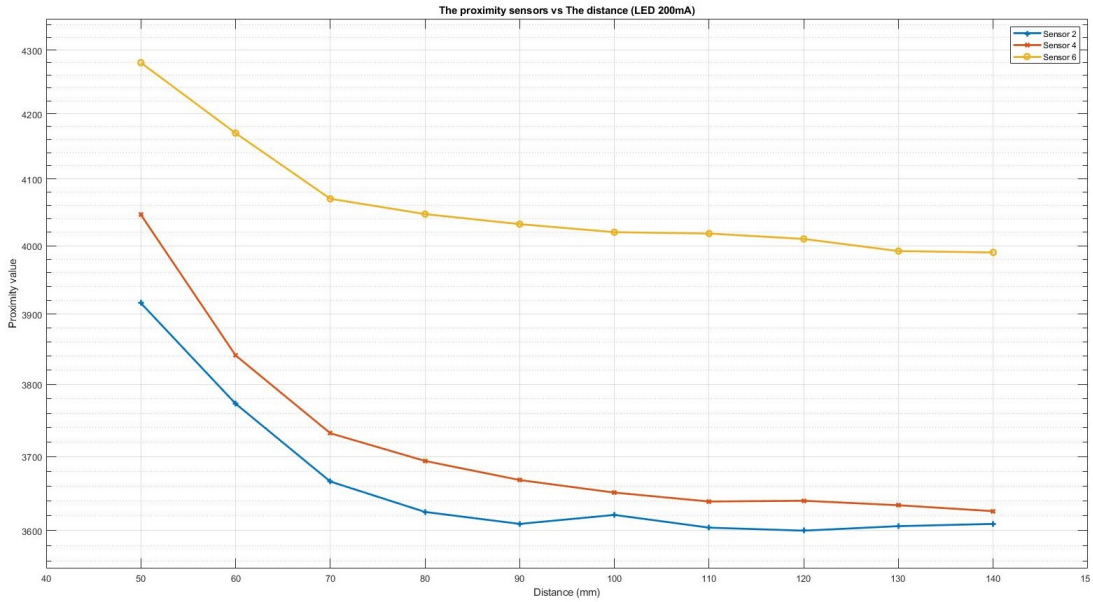

Figure 6.3: Sensor placed outside actuator

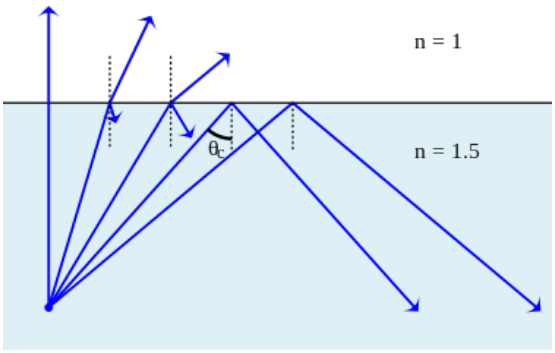

Figure 6.4: Refraction law

A support plate that is used to hold the actuator is made from a transparent plexiglas of 3mm thickness. The sensor is placed under this plexiglas at 10mm height, and the direction of emitted light is perpendicular to the plexiglas. This emitted light is able to pass through the plexiglas and reach the top surface. The behaviour line of the sensor is shown as in Figure 6.3. In general, the behaviour lines of these sensors follow a similar pattern. However, these sensor values significantly increase, doubling the values which are recorded in the previous experiment of fundamental measurement. The increase in sensor values is resulted from the fact that the plexiglas is placed above and close to the sensor. Indeed, when the emitted light passes through the boundary between two different environments, the direction of emitted light is changed in accordance with the Snell's Law, as shown in Figure 6.4. A small density of emitted light is reflected immediately after reaching the boundary of the plexiglas. When the emitted light that passes through the plexiglas reaches the top surface, it is then reflected again. This reflected light approaches the boundary between two different environments, and is refracted, following the Snell's Law.

Consequently, the total energy of reflected light considerably increases. When the actuator elongates within the range from 50mm to 100 mm, its behavior line shows a steep incline; therefore, the height of the actuator is measured with higher accuracy

than that in the first experiment for sensor calibration. Nevertheless, when the actuator goes far away from 100mm to 140mm, there are insignificant changes in the behaviour line of the sensor 2, specifically from 3610 to 3600. This change is only 10 sensor raw units because of the disturbances from the refraction process. It is therefore very hard to measure the changes in the height of the actuator within this range.

Sensor embedded inside the actuator

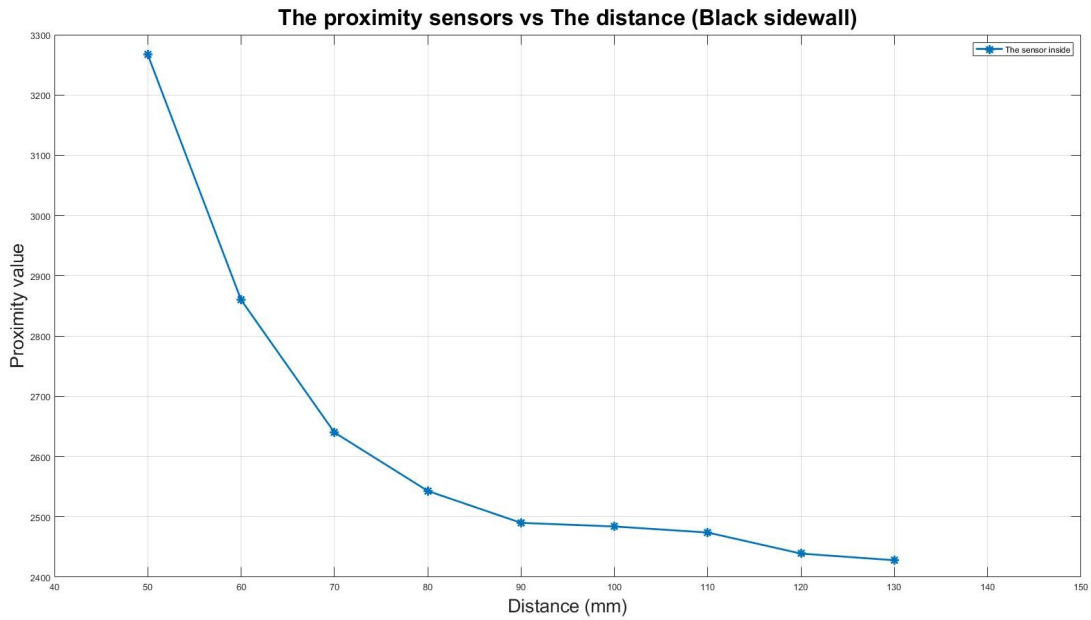

Figure 6.5: Sensor embedded inside actuator

In this experiment, the sensor is placed inside the actuator. It means that there is no obstacle in between the sensor and the actuator. Most of the emitted light travels to touch the top surface, and the density of reflected light is higher, as shown in Figure 6.5. The behaviour line that shows the changes in the height of the actuator within a range from 50mm to 130mm, changes dramatically to nearly 850 sensor units, from 3280 to 2430. This value increases by approximately threefold compared to the value that is recorded in the experiment with the sensor being placed outside the actuator. In addition, the behaviour line from 90mm to 130mm is shown with steep gradient since

the sensor value decreases considerably by about 100 sensor units.

Figure 6.6: Assembly of actuator and sensor

From the above-mentioned findings, it can be concluded that the sensor placed inside the actuator presents the best performance. Technically, disturbances from the environment are removed. With regards to the criteria about the air tightness and sensor placement, design 3 is finally selected, as shown in Figure 6.6. There is a support plate above which the sensor is mounted on top. The connecting pins and supply pipe are drilled through this plate to connect to the outside. These components are linked by screws for the easy assembly and maintenance.

6.1.3 Effects of sidewall colour

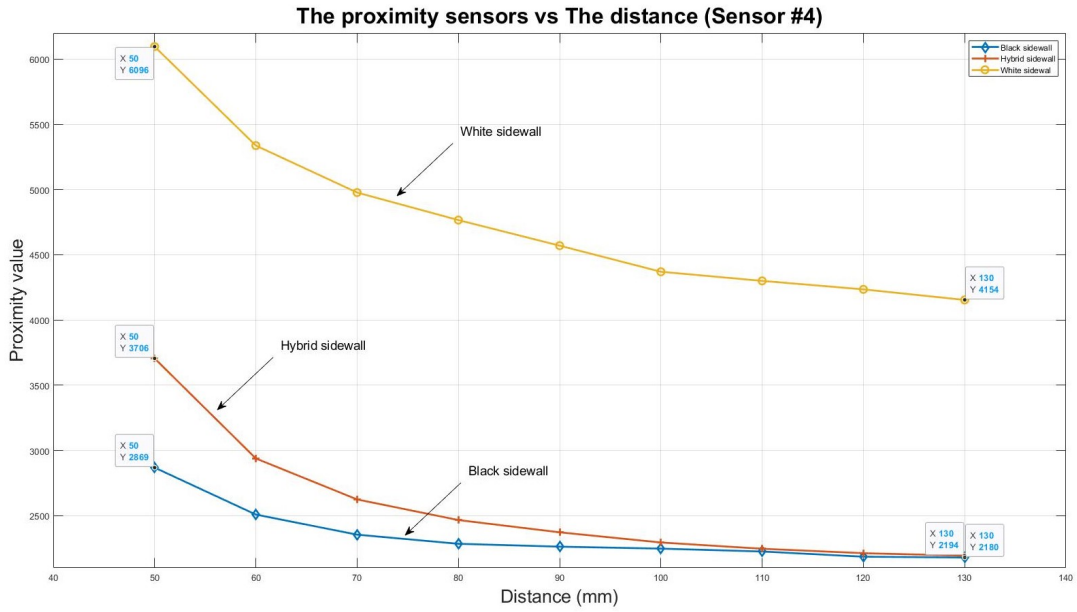

Figure 6.7: Colour effects on sidewall

Three experiments have been conducted to validate the effects of the sidewall colour. These findings are shown in Figure 6.7. Generally, the shape of the sensor's behaviour lines are quite similar. They drop fast in the first 30mm, and then, reduce gradually in the next range. In the case of the black sidewall, only the upper layer is pigmented in white colour, and sidewall around is pigmented in black. The black colour can highly absorb energy from IR light, so a part of reflected light is absorbed by a black sidewall, which reduces the density and energy of the reflected light. In particular, if the sidewall is painted in black color, in the working range of actuator from 90mm to 130 mm, the working range of sensor is only 100 raw units. On the other hand, when the white-painted area of the sidewall is larger, the density of the reflected light also rises proportionally. The white area spreads out to account for 50% of the sidewall, the working range of sensor from 90mm to 130 mm is 206 raw units, from 2400 to 2194. This value is twice as large as that recorded for the black sidewall. Finally, when

the whole sidewall is pigmented in white, the whole working range of sensor from 50mm to 130 mm increases and reaches 1942 raw units, from 6096 to 4154 raw units, as shown in Figure 6.7. This value is nearly threefold larger than that recorded for the black sidewall and larger than that recorded for the black-white sidewall by 20 percent. Especially, within working range of sensor from 90mm to 130 mm, the white sidewall presents the best performance when its value is nearly 450 raw units in comparison with 206 raw units of the black-white sidewall and 100 raw units of the black sidewall. The conclusion here is that the actuator with the whole inside sidewall painted in white shows the best performance.

To generalize the results from these experiments, various sensors have been tested with the whole white sidewall. The experiments' results show that the behaviour lines of the sensors similarly have steep gradients, especially when the actuator goes far away within range from 90mm to 130mm, these working range of sensor 2, sensor 6, and sensor 9 are approximately 550, 450, and 500 raw unit respectively, as shown in Figure 6.8. Therefore, the white colour is finally proved to be the most appropriate for this design.

Based on the findings of these experiments, with the reference to the studies conducted by Thien et al. (2016) and Mollah (n.d.), it comes to the conclusion that the white colour pigmented on the whole inside of the air chamber brings about more effective performance of the IR proximity sensor.

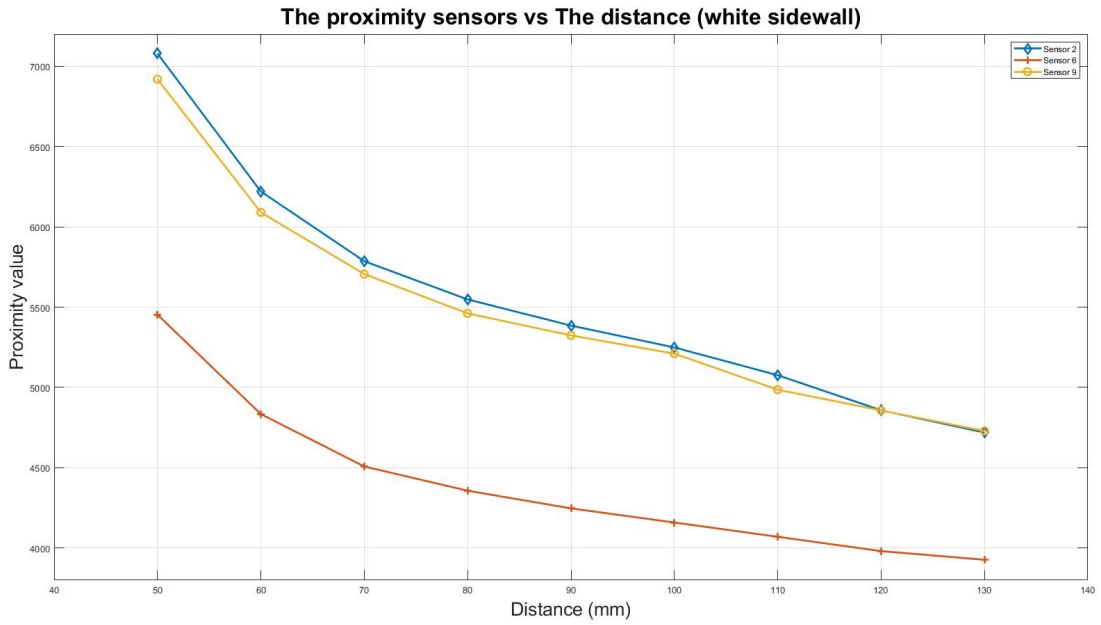

Figure 6.8: Behaviour lines of three different sensors with white sidewall

To sum up this section, the soft origami actuator with white sidewall and embedded IR sensor has been finalized, as shown in Figure 6.6. It suffices to meet the requirements of the research with regards to the air tightness, easy assembly, easy maintenance, and accurate measurement of sensor's height. This proposed model has sorted out the drawbacks that are revealed in the previous studies. The Braille design (Mosadegh et al., 2014) is only capable of working with round objects by inflating air into balloon actuators. The design of Deng et al. (2016) is improved since it is able to manipulate the flat objects. However, both of these designs are subjected to the deformation characteristics of the surface layer. It leads to the limitations in their working range because the actuators are not capable of expanding to a large area. Maratas's design (2018) introduces an origami actuator which is capable of working in a wider range. However, his model shows several drawbacks regarding the manufacturing and control process. The proposed model in this research has been inspired by the origami structure of Maratas's (2018) prototype to enhance the contraction and extension ability of the actuator. It is not only creating the surface deformation but also elongating this surface

in a larger range following the vertical direction. Consequently, the Tabbot wave that is made on the top surface by the elongation of the actuators has larger amplitude and changeable phase.

Finally, it is evident that the practical model with embedded IR sensor has been produced successfully based on the designs and the principles raised in the previous studies. This research has proposed the new actuator which adopts the state-of-art technique including the origami structure and embedded sensor. It is proved to be easy to install or uninstall the actuator during the operating process, and it can still ensure the air tightness and proper performance. Another important step to build up the table robot is to develop the closed-loop controller.

6.2 Testing control system

There are three major factors which significantly affect the performance of the control system: finalizing a regression function of the sensor, linearizing a soft actuator model, and developing a PID controller. These factors are discussed in this section.

6.2.1 Regression function of the sensor

The sensor that is adopted in this study has a non-linear dependency between the sensor raw unit and the height unit. Therefore, it is challenging for the movement of actuator to be programmed directly with the raw sensor unit, since the desired height of the actuator is difficulty estimated from this raw unit. A regression function is thus necessary to clarify the operation of the control system. When conducting the experiments to test the effects of colors painted on the actuator sidewall and sensor placement, the data about the actuator's deformation are collected to build up a data set of deformation. This data set is analysed to determine the regression function. This regression function is to

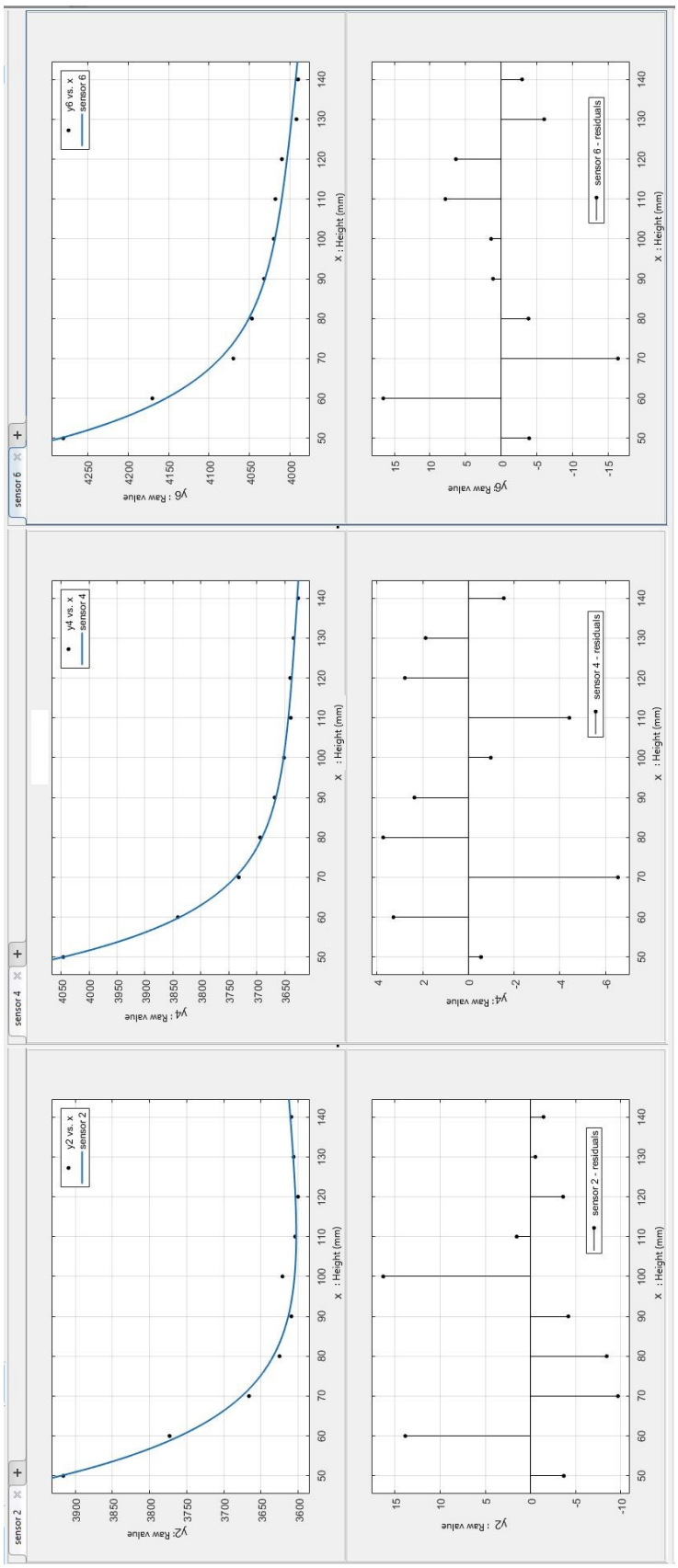

Figure 6.9: Fitting curve of 3 sensors embedded outside

converse raw sensor value into height unit measured in millimeter. A curve fitting tool in MATLAB software is used to maximize the process of determining the regression function.

When the sidewall is painted black, and the sensor is placed outside the actuator, the data collected from three sensors are shown in Figure 6.9. Although the residual in these three measurements is not too large when compared to the fitting curve, the shape of these curves is considered inappropriate. The values of sensors plummets in the first range from 50mm to 90mm. When the height of actuator exceeds 90mm, these fitting curve lines tend to fluctuate slightly, and the gradient of the fitting curve lines within this range is not steep enough to differentiate the actuator's height (i.e. the difference in the sensor's raw values at 90mm and 130mm is about 100 raw units). Consequently, placing the sensor outside the actuator does not show the acceptable result to develop the general regression function of the sensor.

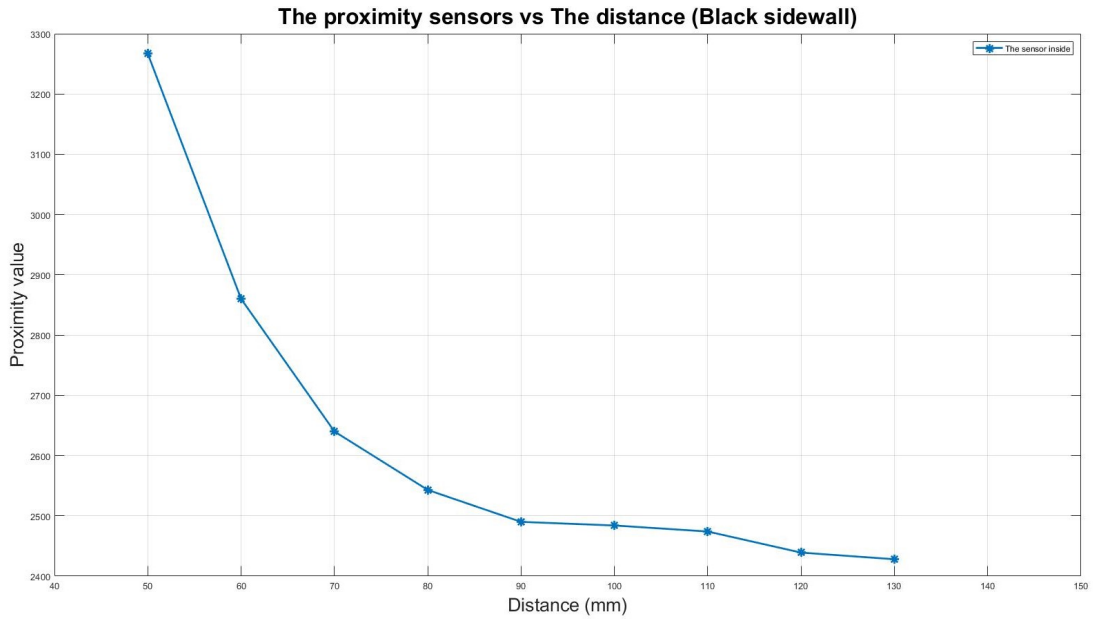

(a) Black sidewall with sensor inside

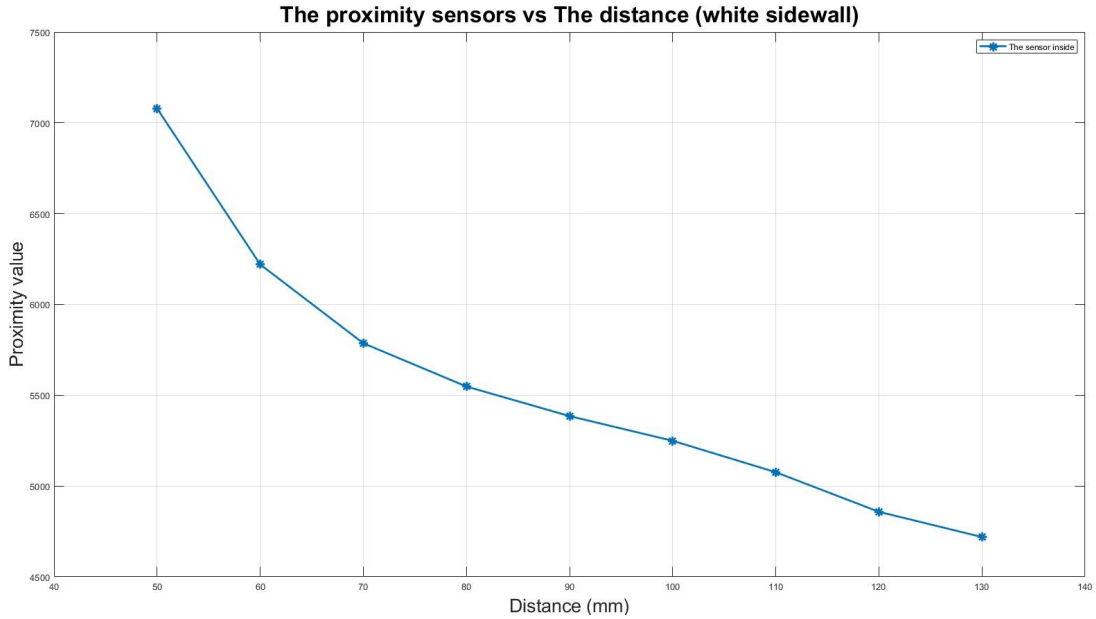

(b) White sidewall with sensor inside

Figure 6.10: Fitting Curve

When the sensor is placed inside the actuator, two colours (black and white) of the actuator sidewall are tested. The data are also collected, analysed, and finally presented in Figure 6.10. The behaviour line of the sensor with white sidewall has steeper gradient

than that recorded for the black sidewall. The behaviour line of the white sidewall is capable of measuring the actuator's height precisely within range from 50mm to 130mm. Based on this result, a regression function is determined to converse from the raw sensor value to the height unit. Several regression functions are studied including polynomial, power, rational, exponential, and Fourier form. For example, in the sensor 2 with the white sidewall, as shown in Figure 6.11, several regression functions are presented in the equations as below:

- Polynomial equation degree 2

$$f(x) = p_1 x^2 + p_2 x + p_3 \tag{6.1}$$

- Exponential equation

$$f(x) = a \exp(bx) \tag{6.2}$$

- Power equation

$$f(x) = ax^b \tag{6.3}$$

- Fourier equation

$$f(x) = a_0 + a_1 \cos(xw) + b_1 \sin(xw) \tag{6.4}$$

The constants in these equations that are generated by the Matlab software include $p_1, p_2, p_3, a, b, a_0, a_1, b_1$. The variable x is the representative for the raw value of sensor, and the variable f(x) is the representative for the height units measured in millimeter.

To determine which fitting curve best illustrates the operating characteristics of sensors and actuators, both graphical and numerical fits need to be examined. The criteria with regards to the sum of square due to error (SSE), the square of the correlation

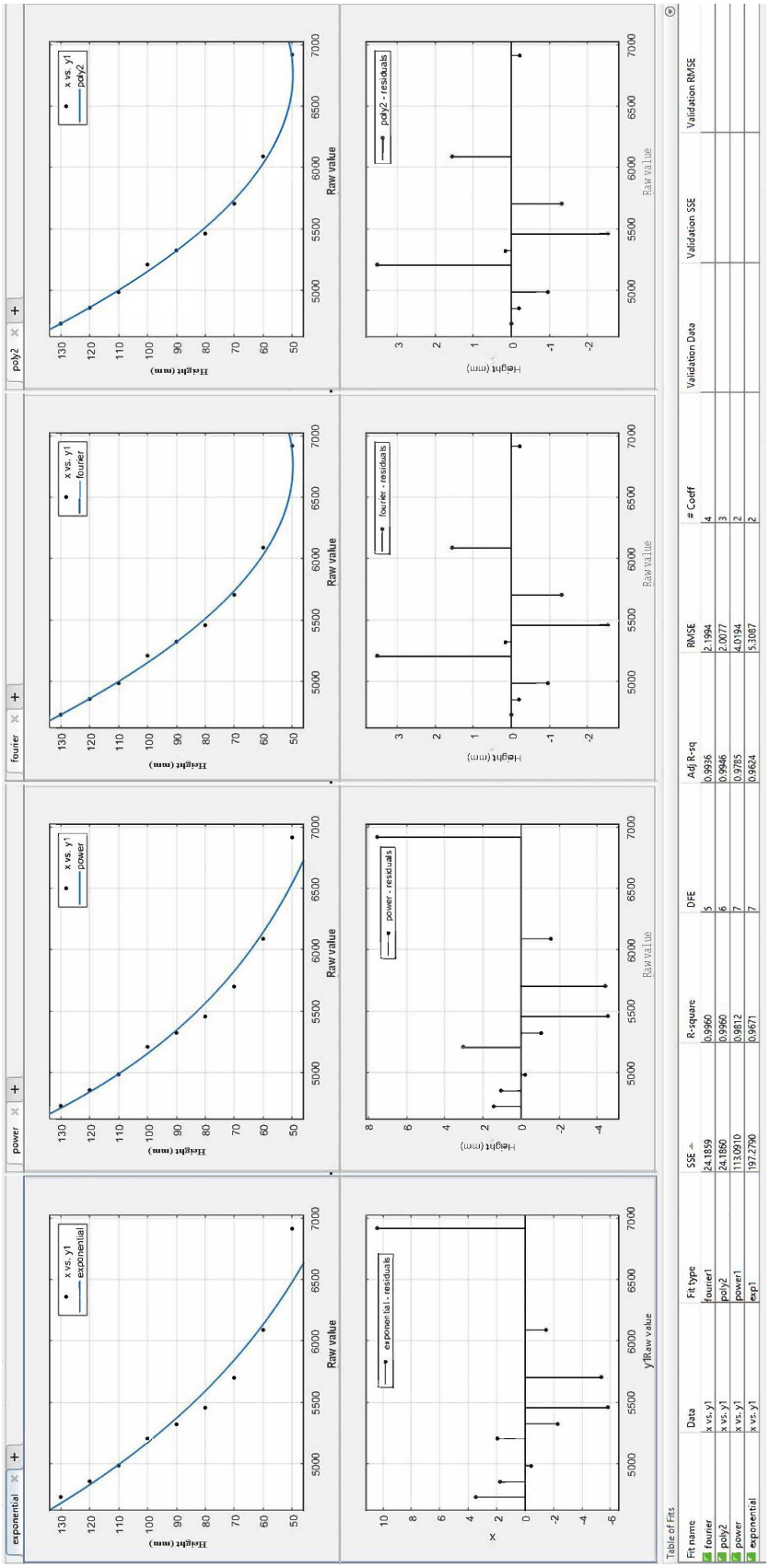

Figure 6.11: Form of regression function for sensor 2

between the response values and the predicted response values (R-square) are considered. When SSE value is close to zero, and R-square value is close to 1, the fitting curve is the most appropriate to represent the behaviour line of the sensor. Also, the roots of these equations are also considered since they affect the real value of the sensor after being conversed from the raw unit to the height unit.

Based on these findings, the power form has its SSE approach nearly zero (at 113.0910), while the values of the fourier, polynomial degree 2, and exponential form are 24.1859, 24.1860, and 197.2790 respectively. R-square of the power form is nearly to 1 (at 0.9812), while R-squares of fourier, polynomial degree 2, and exponential form are 0.9960 0.9960, and 0.9671 respectively. However, the graphical fitting curve of the power form provides the best illustration of the operating characteristics of sensors and actuators since their gradient is steeper than those observed in the other curves. Furthermore, the root of the power form is single, thus giving higher accuracy in the conversion.

To validate the application of the power form in developing the regression function, four different sensors are tested. Since each sensor has its own working range, it is challenging to determine one specific equation applied for all sensors. Therefore, it is only possible to determine a general form of equation to calibrate these sensors according to their characteristics. The data related to fitting curves of various sensors are shown in Figure 6.12. All of the fitting curves present good values of SSE and R-square which are close to 0 and 1 respectively. Additionally, their gradients are steep enough to differentiate the height of the actuator when the actuator goes far away. In short, the power form of the regression function is concluded as the best for the conversion from the raw units of the sensor to the height units.

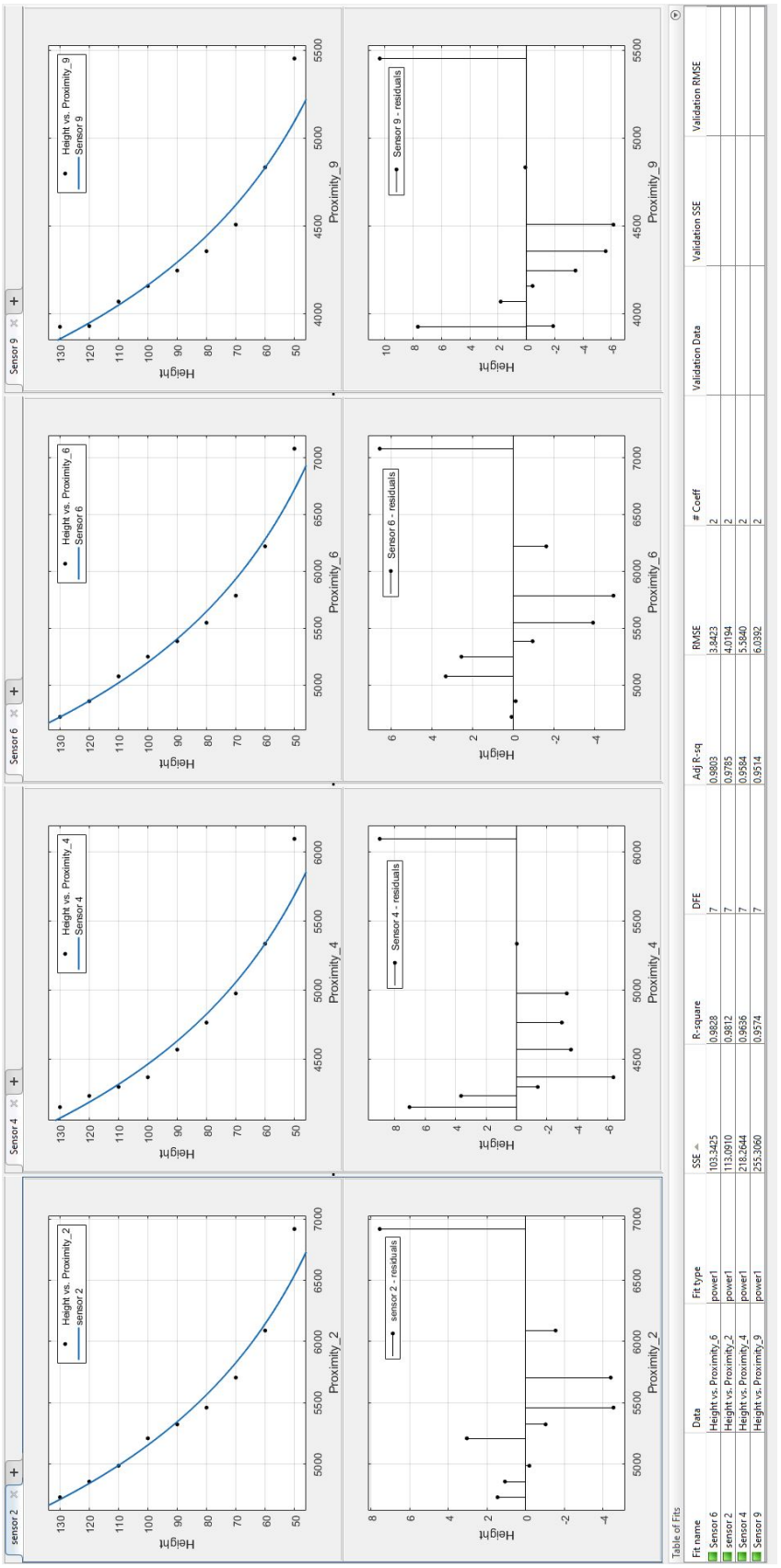

Figure 6.12: Regression function of sensors

In conclusion, the experiments have sorted out two issues related to using non-linear sensors in this research: the feedback signal and non-linear value of the sensor. The general form of the regression function of the sensor is proposed. This form of regression function is applied to create the feedback signal and linearize non-linear characteristics of the sensor to support the control code programming.

6.2.2 Linearizing a soft actuator model

Table 6.1: Dataset of velocity of actuator

No	PWM (%)	Time (s)	inflate			deflate		
			postion start (mm)	postion stop (mm)	velocity up (mm/s)	postion start (mm)	postion stop (mm)	velocity down (mm/s)
1	0.25	3	60	65	1.67	142	138	1.33
2	0.25	3	65	70	1.67	138	134	1.33
3	0.25	3	70	75	1.67	134	130	1.33
4	0.25	3	75	80	1.67	130	127	1.00
5	0.25	3	80	85	1.67	127	124	1.00
6	0.25	3	85	90	1.67	124	120	1.33
7	0.25	3	90	94	1.33	120	117	1.00
8	0.25	3	94	99	1.67	117	112	1.67
9	0.25	3	99	103	1.33	112	108	1.33
10	0.25	3	103	107	1.33	108	102	2.00
11	0.25	3	107	110	1.00	102	98	1.33
12	0.25	3	110	114	1.33	98	92	2.00
13	0.25	3	114	118	1.33	92	86	2.00
14	0.25	3	118	121	1.00	86	80	2.00
15	0.25	3	121	125	1.33	80	75	1.67
16	0.25	3	125	128	1.00	75	70	1.67
17	0.25	3	128	131	1.00	70	65	1.67
18	0.25	3	131	134	1.00	65	60	1.67
19	0.375	3	60	72	4.00	145	137	2.67
20	0.375	3	72	83	3.67	137	131	2.00
21	0.375	3	83	93	3.33	131	125	2.00
22	0.375	3	93	103	3.33	125	118	2.33
23	0.375	3	103	113	3.33	118	110	2.67
24	0.375	3	113	120	2.33	110	100	3.33
25	0.375	3	120	128	2.67	100	90	3.33
26	0.375	3	128	134	2.00	90	79	3.67
27	0.375	3	134	139	1.67	79	69	3.33
28	0.375	3	139	145	2.00	69	60	3.00
29	0.5	3	60	74	4.67	145	137	2.67
30	0.5	3	74	88	4.67	137	129	2.67
31	0.5	3	88	100	4.00	129	120	3.00
32	0.5	3	100	112	4.00	120	108	4.00
33	0.5	3	112	123	3.67	108	95	4.33
34	0.5	3	123	132	3.00	95	83	4.00
35	0.5	3	132	139	2.33	83	70	4.33
36	0.5	3	139	145	2.00	70	58	4.00
37	0.625	3	58	76	6.00	150	139	3.67
38	0.625	3	76	93	5.67	139	129	3.33
39	0.625	3	93	108	5.00	129	118	3.67
40	0.625	3	108	122	4.67	118	103	5.00
41	0.625	3	122	131	3.00	103	89	4.67
42	0.625	3	131	141	3.33	89	72	5.67
43	0.625	3	141	150	3.00	72	58	4.67
44	0.75	3	58	79	7.00	149	136	4.33
45	0.75	3	79	97	6.00	136	123	4.33
46	0.75	3	97	114	5.67	123	111	4.00
47	0.75	3	114	129	5.00	111	96	5.00
48	0.75	3	129	139	3.33	96	78	6.00
49	0.75	3	139	149	3.33	78	60	6.00
50	0.875	3	60	83	7.67	155	141	4.67
51	0.875	3	83	103	6.67	141	129	4.00
52	0.875	3	103	120	5.67	129	115	4.67
53	0.875	3	120	132	4.00	115	98	5.67
54	0.875	3	132	144	4.00	98	78	6.67
55	0.875	3	144	155	3.67	78	58	6.67
56	1	3	58	84	8.67	154	139	5.00
57	1	3	84	108	8.00	139	123	5.33
58	1	3	108	127	6.33	123	105	6.00
59	1	3	127	142	5.00	105	81	8.00
60	1	3	142	154	4.00	81	59	7.33

Although the system is non-linear due to the characteristics of the soft materials, a linearized plant model is developed to simulate the operating process of this actuator. A black box is used to represent the plant model with an input being PWM value and output being the velocity of actuator. The data set of upward velocity and downward velocity is shown in Table 6.1. These data set collected from actual measurements are

analyzed to determine the behaviour velocity of the actuator during its working process, as shown in Figure 6.13.

As shown in Figure 6.13a, the upward velocity has tendency to reduce gradually when the actuator travels from the minimum height to the maximum height. The reduction in upward velocity is clearly presented when the PWM value is set at the maximum power, and the actuator velocity is nearly linearized. However, some slight fluctuations in this velocity value are observed at the minimum PWM value since the resolution of measurement is low. The resolution of the ruler is 1mm, and the travel length of the actuator in each three-second period is from 5mm to 25mm, depending on the PWM value. Small changes in the measurement may lead to considerable errors. As shown in Figure 6.13b, the behaviour of the downward velocity is similar. However, a small difference is recorded in the first segment in which the velocity increases slightly prior to decreasing continuously. This difference is caused by two factors. Firstly, there is a marked difference between flowing pressure and vacuum pressure of the air pump. The flowing pressure is always higher than the vacuum pressure. Secondly, the actuator operates like the spring, so there is an equivalent stiffness coefficient in the actuator *(the stiffness coefficient of the actuator is not investigated in this research)*. This stiffness coefficient restricts the movement of the actuator, so the velocity value tends to reduce when the actuator goes far away from the rest position.

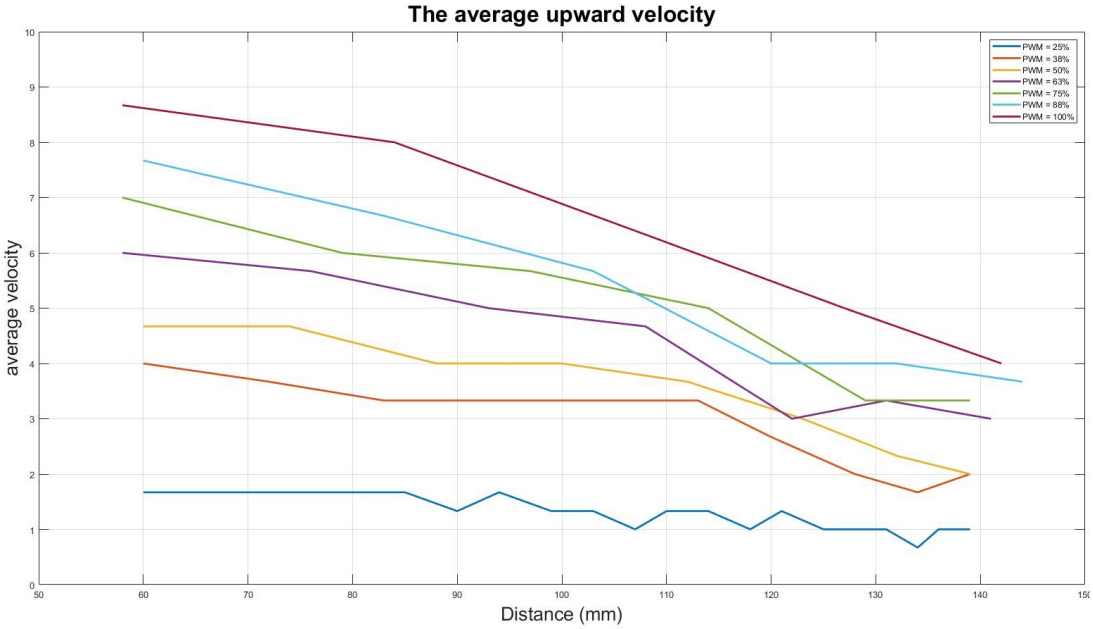

(a) Upward velocity

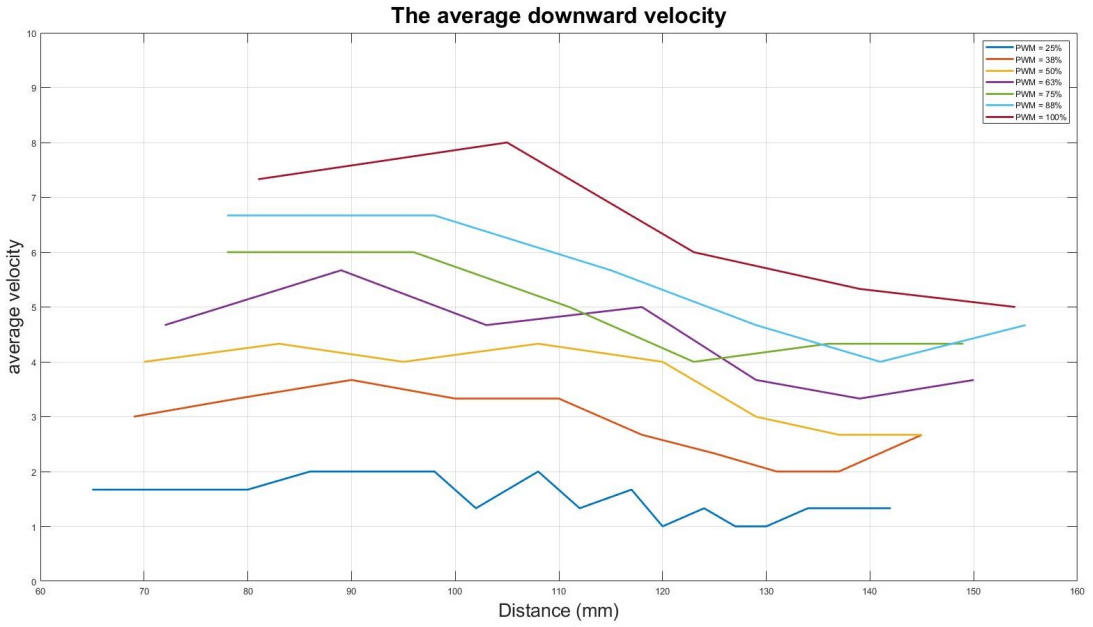

(b) Downward velocity

Figure 6.13: Behaviour velocity of actuator

Based on the above-mentioned findings, a look-up table is proposed, as shown in Table 6.2 & 6.3 to represent the plant model of the physical system including the air pumps and actuators.

Table 6.2: Look-up table of upward velocity

Breakpoints	Column	(1)	(2)	(3)	(4)	(5)	(6)	(7)	(8)	(9)	(10)	(11)
Row		50	60	70	80	90	100	110	120	130	140	150
(1)	0	0	0	0	0	0	0	0	0	0	0	0
(2)	0.25	1.67	1.67	1.67	1.67	1.33	1.33	1.33	1	1	1	1
(3)	0.38	4	4	3.67	3.67	3.33	3.33	2.67	2.33	2	1.67	1.67
(4)	0.5	4.67	4.67	4.67	4.67	4	4	3.67	3.33	2.67	2.33	2
(5)	0.63	6	6	5.67	5.67	5	5	4.67	3.67	3.33	3	2.67
(6)	0.75	7	7	7	6	6	5.67	5.33	5	4	3.67	3.33
(7)	0.88	7.67	7.67	7.67	6.67	6.67	6	5.67	4.67	4	3.67	3.67
(8)	1	8.67	8.67	8.67	8	7.67	7.67	6.33	6	5	5	4

Table 6.3: Look-up table of downward velocity

Breakpoints	Column	(1)	(2)	(3)	(4)	(5)	(6)	(7)	(8)	(9)	(10)	(11)
Row		50	60	70	80	90	100	110	120	130	140	150
(1)	0	0	0	0	0	0	0	0	0	0	0	0
(2)	0.25	1.67	1.67	1.67	2	2	1.67	1.67	1.33	1.33	1.33	1
(3)	0.38	3	3	3.33	3.67	3.33	3.33	2.67	2.67	2.33	2	2
(4)	0.5	4	4	4.33	4.33	4.33	4	4	3	3	2.67	2.67
(5)	0.63	4.67	4.67	5.67	5.67	5	5	4.67	4.67	4	4	3.33
(6)	0.75	6	6	6	6	5	5	4.67	4.67	4.67	4	4
(7)	0.88	6.67	6.67	6.67	6.67	5.67	5.67	5	5	4.67	4.67	4
(8)	1	7.33	7.33	7.33	8	8	6	5.33	5.33	5.33	5	5

The primary purpose in this experiment is to develop the plant model to represent operation characteristics of a pair of one air pump and one actuator. To ensure the accuracy of the measurement, a typical PWM value is set at 50% to control the air pump, and the measurement is conducted and recorded three times in order to maintain the validity and reliability. The results are shown in Table 6.4 and illustrated in Figure 6.14. These behaviour lines generally go down gradually in three measurements. The error in three measurements is resulted from the errors in measurement of the distance, accumulated errors, and large intervals in the measuring process. Similarly, the downward velocity is also presented in Figure 6.15, and these values are shown in Table 6.5. However, the downward velocity is separated into two segments: an increasing segment within the range from 70mm - 90mm and decreasing segment within the range from 90mm to 140mm. The results of these three different measurements show the similarity in the behaviour of the actuator and the air pump.

Table 6.4: Measuring upward velocity of actuator 6 in three measurements

1st measurement		2nd measurement		3rd measurement	
Height	Velocity	Height	Velocity	Height	Velocity
63	4.33	60	4.67	62	5.33
76	4.67	74	4.67	78	5.00
90	4.00	88	4.00	93	3.67
102	4.00	100	4.00	103	4.00
114	3.33	112	3.67	115	3.00
124	2.67	123	3.00	123	2.67
132	2.33	132	2.33	130	2.33

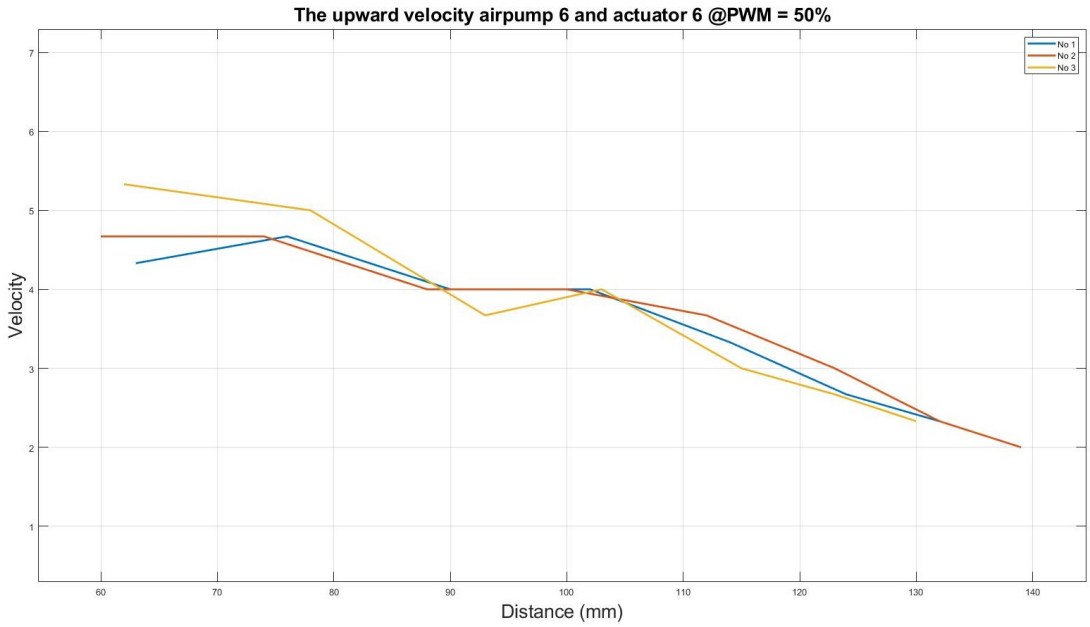

Figure 6.14: upward velocity of actuator 6 at PWM = 50%

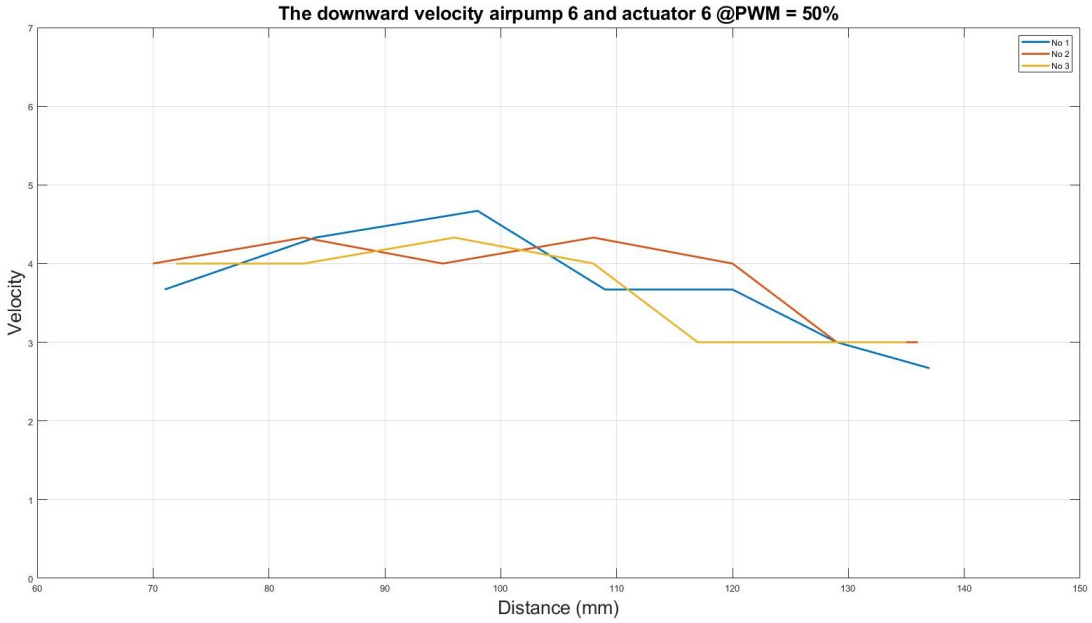

Figure 6.15: downward velocity of actuator 6 at PWM = 50%

Table 6.5: Measuring downward velocity of actuator No.6 in three measurements

1st measurement		2nd measurement		3rd measurement	
Height	Velocity	Height	Velocity	Height	Velocity
71	3.67	70	4.00	72	4.00
84	4.33	83	4.33	83	4.00
98	4.67	95	4.00	96	4.33
109	3.67	108	4.33	108	4.00
120	3.67	120	4.00	117	3.00
129	3.00	129	3.00	125	3.00
137	2.67	136	3.00	135	3.00

In addition, two other pairs of air pump and actuator are then experimented. The results are shown in Figure 6.16. The behaviour velocities of the actuators in both pairs are similar, which proves the accuracy of the proposed plant model. In other words, the plant model manages to determine the position of the actuator in every period

when it receives the PWM value from the micro-controller. Combining these two input parameters, the plant model can be operated at the suitable velocity. Finally, a visual model of the plant model is developed in MATLAB/SIMULINK software, as shown in Figure 6.17. This visual model properly simulates the whole operating process of the actuator and air pump. The detailed discussion regarding this visual model is provided in the next section about the PID model.

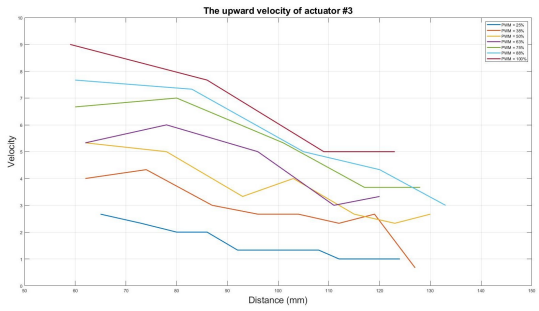

(a) Actuator 3 going up

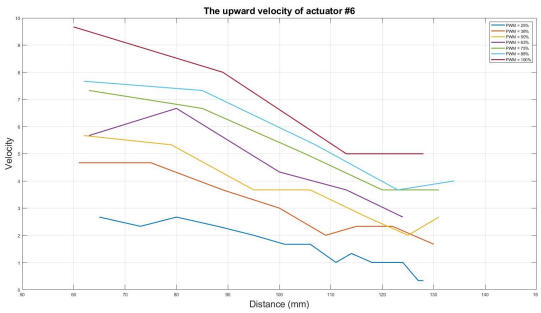

(b) Actuator 6 going up

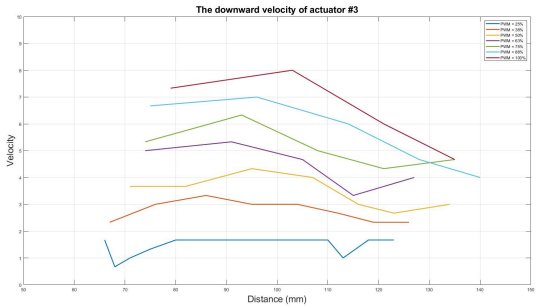

(c) Actuator 3 going down

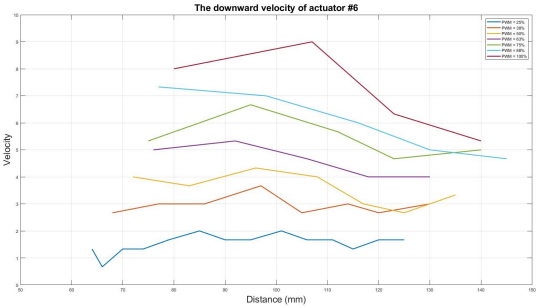

(d) Actuator 6 going down

Figure 6.16: Velocity behaviour of actuator 3 and actuator 6

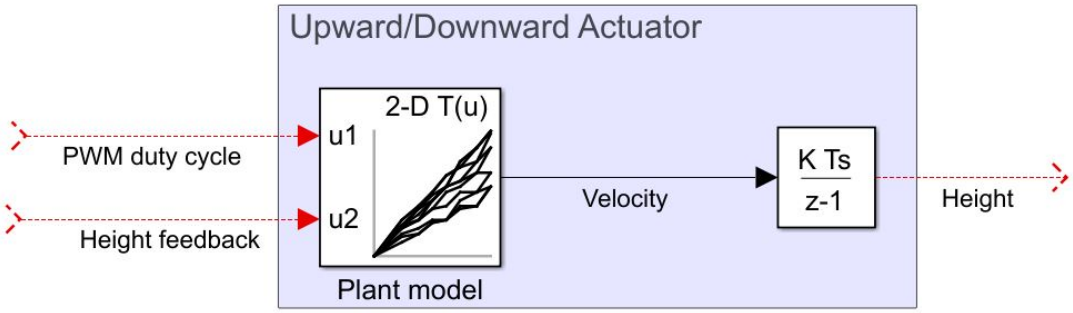

Figure 6.17: Plant model in Simulink Software

6.2.3 Constructing PID controller

PID controller is an exciting topic which has attracted numerous studies, and a variety of methods have been proposed. In the scope of this research, the continuous-time and discrete PID controller are investigated to determine the most effective method to control the system.

Continuous-time PID

A prototype of the continuous-time PID controller is constructed to control the plant model. In this case, the powers of the air pump and motor driver are always smaller or equal to 100% of its energy. Thus, a clamping controller is applied to the PID controller to ensure that the PWM value of this simulated PID block is always within the range from 0% to 100% of the energy level of the motor driver. Apart from the plant model mentioned the previous section, the simulated model of the whole system is constructed to simulate the entire operation of the system, as shown in Figure 6.18.

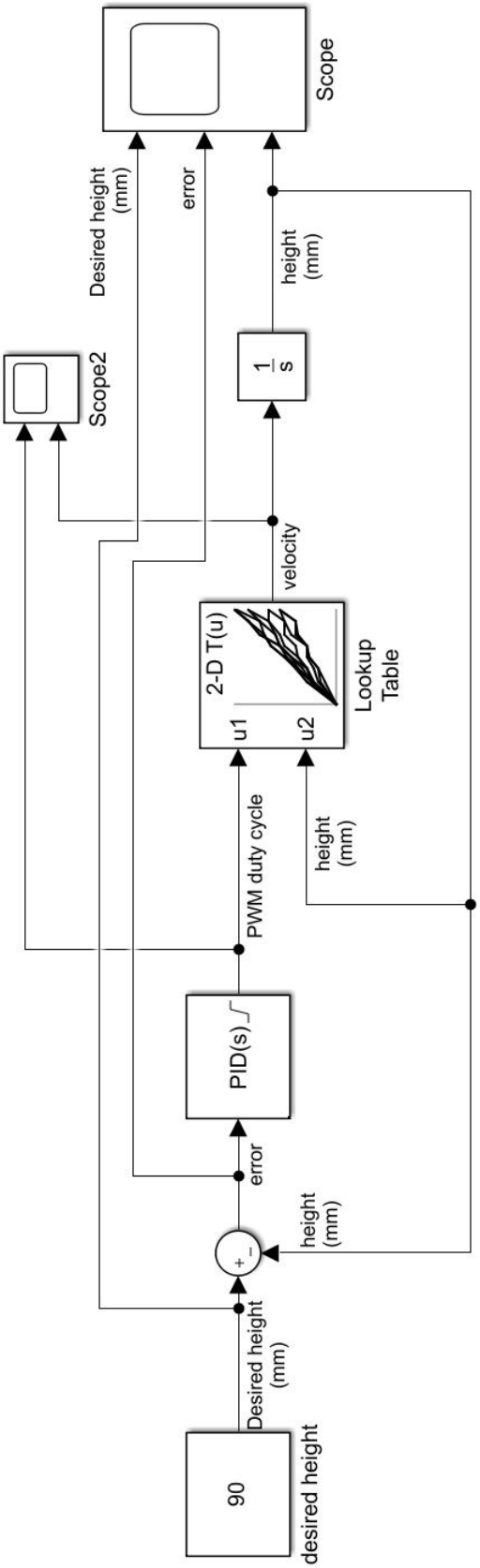

Figure 6.18: Continuous-time PID system

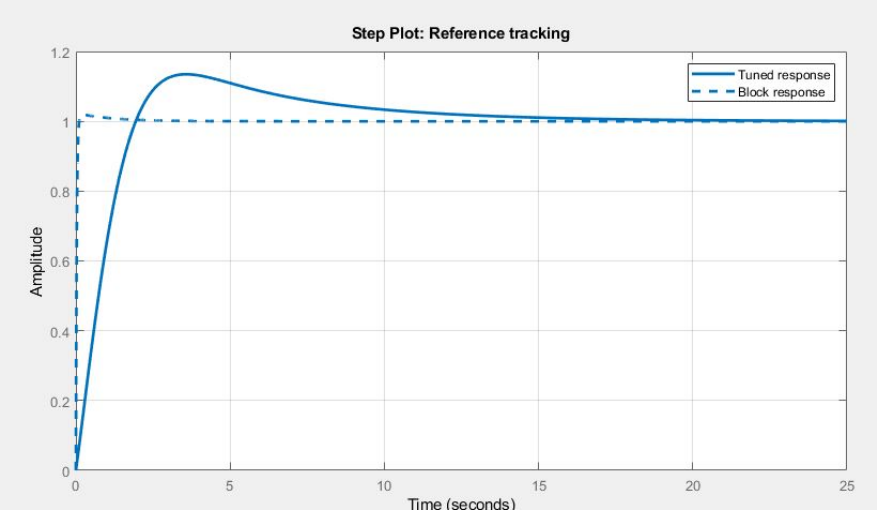

(a) PID responsive line

Controller Parameters

	Tuned	Block
P	0.092719	3.5
I	0.017736	3
D	-0.019539	0.005
N	1.7204	50

Performance and Robustness

	Tuned	Block
Rise time	1.43 seconds	0.0541 seconds
Settling time	12.2 seconds	0.0879 seconds
Overshoot	13.5 %	1.91 %
Peak	1.13	1.02
Gain margin	-Inf dB @ 0 rad/s	Inf dB @ 0 rad/s
Phase margin	69 deg @ 1 rad/s	90.7 deg @ 39.9 rad/s
Closed-loop stability	Stable	Stable

(b) Continuous-time PID parameter

Figure 6.19: Outcomes of PID controller

The height of actuator is sensed by the embedded sensor. This value is sent back in two paths. One path is connected with the plant model. This parameter is to specify the

position of the actuator continuously. In accordance with the specific height, a relevant PWM energy level is presented to control the actuator to reach the desired height. The other path is fed into the sum block to make comparison between the desired height and the current height. The magnitude of the error determines the equivalent PWM energy level to control the actuator as precisely and fast as possible. Based on these parameters of the proposed plant model, the simulated model and the characteristics of the system, a set of P, I, D gains is selected, as shown in Figure 6.19b P = 3.5; I = 3; D = 0.005). After many experiments are conducted, the PID gains are considered the most appropriate for the simulated model since the overshoot gain is 1.91%, the rise time is 0.0541 seconds, the settling time is 0.0879 seconds, and the closed-loop stability is maintained stable.

For instance in Figure 6.20a, the initial position of the actuator, which is at the minimum height, at 50mm. The desired height is set at 140mm. At this time, the error between the desired height and the current height is 90mm. The air pump is, hence, driven with the maximum value. This maximum value of the air pump is kept in about 7.643 seconds until the error reduces to 21.21mm. Under the effect of stiffness co-efficient of the actuator, the velocity of actuator gradually drops in 1.473 seconds before the PID controller is activated. This behaviour of actuator observed from the experiments is synthesised and represented in the plant model in Section (6.2.2). After that, the PID controller is initiated at 8.242mm away from the desired height. At this time, the PWM energy level is adjusted quickly to reduce the velocity of actuator. It takes about 4.884 seconds for the actuator to reach the desired height at 140mm. Apart from the presented PID gains, the estimate overshoot gain of this system is 1.91%, and the actuator is thus able to reach the desired height without overshoot, as shown in Figure 6.20b. However, the quality of this PID controller is not smooth with a few disturbances in the PWM signal. These disturbances cause fluctuations in the velocity

of the actuator. The gradient representing the velocity of actuator is erratic, while the gradient representing the height of actuator is smooth.

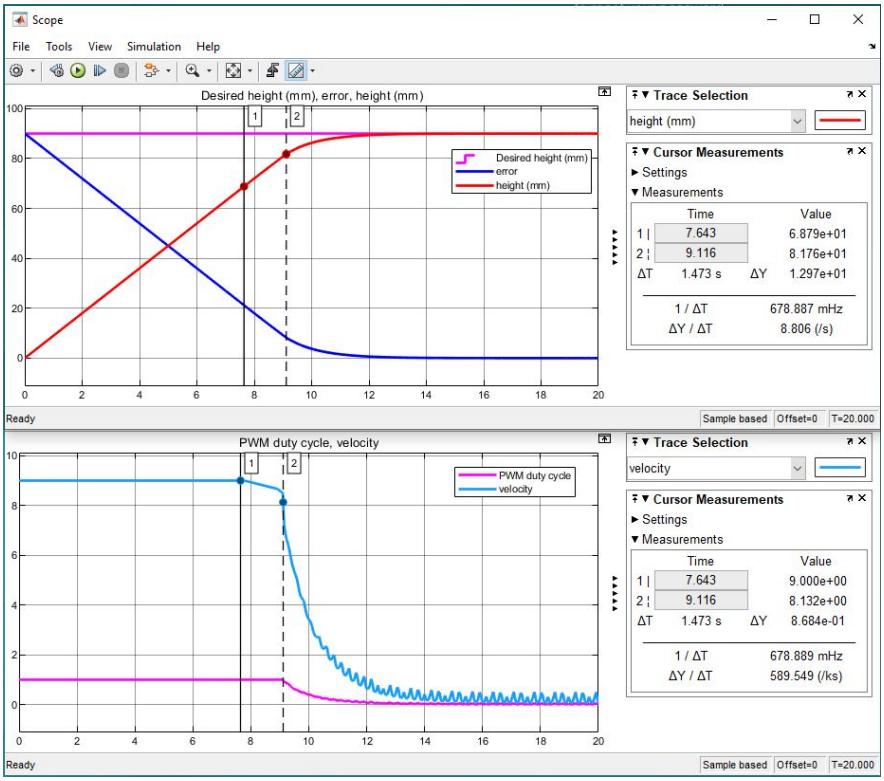

(a) Example of continuous PID controller

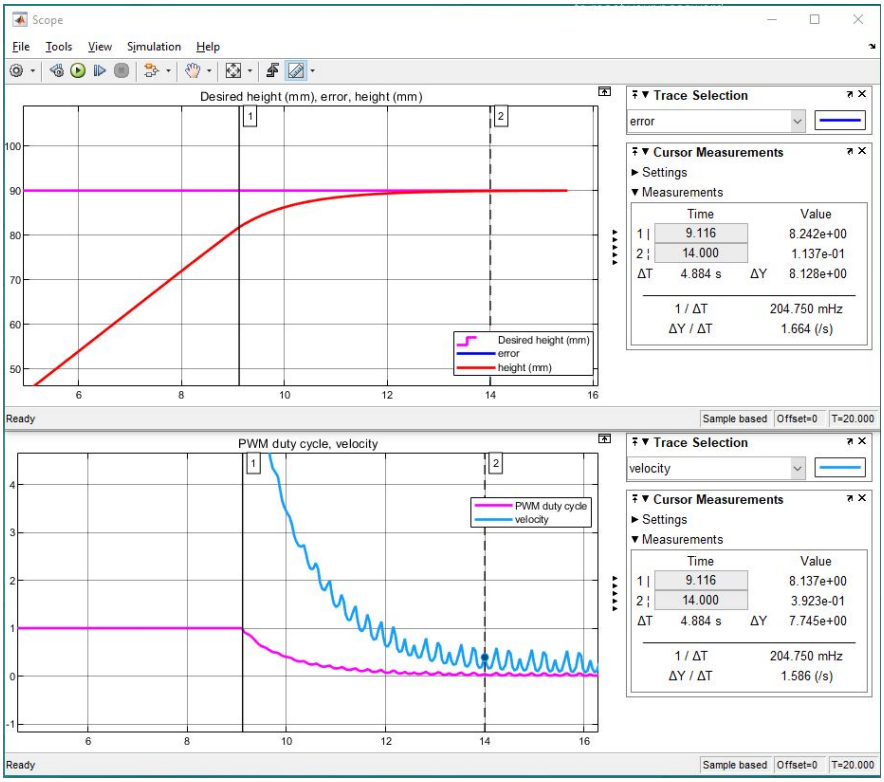

(b) PID working process

Figure 6.20: Continuous PID controller

Discrete PID controller

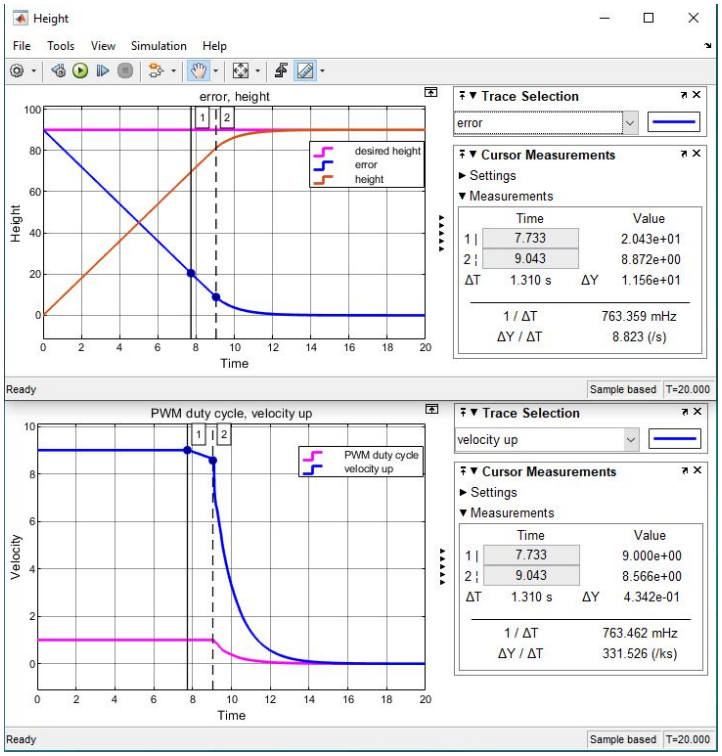

(a) Example of discrete PID controller

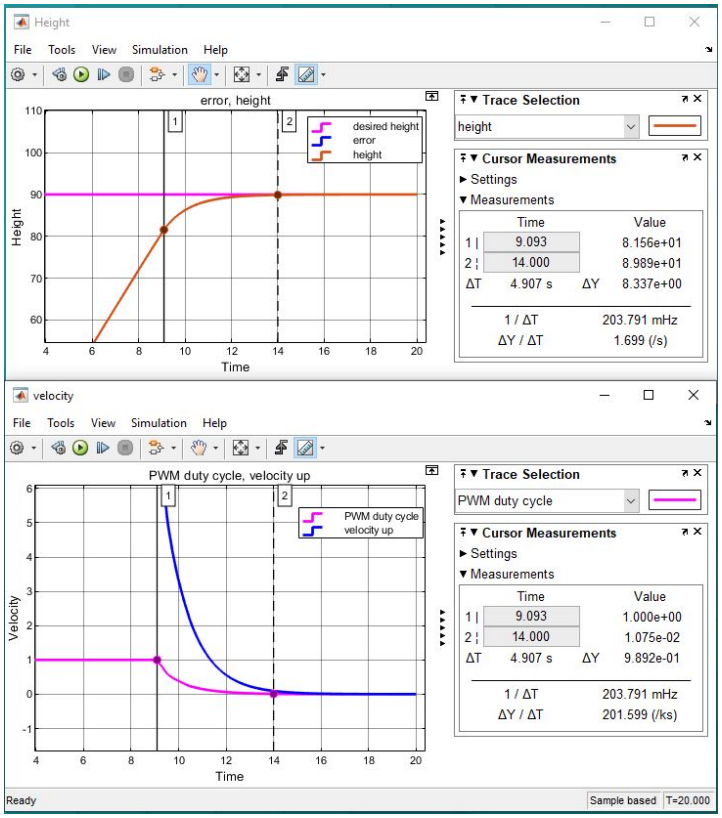

(b) Discrete PID working process

Figure 6.21: Discrete PID controller

Thanks to the advancement of digital processors, the digital signal has been processed with high accuracy, fast response, and similarity to the continuous signal. Furthermore, every continuous signal is converted from analogue to digital prior to being fed into the digital processor. A digital controller is thus adopted to reduce the errors in the conversion and control process. In particular, a discrete PID controller with the same PID gains is used to replace the continuous PID controller, as shown in Figure 6.17. It proves to have more stable velocity and more stable PID control signal than those of the continuous PID controller, as shown in Figure 6.21. In particular, the changes in velocity in the first 9.043 seconds are caused by the natural behaviour of the actuator. The velocity stays constant at 9mm/s in the first 7.733 seconds prior to dropping slightly to 8.56mm/s in the next 1.310 seconds before the discrete PID is activated. The discrete PID is initiated at 8.872mm away from the desired height, and it takes 4.907 seconds for the actuator to reach the desired height. The Figure 6.21b presents a better adjustment of the velocity. The gradients representing the velocity and PWM duty cycle are smoother. This operation of simulated model is similar to that of the practical model.

To sum up, the discrete PID controller has been selected with the most appropriate PID gains including P = 3.5; I = 3; D = 0.005. A clamping mode is also added to keep the PID output within the working range. The rise time is short at only 0.0541 seconds. The settling time is after 0.0879 seconds, and the overshoot gain is only 1.91%. Therefore, the discrete PID controller has provided more advantages than the continuous-time PID controller. Moreover, the discrete PID controller and the closed-loop controller together create a complete feedback control system. It is considered a significant contribution to the field since the previous research studies does not have a control system; they otherwise just present it in theory and prototype. Feedback control system manages to detect and monitor the deformation of the actuator since it has IR proximity sensor embedded inside the actuator.

6.3 Movement algorithm

Together with the above-mentioned results regarding the sensor regression function and simulated system, the movement algorithm shows the proper response as raised in the requirements of this current research. It creates the Tabbot wave on the top surface. Based on the desired movement, either the translational movement or rotational movement, the system controls an equivalent sequence of various actuators. The continuous Tabbot waves in the same direction are to translate the object, meanwhile pairs of continuous Tabbot waves in the opposite direction are to rotate the objects.

6.3.1 Translational movement

A square object is located on the table's surface. Initially, the Tabbot is at rest position, the table's surface and square object are in parallel, following the horizontal direction. The object is far away from the origin by 35mm. After 9 seconds, when the G3, G2, and G1 reach the highest, middle, and lowest position respectively, the left end of the object is lifted up, following the pattern of the top surface. The propagated Tabbot wave is translated consecutively from G3 to G2, and then to G1. This principle is mentioned in Chapter 3 and Chapter 4. Initially, T_0 = $0second$, the object is at 35mm far from the origin. After T_8 = $85seconds$, the object travels by 67mm. It means that the object's velocity is approximately 0.79 mm/seconds, equal to 47 mm/min. The object is manipulated by 65mm after 85 seconds by the Tabbot with seven actuators, as shown in Figure 6.22. Compared to the Deng et al.'s experiment (2016), he adopted six actuators with 24 air chambers to manipulate the object (each actuator has four air chambers). The object's velocity is approximately 30 mm/min. In this current research, with seven actuators, the Tabbot is capable of manipulating the object faster than Deng et al.'s prototype by about 15%. Furthermore, the actual actuation of the Tabbot is similar to the proposed theory and model.

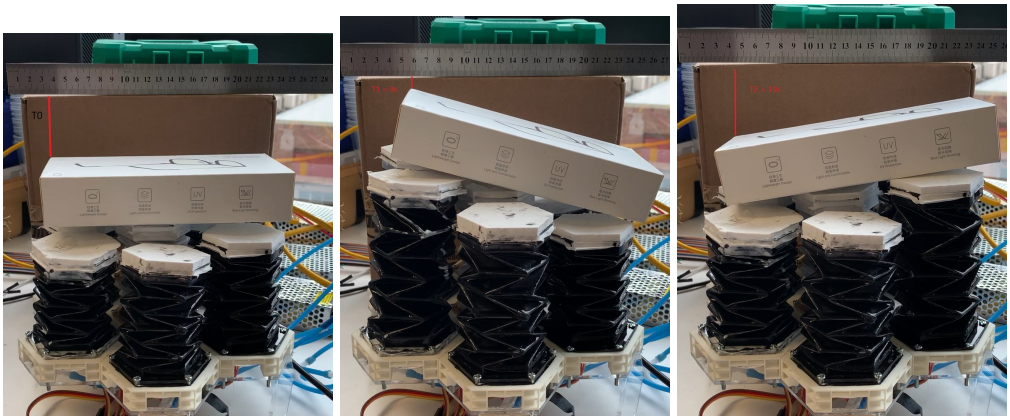

(a) T_0 = 0s (b) T_1 = 9s (c) T_2 = 19s

(d) T_3 = 25s (e) T_4 = 36s (f) T_5 = 42s

(g) T_6 = 54s (h) T_7 = 59s (i) T_8 = 85s

Figure 6.22: Example of translational movement

(Note: Cover plate on top is removed to have a better look inside the Tabbot)

In summary, this proposed Tabbot has successfully addressed the research questions in this study. It reveals how the soft origami actuator operates, and how the IR sensor

works inside the actuator. Finally, it has also proven the efficiency of the closed-loop controller in controlling the actuator movement.

6.3.2 Rotational movement

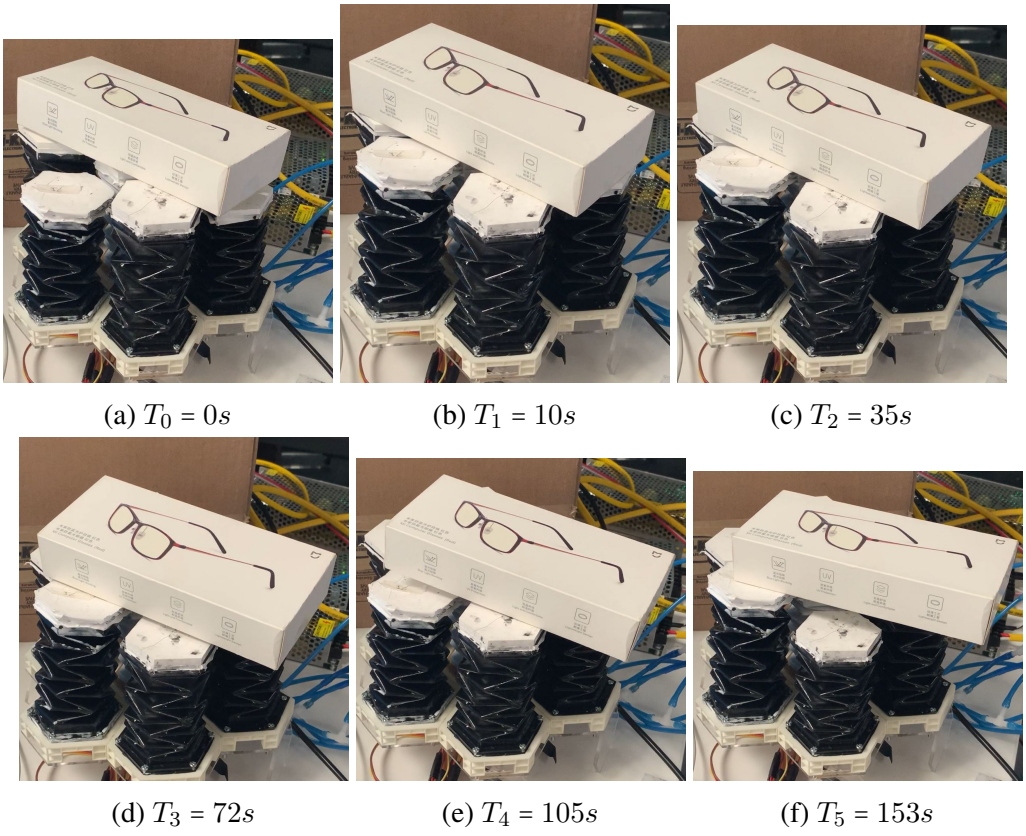

(a) T_0 = 0s (b) T_1 = 10s (c) T_2 = 35s

(d) T_3 = 72s (e) T_4 = 105s (f) T_5 = 153s

Figure 6.23: Example of rotational movement

(Note: Cover plate on top is removed to have a better look inside the Tabbot)

In this experiment, pairs of propagated Tabbot waves, which are in opposite direction, are made to rotate the object. As shown in Figure 6.23, the object that is located on the top surface is reoriented after 153 seconds, and the rotational angle is about 20 degrees, as shown in Figure 6.24. It means that the angular velocity of the object is approximately 0.13 degree/second. This angular velocity is smaller than that recorded from Deng et al.'s experiment (2016) at 1 degree/second.

Besides, not only the rotational movement but also the translational movement are created by the propagation of the Tabbot waves. A pair of Tabbot waves in the opposite direction is similar to the torques, thus producing rotational movement. At the same time, the propagation of Tabbot waves creates translational movement.

Due to the small dimensions of this table, there are only two pairs of the opposite waves: (G1-G2) and (G2-G3) and a small number of the actuators. The number of pairs of torques applied to the object is not enough. Therefore, when the object travels throughout one of the two pairs, the torques is just applied at a certain part of the object. Indeed, the force is not powerful enough to rotate the object with a larger angular velocity. When these fundamental cells are built up together to increase the number of actuators, more pairs of the opposite Tabbot waves are made, thus creating more pairs of the torques. As a consequence, the object is able to be rotated with the higher angular velocity while reducing the translating movement since these torques are homogeneously distributed on the object.

(a) Angle at T = 0s (b) Angle at T = 153s

Figure 6.24: Angle of the object at a different time

The actual operation of the system is similar to the simulated operation and able to respond properly to the control signal. The PID controller has controlled the actuators to reach the desired height with the best performance. The feedback signal creates the closed-loop system. The system in this study has sorted out the drawback in the research of Deng et al.. Apart from the origami table model, Maratas's (2018) prototype does not prove its ability of making movements. In this research, a small scale table with seven actuators is capable of translating the object by 65mm in 85 seconds and rotating it in about 20-degree angel in 153 seconds.

To recap the discussion and analysis, the actual prototype of the Tabbot is proposed successfully in this research, as shown in Figure 6.25. The Tabbot addresses all research questions with its major improvements made on the origami actuator with the embedded sensor, the ability to create the translational and rotational movement, and the closed-loop controller.

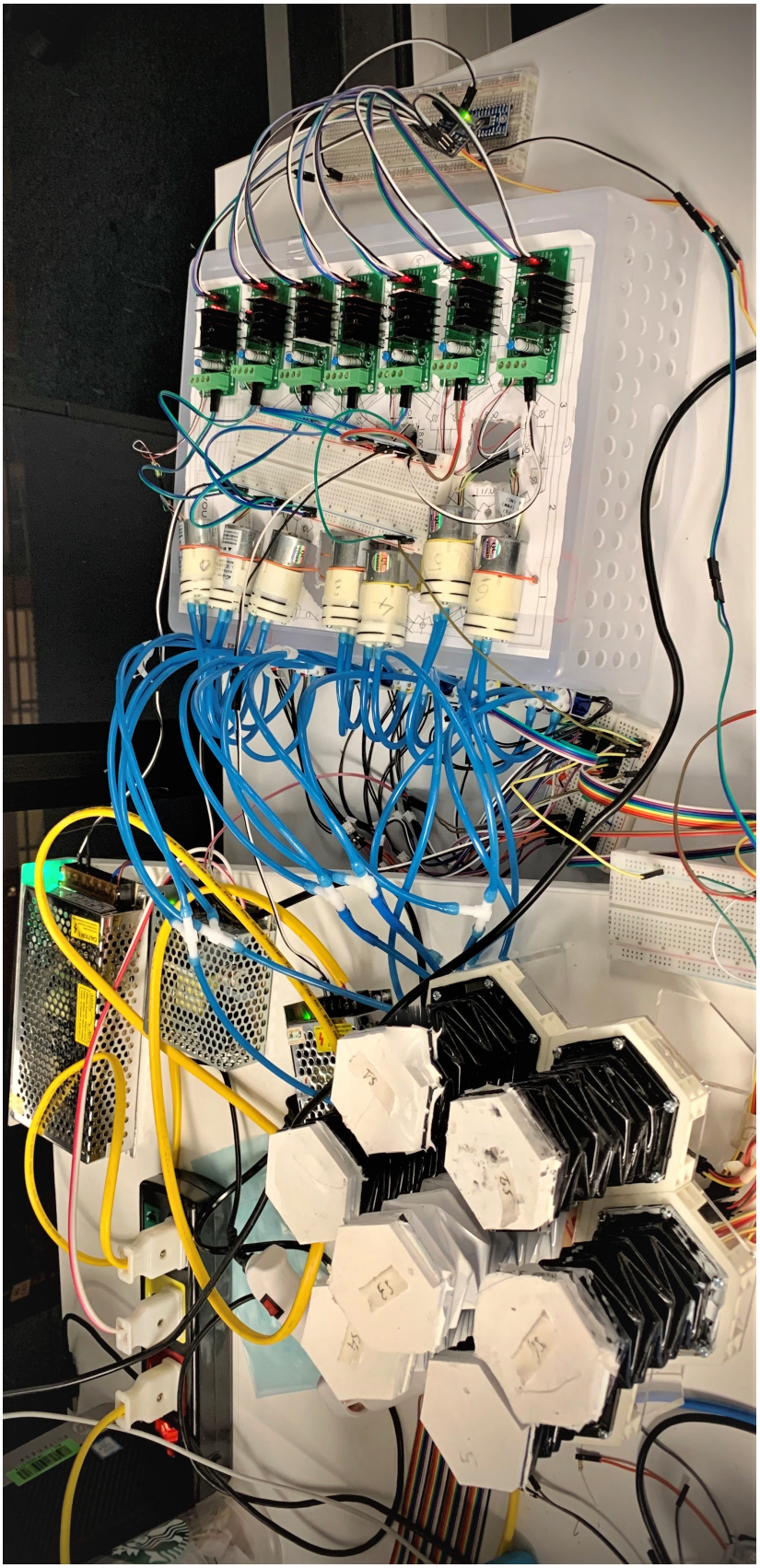

Figure 6.25: Tabbot

Chapter 7

Conclusion

This chapter begins with an overview of what the thesis has achieved to answer three research questions. It then summarizes how the research has been done with various experiments undertaken to investigate various fields such as mechanical, electrical, and programming engineering and successfully establish an actual prototype including the soft origami table robot and closed-loop controller. From here, the practical implications are reviewed before highlighting the contributions of this research to the field of soft robotics. Finally, areas of further research are sketched out in relation to the limitations raised in this current research.

7.1 Overview of achievements

This thesis makes a step towards the theoretical and practical principle of the soft origami table robot. It is the first table robot in which the closed-loop controller is employed, and the sensor is embedded inside the soft origami actuator. It offers solutions to the drawbacks found in the previous studies. In particular, the table robot with embedded sensor manages to eliminate obstacles during the measurement of the deformation on the top surface and effectively handle with both of round work-pieces

and flat work-pieces within a broad elongation of the actuator. Each of the components in this system shows significant improvements compared to other existing research.

The soft origami actuator has been manufactured with improvements. This origami structure is covered by ecoflex00-30 silicone to make it stronger and stand straight along the vertical direction. Furthermore, the elongation of the actuator is proved to increase dramatically, from 50mm to 130mm. With regards to the structure of the Tabbot, by using cantilevers, the top layer is moulded with the origami cylinder. These cantilevers are useful to fix the origami cylinder in the moulding process and keep uniformity among the manually manufactured actuators. The bottom layer is supported by the fringe to increase the contact area between the actuator and the stage. As a result, it helps to avoid the air leakage. The actuator's sidewall is coloured in white to increase the density of the reflected light to the sensor. The precision in the sensor's operation is improved dramatically, and the sensor is embedded inside the actuator. The actuator can be maintained easily thanks to its simple assembly.

The Tabbot is the first proposed prototype in which a sensor is successfully embedded inside the actual actuator. This sensor is capable of detecting the actuator's elongation. The research has proved that this sensor performs better with the white colour painted on the upper layer and sidewall. The challenge here is its non-linear value when being conversed from the raw value of the sensor to the height unit. Nevertheless, this study manages to establish a general equation that can be applied to these sensors. It is useful to calibrate the sensors and can run properly in the closed-loop controller.

The non-linear characteristic of the soft system raises a challenge in other studies in this field. However, based on the findings of this research, the plant model of the soft actuator is proposed and evaluated in MATLAB/SIMULINK software. The operation

of the simulated and actual system show their correspondence. Consequently, PID gains are identified and quickly adjusted to suit the specific behaviours of the air pump.

The electrical system is also improved. With only one air pump and two 3/2-way solenoid valves, this system is capable of inflating and deflating to create upward and downward movements of the actuator respectively. The other research adopts two separated air pumps for inflating and deflating process. Therefore, with such as large number of components in the system, it is difficult to scale up to a larger model. The electrical system in the current research has maximized its performance by reducing the number of components and minimizing the physical size of the system. The proposed Tabbot is thus proved to be more reliable, cost-effective, and efficient.

Finally, the thesis has proposed the actual prototype of the soft origami table robot. This Tabbot is able to manipulate the objects in both translational and rotational movement. It also shows a significant benefit in handling the delicate objects in round and flat shape. Moreover, the operation states of the system are simultaneously monitored by the feedback signal, and this system is automated completely. Due to the time limitation, this research however only presents the fundamental cell of the soft table robot with seven actuators integrated. This fundamental cell is considered the principle to pave the way for the further development of a large scale table robot.

7.2 Contributions

The objectives of this project have been accomplished to present several contributions in the field of soft robotics, and answers have been provided to the questions which were originally posed in the first chapter of the thesis:

1. How can a sensor embedded inside the soft origami actuator operate properly?

Based on the actuator's design, the sensor is embedded and maintained inside the actuator.This research has also verified the principle of the colour of the upper layer in the previous research; white color shows the best reflective co-efficient. Also, it has made an evaluation on the effects of the sidewall's colour on the operation of the IR sensor. White colour pained on both the upper layer and the sidewall is proved to have the best reflective co-efficient. A new method of manufacturing the origami actuator has been pointed out with a fringe at the bottom and the upper layer being cast directly with the cylinder. It therefore ensures that the proposed actuator with the embedded sensor inside is tight, flexible, efficient, cost-effective, and easy to be maintained.

2. How can a soft origami actuator operate to create translational and rotational locomotion?

   Firstly, based on the separate control principle for movement of each actuator, a combination of discrete actuators has been made to create sinusoidal movement on top surface. This moving control ensures that the objects on top are able to be manipulated in the translational and rotational movement.

   In addition, with the adoption of the origami structure, these actuators have longer elongation to create a larger amplitude of the Tabbot's waves on the top surface. As a result, this proposed prototype is able to handle the delicate objects in either round or flat shaped objects.

3. How can the prototype be controlled by a closed-loop controller?

   By successfully embedding the sensor inside the actuator, difficulties in sensing the actuator's deformation are sorted out. It is a key point to automate the soft table robot completely. Besides, the plant model of the soft actuator has been simulated in the MATLAB/SIMULINK software based on the lookup-table. This

lookup-table is constructed from the collected data that are representative for the actuator's behavior. In addition, the lookup-table manages to linearize the non-linear behaviour of the soft actuator. Moreover, the closed-loop controller has been developed from the regression function of the sensor and the plant model of the actuator to monitor the operating states of the system simultaneously. In short, this prototype is studied and validated by the simulated and actual results of the system.

To sum up, the research findings has been discovered regarding the embedded sensor, determining the regression function of the sensor and the effect of the sidewall's colour, linearizing the origami soft actuator and moving algorithm. All of them have been adopted to construct the actual soft origami table robot to manipulate the delicate objects.

7.3 Limitations and Future research

Although a completed prototype of the soft origami table robot has been proposed and evaluated thoroughly, some limitations are still present. With the initial achievements, the research is able to open some promising topics to learn more about:

1. Practical scale table

   Due to the time constraint, the research has only shed light on the principal cell of the soft origami table robot with its full functions. Future work could address the synchronization of actuators in a large scale table. It is such a big challenge to combine different cells since it is related to the synchronization of the control signal of these cells to create the larger sinusoidal waves.

2. Controlling and moving algorithm

To be applied to a larger scale table, a high level of control algorithm could be investigated. It is first necessary to detect an object's location on the top surface properly, and a far more complicated algorithm is required to manipulate the objects to travel in a specified trajectory or optimise the travelling path.

3. Linearizing the soft model

   Linearizing the soft model has posed a big challenge in the previous studies. A transfer function and state-space model of the soft actuator have been proved to be helpful to calculate and analyse the states of the system properly during the whole operation, so another long term research project would be to develop an accurate non-linear model of the actuators from the first principle.

4. Sensor techniques

   The infrared sensor is quite simple and effective to be adopted in the small systems. However, it is challenging to present the correct results because of the errors in the conversing process, especially in large systems. Therefore, to improve the precision and stability of the system, a new type of sensor that can measure the distance directly is a worth-investigating proposal to reduce disturbance in the control process.

By the way of conclusion, the findings in this research have successfully solved important issues raised in the soft robotics literature and proposed potential areas for future research. It also presents practical applications of soft robotics in the industries and life.

References

Adafruit. (n.d.). *Adafruit pca9685 16-channel servo driver.* Retrieved from `https://learn.adafruit.com/16-channel-pwm-servo-driver`

Adriaens, H., De Koning, W. L. & Banning, R. (2000). Modeling piezoelectric actuators. *IEEE/ASME transactions on mechatronics*, *5*(4), 331–341.

Al-Ibadi, A., Nefti-Meziani, S. & Davis, S. (2018). Design, implementation and modelling of the single and multiple extensor pneumatic muscle actuators. *Systems Science & Control Engineering*, *6*(1), 80–89.

Araki, M. (2009). Pid control. *Control Systems, Robotics and Automation: System Analysis and Control: Classical Approaches II*, 58–79.

Benniu, Z., Junqian, Z., Kaihong, Z. & Zhixiang, Z. (2007). A non-contact proximity sensor with low frequency electromagnetic field. *Sensors and Actuators A: Physical*, *135*(1), 162–168.

Benslimane, M. Y., Kiil, H.-E. & Tryson, M. J. (2010). Dielectric electro-active polymer push actuators: performance and challenges. *Polymer International*, *59*(3), 415–421.

Bihlmaier, J. A. (1982, June 22). *Pneumatic-hydraulic actuator system.* Google Patents. (US Patent 4,335,867)

Chee, C. Y., Tong, L. & Steven, G. P. (1998). A review on the modelling of piezoelectric sensors and actuators incorporated in intelligent structures. *Journal of Intelligent Material Systems and Structures*, *9*(1), 3–19.

Chen, A., Yin, R., Cao, L., Yuan, C., Ding, H. & Zhang, W. (2017). Soft robotics: Definition and research issues. In *2017 24th international conference on mechatronics and machine vision in practice (m2vip)* (pp. 366–370).

Dai, J. & Caldwell, D. (2010). Origami-based robotic paper-and-board packaging for food industry. *Trends in food science & technology*, *21*(3), 153–157.

Deng, Z., Stommel, M. & Xu, W. (2016). A novel soft machine table for manipulation of delicate objects inspired by caterpillar locomotion. *IEEE/ASME Transactions on Mechatronics*, *21*(3), 1702–1710.

DiCola, T. (n.d.). *Using vcnl4010 proximity sensor.* Retrieved from `https://learn.adafruit.com/using-vcnl4010-proximity-sensor`

Fadali, M. S. & Visioli, A. (2013). *Digital control engineering: analysis and design*. Academic Press.

Gardiner, M., Aigner, R., Ogawa, H. & Hanlon, R. (2018). Fold mapping: Parametric design of origami surfaces with periodic tessellations. In *7th origami science*

mathematics and eductation conference. presented at the 7osme, oxford, great britain.

Hashem, R., Smith, B., Browne, D., Xu, W. & Stommel, M. (2016). Control of a soft-bodied xy peristaltic table for delicate sorting. In *2016 ieee 14th international workshop on advanced motion control (amc)* (pp. 358–363).

Ilievski, F., Mazzeo, A. D., Shepherd, R. F., Chen, X. & Whitesides, G. M. (2011). Soft robotics for chemists. *Angewandte Chemie International Edition*, *50*(8), 1890–1895.

Johnson, M., Chen, Y., Hovet, S., Xu, S., Wood, B., Ren, H., ... Tse, Z. T. H. (2017). Fabricating biomedical origami: a state-of-the-art review. *International journal of computer assisted radiology and surgery*, *12*(11), 2023–2032.

Johnston, A. R. (1977). Proximity sensor technology for manipulator end effectors. *Mechanism and Machine Theory*, *12*(1), 95–109.

Kamoer. (n.d.). *Kvp04 vacuum pump.* Retrieved from `http://kamoer.com/Products/showproduct.php?id=263&lang=en`

Kier, W. M. & Stella, M. P. (2007). The arrangement and function of octopus arm musculature and connective tissue. *Journal of Morphology*, *268*(10), 831–843.

Kim, S., Hawkes, E., Choy, K., Joldaz, M., Foleyz, J. & Wood, R. (2009). Micro artificial muscle fiber using niti spring for soft robotics. In *2009 ieee/rsj international conference on intelligent robots and systems* (pp. 2228–2234).

Kim, S., Laschi, C. & Trimmer, B. (2013). Soft robotics: a bioinspired evolution in robotics. *Trends in biotechnology*, *31*(5), 287–294.

Laschi, C., Cianchetti, M., Mazzolai, B., Margheri, L., Follador, M. & Dario, P. (2012). Soft robot arm inspired by the octopus. *Advanced Robotics*, *26*(7), 709–727.

Lin, H.-T., Leisk, G. G. & Trimmer, B. (2011). Goqbot: a caterpillar-inspired soft-bodied rolling robot. *Bioinspiration & biomimetics*, *6*(2), 026007.

Mao, S., Dong, E., Jin, H., Xu, M., Zhang, S., Yang, J. & Low, K. H. (2014). Gait study and pattern generation of a starfish-like soft robot with flexible rays actuated by smas. *Journal of Bionic Engineering*, *11*(3), 400–411.

Maratas, J. (2018). *A novel machine table using origami inspired pneumatic soft actuator* (Bachelor's Dissertation). Auckland University of Technology, New Zealand.

MathWorks, I. (n.d.). *Pid controller.* Retrieved from `https://au.mathworks.com/help/simulink/slref/pidcontroller.html`

Mohamed, N. M., Abdalaziz, A. A., Ahmed, A. A. & Ahmed, A. A. (2017). Implementation of a pid control system on microcontroller (dc motor case study). In *2017 international conference on communication, control, computing and electronics engineering (iccccee)* (pp. 1–5).

Mollah, R. (n.d.). Effect of infrared radiation on coloured surface.

Morgan, J., Magleby, S. P. & Howell, L. L. (2016). An approach to designing origami-adapted aerospace mechanisms. *Journal of Mechanical Design*, *138*(5), 052301.

Mosadegh, B., Mazzeo, A. D., Shepherd, R. F., Morin, S. A., Gupta, U., Sani, I. Z., ... Whitesides, G. M. (2014). Control of soft machines using actuators operated by

a braille display. *Lab on a Chip*, *14*(1), 189–199.

Ogata, K. & Yang, Y. (2010). *Modern control engineering* (Vol. 17). Pearson Upper Saddle River, NJ.

Oguntoyinbo, O. et al. (2009). Pid control of brushless dc motor and robot trajectory planning simulation with matlab®/simulink®.

O'Halloran, A., O'malley, F. & McHugh, P. (2008). A review on dielectric elastomer actuators, technology, applications, and challenges. *Journal of Applied Physics*, *104*(7), 9.

Shepherd, R. F., Ilievski, F., Choi, W., Morin, S. A., Stokes, A. A., Mazzeo, A. D., ... Whitesides, G. M. (2011). Multigait soft robot. *Proceedings of the national academy of sciences*, *108*(51), 20400–20403.

Stommel, M. & Xu, W. (2015). Optimal, efficient sequential control of a soft-bodied, peristaltic sorting table. *IEEE Transactions on Automation Science and Engineering*, *13*(2), 858–867.

Stommel, M., Xu, W., Lim, P. & Kadmiry, B. (2014). Robotic sorting of ovine offal: Discussion of a soft peristaltic approach. *Soft Robotics*, *1*(4), 246–254.

Tachi, T. (2010). Geometric considerations for the design of rigid origami structures. In *Proceedings of the international association for shell and spatial structures (iass) symposium* (Vol. 12, pp. 458–460).

TexasInstruments. (n.d.-a). *Tca9548a low-voltage 8-channel i2c switch with reset.* Retrieved from `http://www.ti.com/lit/ds/symlink/tca9548a.pdf`

TexasInstruments. (n.d.-b). *Uln2803a darlington transistor arrays.* Retrieved from `http://www.ti.com/lit/ds/symlink/uln2803a.pdf`

Thien, H., Stommel, M., Le Daheron, F., Le Page, A., Deng, Z. & Xu, W. (2016). Embedded infrared imaging to measure the deformation of a soft robotic actuator. In *2016 international conference on image and vision computing new zealand (ivcnz)* (pp. 1–6).

Thomas, M. B., Maul, G. P. & Jayawiyanto, E. (2005). A novel, low-cost pneumatic positioning system. *Journal of manufacturing systems*, *24*(4), 377–387.

Van Varseveld, R. B. & Bone, G. M. (1997). Accurate position control of a pneumatic actuator using on/off solenoid valves. *IEEE/ASME Transactions on mechatronics*, *2*(3), 195–204.

Whitesides, G. M. (2018). Soft robotics. *Angewandte Chemie International Edition*, *57*(16), 4258–4273.

Wilson, J., Li, D., Chen, Z. & George, R. (1993). Flexible robot manipulators and grippers: Relatives of elephant trunks and squid tentacles. In *Robots and biological systems: Towards a new bionics?* (pp. 475–494). Springer.

Wilson, L., Pellegrino, S. & Danner, R. (2013). Origami sunshield concepts for space telescopes. In *54th aiaa/asme/asce/ahs/asc structures, structural dynamics, and materials conference* (p. 1594).

Zhakypov, Z., Huang, J.-L. & Paik, J. (2016). A novel torsional shape memory alloy actuator: Modeling, characterization, and control. *IEEE Robotics & Automation Magazine*, *23*(3), 65–74.